THE
PHYSICAL REVIEW

A Journal of Experimental and Theoretical Physics Established by E. L. Nichols in 1893

VOL. 58, No. 11 DECEMBER 1, 1940 SECOND SERIES

Proton Induced Radioactivity of Manganese*

ARTHUR HEMMENDINGER†
University of Oklahoma, Norman, Oklahoma

(Received September 23, 1940)

The reaction Cr^{52} (p, n) Mn^{52} at 6.6-Mev proton energy produces isomers with period 21.3 min. and 6.5 days. These are positron emitters with maximum positron energy of 2.2 Mev (21 min.) and 0.77 Mev (6.5 day). The gamma-ray spectrum for each isomer has been investigated. There are 2 gamma-rays per positron in the short period activity. The gamma-radiation in the 6.5-day activity is so intense that 95 percent of these disintegrations must be due to *K*-electron capture; this is followed by emission of probably two gamma-rays. In the remaining 5 percent the positron emission is followed by three gamma-rays. The threshold for the 21-min. activity and the yield for both periods have been determined.

SAMPLES of metallic chromium have been bombarded with 6.6-Mev protons produced in the University of Rochester cyclotron. Positron activities of two periods were observed and studied: 21.3 min. and 6.5 days. These periods have been observed in other reactions, and Livingood and Seaborg,[1] assign them to isomers of Mn^{52}. This conclusion is consistent with results to be presented here.

I. MEASUREMENT OF PERIODS

The bombarded samples of metallic chromium weighed about 5 g. The surface of the metal was cleaned by grinding on an emery wheel. The initial activity for the 21-min. period was 67 microcuries per microampere of protons for infinite duration of bombardment at 6.6-Mev proton energy. The initial activity for the 6.5-day period was 4.4 $\mu C/\mu a$ under the same conditions.

The two activities mentioned were identified chemically as Mn. A layer a few tenths of a millimeter thick was dissolved off of the Cr target by immersion in hot HCl. To the acid solution $MnCl_2$ was added for a carrier. NaOH was added until the solution was basic, and it was then oxidized with Na_2O_2. The solution was boiled, diluted, and filtered. The precipitate showed the 21-min. and 6.5-day activities.

The periods were measured with an ionization chamber containing Freon-12 at 2 atmospheres pressure and an FP-54 amplifier arranged for automatic photographic recording of the data.[2] Figure 1 shows the decay curve of a Cr target which had been exposed to 6.8-Mev protons at 0.07 μa for an hour. From this curve we determine the shorter period as 21.3 min. Subtracting the long period activity from the total, we see that the two periods mentioned account for practically all of the observed activity, and there is no

* A preliminary report of this work was made at the Washington meeting of the American Physical Society, December 1938. See Phys. Rev. **55**, 604 (1939).

† A report of work done at the University of Rochester during the summers of 1938 and 1939.

[1] J. J. Livingood and G. T. Seaborg, Phys. Rev. **54**, 391 (1938).

[2] S. W. Barnes, Rev. Sci. Inst. **10**, 1 (1939).

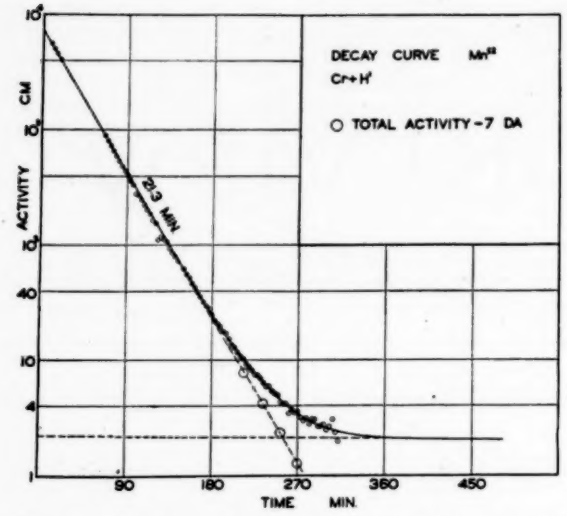

FIG. 1. Decay curve of Mn^{52}. Cr target bombarded at 6.8 Mev for 60 min. at 0.07μa. Measurements start 4 min. after end of bombardment.

evidence for a 46-min. period, which activity occurs at lower proton energies.[3,4] We have also found the 310-day period assigned by Livingood and Seaborg[1] to Mn^{54}, but have not studied it. Figure 2, showing the decay curve of a Mn precipitate several days after bombardment of the parent Cr, gives the half-life as 7.4 ± 1 days. The Cr target was bombarded for 45 min. at a current of 0.5 μa of 6.6 Mev protons. This period is slightly greater than Livingood and Seaborg's value of 6.5 ± 1 days, and since the 310-day activity was not subtracted, it seems reasonable to assume 6.5 days to be the more precise value.

II. Positron Energy

The energies of both sets of positrons were measured by means of a cloud chamber in a magnetic field. Histograms are shown in Fig. 3 and Fig. 4. The cloud-chamber tracks were mostly positrons, distributed in the usual beta-ray spectrum. The upper energy limits of the positron spectra are 2.2 Mev (21 min.) and 0.77 Mev (6.5 day). The energy 0.77 Mev agrees fairly well with the value (0.7) given by Livingood and Seaborg.[1] They do not report the energy of the 21-min. positrons. We have measured the range in Al of these particles and find it to be 0.973 g/cm^2. Using the relation[5]

$$\text{energy} = (\text{range (g/cm}^2) + 0.165)/0.536 \text{ Mev},$$

we get a value of 2.12 Mev.

III. Excitation Function

By bombarding a pile of thin films of chromium the threshold for the 21-min. activity was determined. The intensity of the 6.5-day activity was far too small for such a measurement. Cr films about 0.18μ thick were evaporated onto 2.5μ Al foil. The Cr side of the foil was exposed to the proton beam so that the Mn recoil nuclei could not get away. The stopping power of the pile of eight foils was measured by placing it in the proton beam and observing the decrease in range of the protons. The stopping power of the pile was 6 cm air equivalent. Protons of this energy produce no activity in Al of such a period and intensity to be troublesome even in comparison with the activities of these thin targets. The incident proton energy at the first foil was 6.6 Mev. There was an 0.05 Mev energy

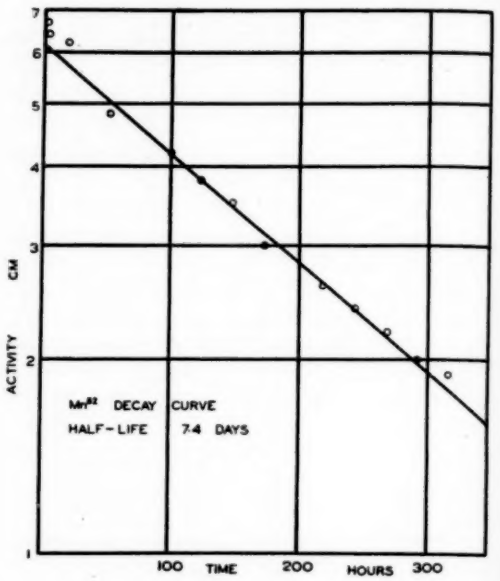

FIG. 2. Decay curve of Mn precipitate. Cr target bombarded at 6.6 Mev for 45 min. at 0.5μa. Measurements start two days after end of bombardment.

[3] Barnes, DuBridge, Wiig, Buck and Strain, Phys. Rev. 51, 775 (1937); DuBridge, Barnes, Buck and Strain, Phys. Rev. 53, 447 (1938).

[4] Delsasso, Ridenour, Sherr and White, Phys. Rev. 55, 113 (1939).

[5] E. E. Widdowson and F. C. Champion, Proc. Phys. Soc. 50, 192 (1938).

loss in each Cr+Al film. The decay curves for the various films are shown in Fig. 5. The initial activities are plotted against the proton energy in Fig. 6. We find the threshold for the 21-min. activity to be 6.3 Mev. The actual reaction energy (threshold corrected for nuclear recoil) is $6.3(52/53)=6.2$ Mev. All we can say about the threshold of the 6.5-day activity is that it does not differ from 6.2 Mev by more than a few tenths of a Mev; at energies lower than 6.3 Mev the 46-min. and 310-day activities are so great compared to the 6.5-day that a more precise determination of this threshold is hardly feasible.

IV. Gamma-Rays

Gamma-ray absorption curves are shown in Fig. 7. The first part of the curve for the 21-min. period has a slope which probably corresponds to annihilation radiation. In the 6.5-day activity the intensity of annihilation radiation is negligible compared to that of higher energy radiation. Using data given by Gentner[6] we estimate the

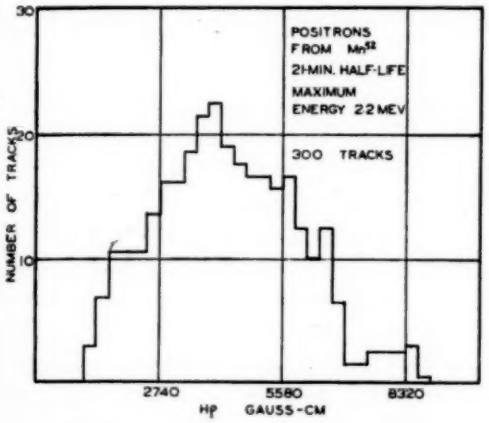

Fig. 3. Distribution of positron tracks from 21-min. Mn^{52}.

average gamma-ray energies as 1.1 ± 0.2 Mev (21 min.) and 0.9 ± 0.2 Mev (6.5 day). Since both gamma-ray spectra are probably complex these energy values are very uncertain.

The source used in plotting the gamma-ray absorption curves (Fig. 7) was a thick Cr target covered with an Al sheet. Thus positrons emitted in any direction were stopped, and for each positron there must be two quanta of annihilation radiation. The ionization current due to the hard component is twice that due to the soft (from Fig. 7), and the ionization per quantum of the hard radiation will possibly be greater than that of the 0.5-Mev radiation. This suggests that there may be about two 1.1-Mev quanta per positron. The assumption that there are two 1.1-Mev gammas per positron is also necessary to account for the observed threshold of 6.2 Mev, since the upper limit of the positron spectrum is only 2.2 Mev, leaving 2.2 Mev for the gamma-ray energy.

We can estimate the intensity of the gamma-radiation in the 6.5-day activity by calculating the ratio $\Gamma=\gamma/(\gamma+\beta)$ of ionization produced by gammas to total ionization, the former being measured with an Al absorber thick enough to stop all positrons.

These ratios are 0.025 (21 min.) and 0.24 (6.5 day). For the 21-min. activity $\gamma/\beta=2.5$ percent, of which two-thirds is for hard gamma-rays. For these only, $\gamma/\beta=1.6$ percent. For the 6.5-day activity $\gamma/\beta=32$ percent. Since the sensitivity of the ionization chamber does not vary greatly with energy in this region, and since the gamma-rays have nearly the same absorption coefficients, the number of gammas per positron in the 6.5-day activity is $32/1.6=20$ times as many in the 21-min. activity, which means 40 gammas per positron.

We conclude that the 6.5-day isomer decays not only by positron emission, but also by K-electron capture followed by emission of gamma-radiation. Presumably 3 gammas accom-

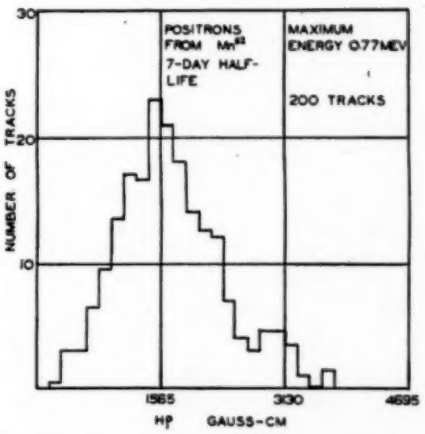

Fig. 4. Distribution of positron tracks from 6.5-day Mn^{52}.

[6] W. Gentner, J. de phys. et rad. 6, 274 (1935).

pany the positron, leaving the other 37 for K capture. Assuming 2 gammas per K capture, then there are about 18 K captures per positron, or positron emission occurs in only 5 percent of the disintegrations.

We have looked for x-rays emitted by the 6.5-day isomer. There is evidently a soft radiation, which we were unable to identify, apparently because of the absorption in air.

V. Coincidence Counter Measurements

The data presented so far show that there might be some interesting features of the disintegration of the 6.5-day isomer, and it seemed at least possible that these could be investigated by means of coincidence counters. Thick-walled alcohol-argon filled counters were used, and an amplifier with a resolving time (τ) of $(9.17\pm0.25)\times10^{-9}$ min. The details of the counters, amplifiers, scaling, circuit, and the technique of measuring τ will be described elsewhere. Counter data were taken for both short and long periods. In each case, measurements were made of single and coincidence counting rates with the thin (0.5 mm) source in both positions A and B of Fig. 8. In position A the source is placed between two Al slabs 0.25 in. thick which serve to stop all positrons. In position B ideally only half of the positrons produce annihilation radiation which affects the counters. Actually, the number of annihilation quanta counted in position B is more than half of the total number, and this ratio must be ascertained by separate measurements.

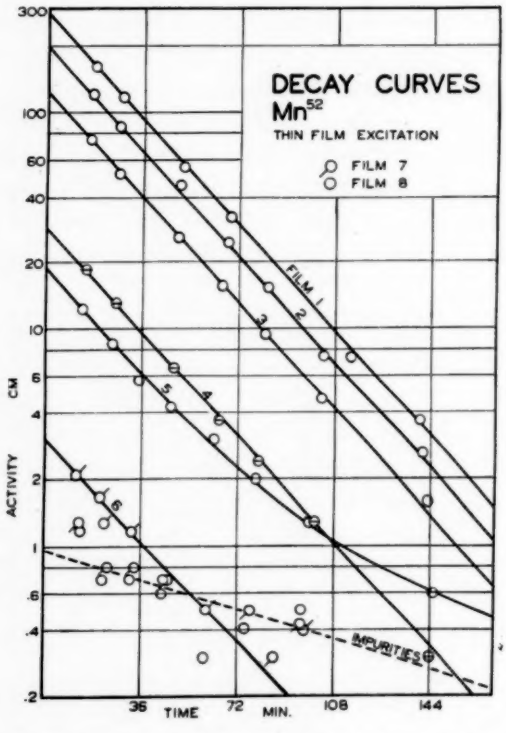

FIG. 5. Decay curves of thin films of Cr bombarded with protons.

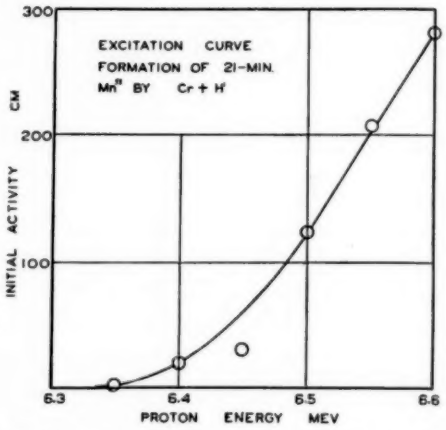

FIG. 6. Excitation curve for the formation of the 21-min. Mn^{52}. Threshold estimated at 6.3 Mev.

If we let N_1=single counting rate, position A; N_2=single counting rate, position B; N_3=coincidence counting rate, position A; N_4=coincidence counting rate, position B; N=number of disintegrations per minute; n=average number of gamma-rays per positron (exclusive of annihilation radiation); S_γ=average gamma-ray sensitivity of the counter including the solid angle; S_a=annihilation radiation sensitivity of counter; and K=a constant to be determined later (with the source in a vacuum, $K=1$), we can write the following equations for the counting rates:

$$N_1=NnS_\gamma+2NS_a, \tag{1a}$$

$$N_2=NnS_\gamma+KNS_a, \tag{1b}$$

$$N_3=NS_\gamma^2n(n-1)+4NnS_\gamma S_a, \tag{1c}$$

$$N_4=NS_\gamma^2n(n-1)+2KNnS_\gamma S_a. \tag{1d}$$

To determine K, separate measurements were made using a source of Zn^{63}. This element emits 2.3-Mev positrons (nearly the same positron energy as the 21-min. Mn^{52}) and no gamma-rays,

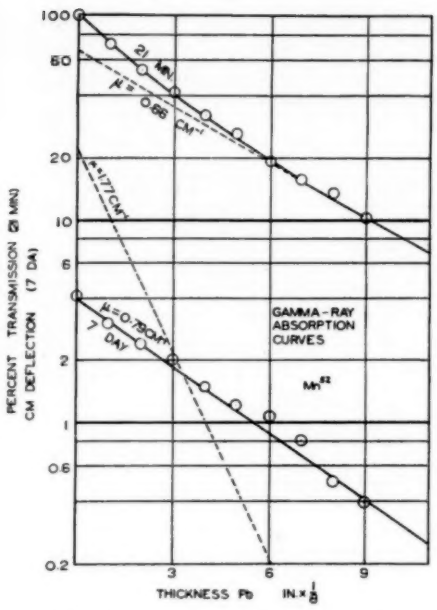

FIG. 7. Absorption curves in Pb of gamma-radiation from Mn^{52}, both isomers.

so that $n=0$. By measuring single counting rates in positions A and B we can solve Eqs. (1a) and (1b), obtaining $K=2N_2/N_1$. The result of such measurement is $K=1.06$.

We can now solve Eqs. (1) for n, N, S_a, S_γ. We are at present interested in the value of n:

$$n=\left[1-2\frac{2N_4-KN_3}{2N_2-KN_1}\cdot\frac{N_1-N_2}{N_3-N_4}\right]^{-1}.$$

In measuring N_1 and N_2 the background of the counters must be subtracted as well as the activity of the 6.5-day Mn^{52} present. The single counting rates of the two counters were nearly the same, and for N_1 and N_2 averages of the rates for the two counters were used. Actually, N_1 and N_2 could not be measured until the coincidence counting rates were too small to measure. In measuring N_3 and N_4 the procedure was to start with a sample which gave about 1000 coincidence counts per min. in position A. Coincidence decay curves in positions A and B were then plotted (with cosmic-ray background subtracted). Since N_1, N_2, and τ are known, the accidental counting rates are known, so one can calculate the true initial coincidence counting rates. The first part of the data (counting rate 1000 coincidences per min.) is useless, for these are mostly accidental coincidences. At best, the method does not yield data of high precision with a source which has a 21-min. period, for the interval of time in which coincidence counts can be made is too short. The data for 21-min. Mn^{52} are as follows:

$N_1=395500\pm120$ (counts/min.)
$N_2=305500\pm90$
$N_3=360\pm17$ (counts/min.)
$N_4=231\pm11$.

The fractional probable errors in N_1 and N_2 were computed in the usual way: 0.67 divided by the square root of the total number of counts. Since N_3 and N_4 are differences of measured and accidental coincidence rates, the probable error was computed for each measured point, and the values of N_3 and N_4 are means weighted according to the inverse square of the probable error. Using Eq. (2) we find $n=1.26\pm0.17$. This suggests that positron emission is followed sometimes by the emission of two 1.1-Mev gamma-rays, and at other times by one 2.2-Mev gamma. Presumably the high energy gamma-radiation is not very intense, for it did not show up at all in the absorption curve (Fig. 7). There is some further evidence for the higher energy gamma-rays in cloud-chamber pictures which show pair production by this radiation in a 2.5-mil Pb foil.

The 6.5-day isomer, which disintegrates 95 percent of the time by K capture, can be investigated by comparison of the ratios N_3/N_1 and

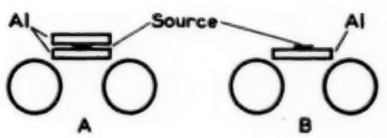

FIG. 8. Geometry of counters and source.

N_4/N_2 for the two isomers. Taking averages of the data for each isomer, we have

ISOMER	N_3/N_1	N_4/N_2
21-min.	$(10\pm0.5)\times10^{-4}$	$(7.5\pm0.3)\times10^{-4}$
6.5-day	$(3.5\pm0.08)\times10^{-4}$	$(2.9\pm0.1)\times10^{-4}$.

Thus the coincidence rate for this activity is less than half that for the short period activity. Remembering that in the 21-min. activity there are 3.3 gammas per disintegration (including annihilation radiation) and never more than 4, it appears that for the majority of 6.5-day dis-

integrations there are at most 2 gamma-rays. For disintegrations in which there is positron emission the energy available for gamma-radiation is 3.6 Mev. If some of this is the same as the 2.2-Mev radiation of the 21-min. isomer, the energy of the additional gamma-ray is 1.4 Mev. The lower absorption curve of Fig. 7 gives the energy of the 6.5-day gamma-radiation, as about 1 Mev. If there were only one gamma-ray of this energy per K capture, an implausibly large amount of energy would have to be assigned to the neutrino. It is more probable that there are two gammas per K capture, one of them being possibly of about 3.2-Mev energy.

VI. Yield

The initial activity of the 6-day isomer of 4.4 μC/μa is given in Section I. The initial activity due to positrons only is $0.75\times4.4=3.3$ μC/μa. If all the disintegrations were by positron emission the initial activity would be $3.3/0.05=66$ μC/μa. Using the calibration data of the ionization chamber, we get the yields for each isomer at 6.6-Mev proton energy:

21 min.	0.40×10^{-6}	radioactive atoms per proton
6.5 day	0.68×10^{-6}	radioactive atoms per proton.

VII.

The data on the two isomers of Mn^{52} are summarized in the following table:

Isomer	Disintegration	β^+ KE	Threshold	Yield
21.3-min.	β^+	2.2 Mev	6.2 Mev	0.40×10^{-6}
6.5-day	β^+ 5% K 95%	0.77		0.68×10^{-6}

The results of the gamma-ray measurements are somewhat uncertain, but all available data are consistent with the following possible scheme: the 21-min. isomer disintegrates with the emission of a positron followed by two 1.1-Mev gammas or one 2.2-Mev gamma. The 6.5-day isomer, disintegrating by positron emission emits 3.6 Mev of energy, probably in 3 quanta; disintegrating by K capture, it emits 4.2 Mev of radiation in two quanta, one of which must be about 1 Mev. An energy level diagram corresponding to this scheme is shown in Fig. 9.

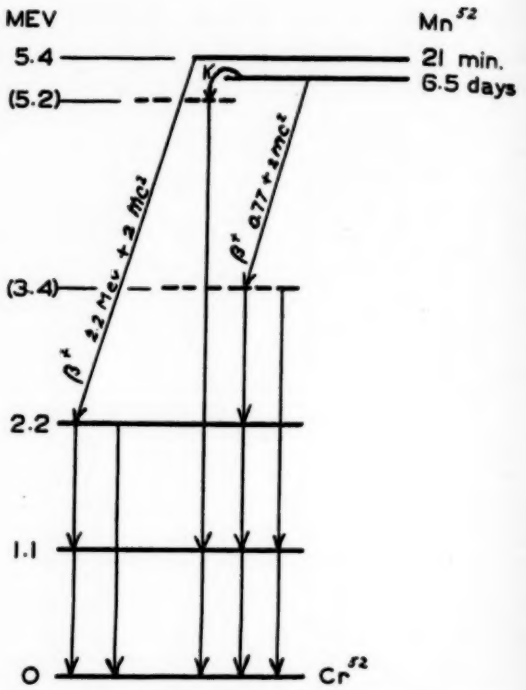

FIG. 9. Energy level diagram consistent with the information available on the isomers Mn^{52}. Uncertain values of energy are in parentheses.

In conclusion I wish to thank Professor L. A. DuBridge for making available laboratory facilities at the University of Rochester, and I am indebted to the whole staff at Rochester for their generous assistance, in particular Dr. S. N. Van Voorhis, Dr. S. W. Barnes and Dr. C. V. Strain. I wish also to thank Dr. L. M. Langer of Indiana University for many helpful discussions regarding the counter work.

Electrostatic Deflection Studies of Alpha-Particles; the Alphas from $Li^6(p,\alpha)He^3$

LEONARD C. MILLER
Ryerson Physical Laboratory, University of Chicago, Chicago, Illinois
(Received October 8, 1940)

A technique is described for studying nuclear reactions in which short range alpha-particles are produced with a yield that is too small for the direct application of the electrostatic deflector. In preliminary experiments a strong polonium source is used to supply alpha-particles to the deflector, and a group of these alphas, homogeneous in energy, passes through the deflector and enters a variable pressure absorption cell and ionization chamber. Cut-off pressures determined for various alpha-particle energies result in a calibrated cell which can then be used to determine the alpha-particle energies in nuclear disintegrations. Application of this method to $Li^6(p,\alpha)He^3$ results in a Q value of 3.94 ± 0.08 Mev. The calibration, extending in alpha-particle energy from 1 to 1.8 Mev, is also used to determine the slope of the range energy curve. The average value of the slope found for this region is 200 kv per mm range.

THE direct measurement of the energies of short range disintegration particles by deflection in an electrostatic field, introduced by Allison[1] and his group, is suitable for high yield reactions. For the study of reactions in which short range alpha-particles are produced, but where the yield is too small to apply the electrostatic deflector directly, the following technique has been devised. A variable pressure absorption cell, suitable for the particles, can be calibrated by using alpha-particles from a strong natural source. These particles are slowed down in air and then allowed to pass through the electrostatic deflector which measures their energies. This cell can then be used to determine the energies of short range alpha-particles, since the solid angle through which the cell will accept particles is much greater than that of the deflector.

This paper describes such a calibration and the application of the method to the alpha-particles from the disintegration of Li^6 by protons. The latter part of the paper shows how this calibration can be used to determine the slope of the range energy curve for alpha-particles in the energy region 1–1.8 Mev.

APPARATUS

The electrostatic deflector and its accompanying high voltage source have been described in previous papers[1,2] from this laboratory. The entrance slit to the deflector was 3 mm wide and 1.3 cm high, and was located 8.9 cm (the focal distance) from the edges of the cylindrical plates of the deflecting electrostatic field. These plates were spaced 0.635 cm apart and had an average radius of curvature of 25.400 cm. They subtended an angle of 90 degrees at their center of curvature and were 8.26 cm high. A collodion foil of 1.5 cm stopping power was placed over the entrance slit to seal up this end of the deflector.

A strong polonium source[3] deposited on silver, with cross section the same as that of the entrance slit, was mounted on a screw arrangement in front of the entrance slit. Movement of the source with respect to the slit changed the portion of the range of the alpha-particles expended in air.

Figure 1 shows the arrangement of the variable pressure absorption cell and ionization chamber which the particles entered after passing through the electrostatic deflector. The opening to the absorption cell, B, 3 mm by 2 cm, served as the exit slit of the electrostatic deflector. Over B was soldered a metal screen, 0.15 mm thick, with about 650 holes per square cm, each hole being about 0.2 mm in diameter. The screen was covered on the higher pressure side by a collodion window with an air equivalent of about 1.7 mm. The brass disk containing the opening B was seated accurately against shoulders on the cylin-

[1] S. K. Allison, L. S. Skaggs, and N. M. Smith, Jr., Phys. Rev. **54**, 171 (1938).
[2] L. S. Skaggs, Phys. Rev. **56**, 24 (1939).

[3] The author is indebted to Miss M. R. Jones of the Chemistry Department for preparing the strong RaD solution used.

drical body of the absorption cell. It was held in place by a collar and sealed by a rubber gasket. The construction was such that the length of the cell was independent of the tightness with which the screws were drawn up to make the seal. The opening A, 6 mm by 2.3 cm, was covered with a similar metal screen but with no collodion film. Thus the pressures in the ionization chamber and absorption cell were the same. The absorption cell had a measured depth of about 0.59 cm and the ionization chamber of about 0.45 cm. The collection voltage of 530 volts for the ionization chamber was applied to the outside brass case as indicated in the figure. The air admitted into the cell was freed of moisture and carbon dioxide by passage through tubes of calcium chloride and sodium hydroxide. Its temperature was measured by a thermometer whose bulb rested on the cell. The pressure was measured in an open tube mercury manometer. A correction was made for the temperature of the mercury. A volume of several liters was placed on the line to stabilize the pressure.

The linear amplifier used in this work was of the resistance-coupled type with a 954 acorn pentode in the first stage. The output of the amplifier was fed into a scale-of-sixteen circuit similar to that described by Stevenson and Getting.[4]

For the study of the Li^6 reaction the high voltage set used was the Cockcroft-Walton circuit described by Hatch.[5] The arrangement of the target chamber and absorption cell-ionization chamber unit was similar to that used in a previous study[6] of this reaction in this laboratory.

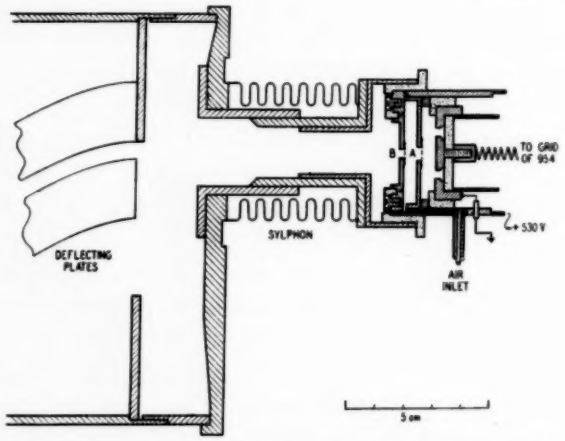

FIG. 1. Arrangement of the absorption cell and ionization chamber for taking number *vs.* pressure curves of particles which have passed through the electrostatic deflector. A pair of brass rods (not shown) keeps the sylphon extended when the deflector is evacuated.

CALIBRATION OF THE ABSORPTION CELL WITH THE ELECTROSTATIC DEFLECTOR

The performance of the variable pressure ionization chamber has been described in a previous communication from this laboratory.[6] In our work the bias on the counting circuit for the main calibration curve was 13 volts, and in a manner to be described later it was determined that a particle must produce about 4100 ion pairs in the ionization chamber in order to be counted. There is a critical operating pressure P_c above which the penetration into the chamber (in terms of air equivalent at standard conditions) required to produce a count should, theoretically, be independent of the pressure. P_c is the pressure at which the particle can produce the number of ions necessary for a count before it reaches the end of the chamber. The reason for the independence of pressure can be briefly stated as follows. The actual length of path of a particle before it loses its ionizing power is inversely proportional to the pressure whereas the specific ionization is directly proportional to the pressure.

The formula for the range of a particle as measured by the cell can be written

$$R=(L/76)(288P/T)+C, \qquad (1)$$

where L is the length of the absorption cell, T the absolute temperature and P the pressure. The first term represents that part of the range expended in the absorption cell, reduced to the standard conditions of 76 cm Hg pressure and 15°C. C represents the air equivalent of the collodion window, assumed to be constant, plus that of the penetration into the ionization chamber. This latter part, then, is also constant so long as the pressure is above P_c, which can be calculated from

$$N_0=\int_0^{D_c} I(x)dx.$$

Here N_0 is the number of ion pairs required to

[4] E. C. Stevenson and I. A. Getting, Rev. Sci. Inst. **8**, 414 (1937).

[5] G. T. Hatch, Phys. Rev. **54**, 165 (1938).

[6] G. J. Perlow, Phys. Rev. **58**, 218 (1940).

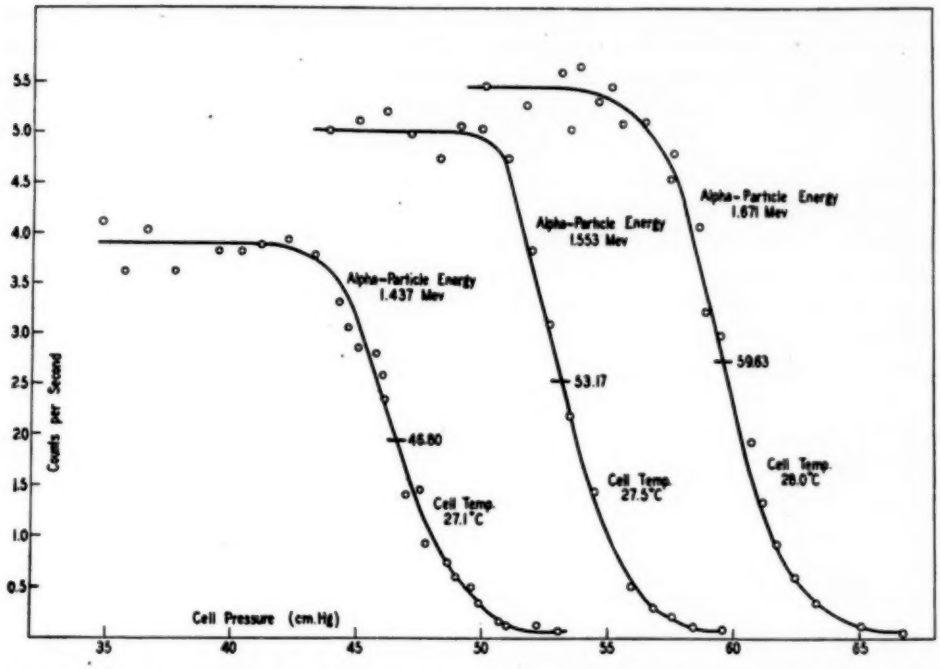

FIG. 2. Curves for determining cut-off pressure as a function of the energy of the alpha-particles.

produce a count, and is equal to 4100 for a 13-volt bias; $I(x)$ is the specific ionization function; $D_c=DP_c/76$ where D is the linear depth of the ionization chamber. If we use the curve of Holloway and Livingston[7] to represent the function $I(x)$ we find that $P_c=27.0$ cm Hg. For this calculation the maximum ordinate of the specific ionization curve has been set at 60,000 ion pairs per cm. Only those number-pressure curves which did not start to drop off until the cell pressure was above 27.0 cm Hg were used in this work.

The quantity N_0 was determined in the following way. A thin polonium source was placed so that its alpha-particles passed through the absorption compartment and entered the ionization chamber near the end of their range. The pressure was then lowered until rough observations with the oscilloscope and counting circuit indicated that the particles traversing the ionization compartment were producing approximately the critical number of ion pairs corresponding to the selected bias. With the pressure held at this value, the distance of the polonium source was readjusted until the pulses showed a maximum height. Then an accurate measurement of the cut-off bias was made by counting at this pressure and varying the bias to get a number bias curve. Such curves were taken at various pressures. Let the pressure associated with a given cut-off bias be P_0. If the linear depth of the ionization chamber is D, then its equivalent depth at P_0 is $D_0=P_0D/76$. The critical number of ion pairs N_0 corresponding to a given bias may then be found from

$$N_0=\left[\int_{\alpha}^{\alpha+D_0} I(x)dx\right]_{\max},$$

where α is to be chosen to give the greatest value for the integral.

Figure 2 shows a set of curves taken with the electrostatic deflector. Each curve was taken at a fixed voltage on the deflector plates, with the ordinates giving counts per second and abscissae the pressure in the cell as read off the manometer. The energy of the alpha-particles passing through the deflector is given[1] by $E=40.00V$ where V is the deflecting potential in volts. An end effect correction[8] equal to $-0.0093E$ must be added on to E. The dispersion is seen to be quite high,

[7] M. G. Holloway and M. S. Livingston, Phys. Rev. **54**, 18 (1938).

[8] S. K. Allison, L. S. Skaggs and N. M. Smith, Jr., Phys. Rev. **57**, 550 (1940).

a 100-kv energy change resulting in a pressure change of about 5 cm Hg. Most of the straggling is range straggling, with small contributions due to noise straggling and ionization straggling. The electrostatic deflector itself contributes a negligible amount, since calculations of its resolving power show[1] that with 3-mm slits the energy spread of the particles passing through it is of the order of 1 percent.

Since the particles leaving the deflector are essentially homogeneous in energy, these curves can be treated as ordinary number *vs.* range curves for a group of alpha-particles all of which have the same initial energy. In our case the pressure at half-maximum can be used as cut-off pressure for the particle of mean range in each group; the values, uncorrected for temperature, are indicated in Fig. 2. Curves for the same alpha-particle energy taken on different days showed variations in cut-off pressures, amounting in the extreme case to about 1.8 cm Hg. These variations were attributed to such factors as changes in the gain of the amplifier or in the constants of the scaling circuit.

Sets of curves were taken on eight different days. On all but two of these days one of the curves was for an alpha-particle energy equal to 1.437 Mev. The average value of 288 P/T, where P is the cut-off pressure and T the absolute temperature, for these curves was 44.72 cm Hg. On the assumption that the gain of the amplifier, constants of the scaling circuit, etc., might be different on different days but essentially constant during the course of one day's runs, all cut-off pressures for the 1.437-Mev curves were adjusted to 44.72 cm Hg, and the pressures for the other curves for each day's runs were shifted by an amount equal to the shift required in the 1.437-Mev curve of that day. Table I shows the unadjusted values when corrected for temperature and the adjusted values.

TABLE I. *Values of (288/T)P for various alpha-particle energies.*

α-Particle Energy (Mev)	Unadjusted Values of (288/T)P (cm Hg)	Adjusted Values
1.730	60.62	60.68
1.671	57.13	56.79
1.553	51.10, 51.05	50.42, 50.71
1.496	47.11*	47.50*
1.437	44.24,* 44.27, 45.40 45.06, 44.79, 44.06	44.72
1.379	40.74*	41.22*
1.333	37.51*, 39.31, 39.37	37.99*, 39.76, 38.69
1.205	33.62, 34.04, 33.62	34.07, 34.07, 32.94
1.086	28.65	28.68

* Old 954 tube.

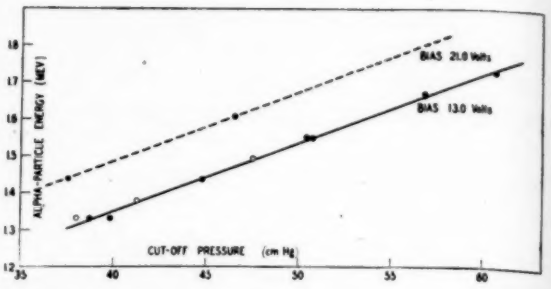

FIG. 3. Energy *vs.* cut-off pressure. The open circles represent points determined with the old 954 tube in the first stage of the amplifier.

Figure 3 shows a plot of energy *vs.* cut-off pressures. After the three points indicated by open circles were taken it was necessary to replace the 954 tube in the first stage. At this point the gain of the amplifier was adjusted so that the cut-off pressure for 1.437 Mev occurred at about the same point as with the old tube. No changes in the amplifier or in any other parts of the circuits were necessary after this. An examination of the cut-off pressures shows that the curve of Fig. 3 would not be altered essentially if the unadjusted points were used.

Use of Cell for Study of $Li^6(p,\alpha)He^3$

The absorption cell-ionization chamber device was placed opposite a thin target of lithium fluoride to detect the alpha-particles at right angles to the incident proton beam. The auxiliary apparatus, such as the amplifier and scaling circuit, was the same as that used in the calibration experiments. Moreover, care was taken to keep unchanged all the wiring connecting various circuits together, such as the leads from the output of the amplifier to the scaling circuit, etc., since changes in these might affect the operation of the circuits.

A metal disk with a 3-mm hole in the center was placed over the absorption cell slit; this opening and the target spot (5.4-mm diameter) served as the limiting aperture widths with a separation between them of 4.0 cm. The proton beam of about 5 microamperes was fed into a

current integrator. The bombarding voltage was 342 kv. This is rather close to the observed 330-kv resonance in F^{19}, but comparison of the curves obtained with those obtained in a previous study[6] of this reaction in this laboratory, made at a bombarding voltage of 370 kv, shows that the alpha-particles from fluorine were avoided. The curves obtained at 370 kv, which is farther above the 330-kv resonance, gave the same ratio of counts on the plateau to counts on the base line as that shown in our curves.

In order that the cut-off pressure should fall within the pressure range for which the cell was calibrated it was found necessary to raise the bias to 21.0 volts. Figure 4 shows a plot of the number of counts *vs.* pressure, the number of counts per point being about 220 on the plateau. The base line represents the long range alphas from Li^7 in addition to the He^3 particles and background noise. Though the points are somewhat scattered, the pressure at half-maximum is fairly well defined at 58.5 cm Hg. When corrected for temperature (28.9°C) this becomes 56.0 cm Hg.

In order to determine the energy corresponding to 56.0 cm Hg at 21.0-volt bias it was necessary to take more data with the electrostatic deflector. The energy *vs.* cut-off pressure curve at this higher bias should be parallel to the one at the lower bias, since it is only the value of C in Eq. (1) that is changed. To check this, two points were determined at the 21.0-volt bias, one with an alpha-particle energy equal to 1.437 Mev, the other 1.612 Mev. These are plotted in Fig. 3. It is seen that the line they determine is parallel to the 13.0-volt bias line. A check was also made at this time at the 13.0-volt bias, and a value of $288P/T$ of 44.03 was found for an energy of 1.437 Mev, which agrees within experimental error with the main curve. From Fig. 3 it is seen that at the higher bias a cut-off pressure of 56.0 cm Hg corresponds to an alpha-particle energy of 1.79 Mev. This gives a Q value for the reaction of 3.94 ± 0.08 Mev, the greatest part of the error resulting from the uncertainty in the cut-off pressure.

The result is in excellent agreement with the other[6] determination of this Q value reported from this laboratory. As pointed out in the report of the previous work this value gives greater consistency with various series of reactions than the previously accepted value, and can be used with other well-established Q values and masses to give a He^3 mass of 3.01688 ± 0.00011 mass units.

The present determination is independent of the slope of the range-energy curve and of the length of the absorption cell. Moreover, it does not depend on the Q value of the reaction $Be^9(p,\alpha)Li^6$ as does the previous determination. In a sense, then, the present work can be considered as a check on the beryllium reaction.

Application to Alpha-Particle Range-Energy Curve

The data of Table I can be used with Eq. (1) to give information about the alpha-particle range energy curve in this region. If L and C were known the curve could be determined absolutely. If only L is known the data can be used to give the slope of the range-energy curve. In those experiments[6] where energies are determined by comparison with particles of known energy, only the slope of the range-energy curve need be used.

In determining the proper value of L to use in the case where the pressure in the ionization chamber is variable, one is confronted with such unknown factors as the point at which the collecting field of the ionization chamber be-

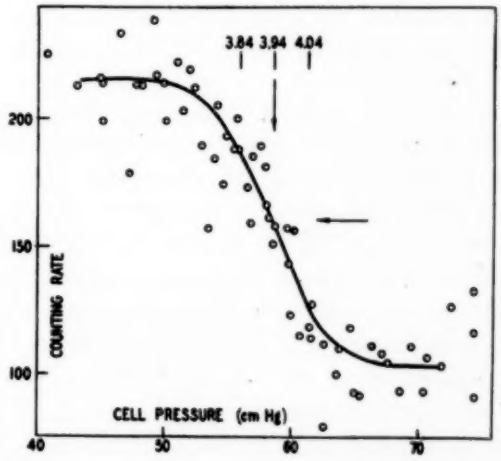

FIG. 4. Counts *vs.* pressure for alpha-particles from Li^6 (p, α) He^3. The base line represents the He^3 particles and the long range alphas from Li^7, plus the background. The horizontal arrow indicates the half-maximum. The lines and numbers at the top indicate where the half-maximum would have to occur to give the various Q values.

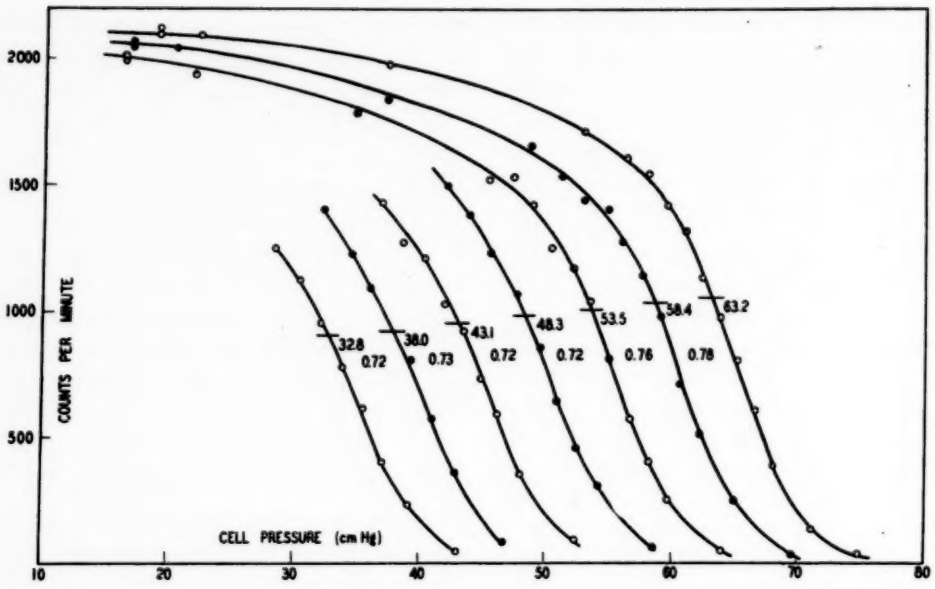

FIG. 5. Determination of the effective length of the absorption cell. The figures between the curves are the computed values of the cell length using adjacent curves. The other figures are cut-off pressures (pressures at half-maximum). Locations of plateaus for the four curves at the lower pressures were determined by solid angle calculations. An average value of effective cell length of 0.740 cm is indicated, with some evidence for a variation in cell length of about 3 percent over region of pressures used.

comes effective and the constancy of that point. In addition the variation in the recombination of ions at different pressures may be significant for such a device. There are also the usual uncertainties in determining the length of a short absorption cell such as the irregularities of the screens and the protruding of the collodion window through the screen apertures. Because of all these factors, the measured length (0.59 cm) of the absorption cell is only an approximation to the effective length.

The following method[6] was used to get the effective length of the cell. An auxiliary chamber was attached in front of the absorption cell and this chamber was kept evacuated. It was thus possible to reduce the pressure in the absorption cell below atmospheric without rupturing the absorption cell window. A thin polonium source, mounted on an accurate metric micrometer, was placed in front of this chamber (which had a front circular opening of one-half inch diameter sealed by a collodion window of 13-mm stopping power) along the axis of the absorption cell-ionization chamber device. A number-pressure curve was taken for a given position of the source. With a cut-off pressure of P at temperature T the range of the particles is given by

$$R=x(p/76)(288/T)+L(P/76)(288/T)+C, \quad (2)$$

where x is the length of path of the particles in air and p is the atmospheric pressure. For another position of the source, that is, for another value of x, we get another equation for R, since the range of the particles is the same. If C is assumed to be constant, the two equations can be solved for L. If p and T do not change between any two curves the value of L is independent of the absolute values of x but depends only on the difference of the x values, which can be accurately read on the micrometer. If p and T do change, the absolute values of x enter only in a small correction term.

Preliminary sets of such curves gave an average value of L of 0.74 cm. Since the discrepancy with the measured value was large the cell length determinations were repeated with a collodion film on the screen between the absorption cell and ionization chamber. This made it possible to keep the ionization-chamber pressure constant at atmospheric so that the device was being used in the conventional way. Two determinations were made under these conditions.

The values obtained were 0.61 cm and 0.60 cm, in good agreement with the measured length of 0.59 cm. These results were taken as evidence that with no window between the two compartments, part of the ionization chamber was effectively part of the absorption cell. Though the entire explanation for this is not known, it seems clear that the correct length to use for the electrostatic deflection experiments, in which the window was not present, is 0.74 cm.

A final set of curves to determine the cell length without a film on the ionization-chamber opening was taken. In these experiments the alpha-particle source on the micrometer screw was moved only one-half mm between curves, in an attempt to find out if the effective cell length varied with pressure. A study of this variation requires the use of curves whose cut-off pressures are close together. A difference in position of the alpha-particle source of one-half mm gives a difference in cut-off pressures of about 5 cm Hg. However, if one uses two such curves to compute the effective cell length, an error in the difference of cut-off pressures of only 3 mm would result in a 6 percent error in the cell length, that is, an error of about 0.04 cm. Since the difference in cut-off pressures for any two positions of the micrometer source is reproducible to within about 3 mm, this method can determine the variation of cell length to an accuracy of about 6 percent.

The set of curves is plotted in Fig. 5. The locations of the plateaus for the four curves at the lower pressures could not be determined experimentally, as they would occur at pressures much below the critical pressure P_c mentioned above, and the ionization chamber would not record all of the particles. These plateaus can, however, be calculated from solid angle considerations, since the number of counts on the plateaus for these experiments changes only because of the change in the solid angle which the opening to the absorption cell subtends at the source. The three plateaus that were determined experimentally checked these calculations. Though some of the points on these plateaus were taken at pressures slightly below P_c, the general appearance of the curves makes it certain that practically all of the counts were being recorded. The gradual decrease from the plateaus which the curves of Fig. 5 exhibit is characteristic of number-distance curves for ordinary thin sources. The effect appears exaggerated in Fig. 5 because of the scale used for abscissae; 10 cm Hg correspond to only about 1 mm distance in air at standard conditions.

The figure between any two curves indicates the cell length computed by using those curves. The average value of 0.74 cm for the cell length over the range of pressures used is substantiated. If the cell length is calculated by using the difference in cut-off pressures between the curve at the highest pressure and that at the lowest pressure, a 3-mm error in this pressure difference results in only a 1 percent error in cell length, that is, an error of less than 0.01 cm. This, then, is a measure of the accuracy with which the average effective cell length is known.

Though the accuracy with which this method can determine the variation in cell length is not high, there does seem to be an indication in Fig. 5 of a downward trend in the effective cell length as the pressure is lowered. A variation in this direction of about 3 percent for the range of pressures used in the electrostatic analyzer data was assumed. The data in Table I was

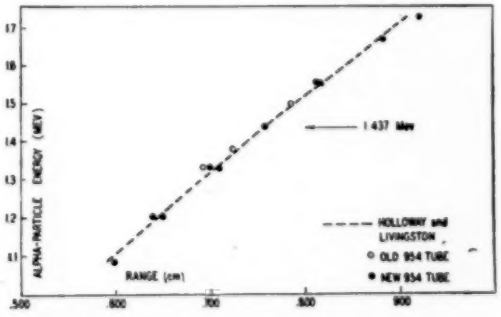

FIG. 6. Points on the range-energy curve in the region studied. The data were matched to the Cornell curve of Holloway and Livingston at 1.437-Mev energy.

used as follows. For pressures greater than 55 cm Hg L was set equal to 0.750 cm, for pressures between 35 and 55 cm a value of 0.740 cm was used for L, and for the two lowest pressures a value of 0.730 cm. An absolute range of 0.758 cm was assigned to the 1.437-Mev alphas, as determined from the latest Cornell[7] curve. This gives C a value of 0.323 cm. The results are plotted in Fig. 6. The points are seen to agree well with the curve of Holloway and Livingston. The spread

of the points is not serious, since the dispersion of the method is so high that the greatest spread corresponds to less than ± 0.01 cm in range. The chief uncertainty is in the value of L used. The results can be said to give an average value of the slope of the range-energy curve in this region of 200 kv per mm range to within 3 percent. This result is independent of the assumption made by Holloway and Livingston (who obtained the range-energy curve in this region by integrating their specific ionization curve) that the ratio between energy loss by ionization and by excitation is constant. Our result, then, is an indication of the validity of this assumption for this region.

The author is greatly indebted to Professor S. K. Allison for his very helpful supervision of this research. He wishes to thank also Dr. L. S. Skaggs and Dr. N. M. Smith, Jr., for their help in performing the experiments.

DECEMBER 1, 1940 PHYSICAL REVIEW VOLUME 58

The Velocity Spectrum of α-Particles

ROY RINGO
Ryerson Physical Laboratory, University of Chicago, Chicago Illinois
(Received September 18, 1940)

A 60° magnetic α-particle spectrograph has been constructed and used on a number of natural α-particle emitters, with photographic plates to detect the particles. The energy of the main group of protoactinium α-particles was found to be 5.053 ± 0.007 Mev. With the thinnest sources of Po, ThC, and ThC′ α-particles, as many as 10 percent of the particles were found to have energies 5 percent or more below the energy of the maximum of any one group.

1. INTRODUCTION

IT is desirable to determine the energy set free in nuclear transformations with the greatest possible precision. This can frequently be done by finding the energies of the charged particles produced in the transformations. The most satisfactory method of measuring the energy of these particles is by their deflection in electric or magnetic fields. The difficulties involved in producing large electric fields make their use less suitable than magnetic fields for the deflection of the heavy particles of mass 1 or more and of energy greater than 2 Mev. Focusing magnetic spectrographs, for measuring the energies of the natural α-particles, have been built by Rosenblum[1] and Rutherford, Wynn-Williams, Bowden and Lewis,[2] using the focusing properties of 180° deflection to increase intensities. Rosenblum, working with the large electromagnet of the Académie des Sciences at Bellvue, detected the α-particles by the blackening they produced on photographic plates. His spectrograph had some disadvantages. The magnet could not be moved, hence it could not be used on reactions produced by artificially accelerated high energy particles. The method also required very strong sources.

Rutherford and his group used an annular electromagnet and detected the particles in an ionization chamber connected to an amplifier and counter. Rays of different velocities were brought into the chamber by varying the magnetic field. The type of magnet used was limited to 180° deflections, this required the source and detector to be in the magnetic field. In addition the sensitivity of the detector was limited by the background counting rate produced by contamination and cosmic rays. These two limitations restricted the usefulness of the instrument mainly to α-particles from strong natural radioactive sources. The energies of all the α-particles from the natural radioactive elements with disintegration rates equal to or greater than that of radium, have been measured by these two instruments.

In this investigation a spectrograph was used which deflected the particles through 60° and which has the source and detector about 40 cm

[1] S. Rosenblum, J. de phys. et rad. [7] 1, 438 (1930).
[2] Rutherford, Wynn-Williams, Bowden and Lewis, Proc. Roy. Soc. A139, 617 (1933).

from the magnetic field. This follows a suggestion of Herzog[3] that the energies of α-particles could be measured conveniently by the use of such deflections. The α-particles are detected in this apparatus by means of a photographic plate in which the tracks made by the individual particles are found by microscopic examination. This method records every particle and has practically no uncertainty due to background. There is also the advantage that exposures of indefinite length can be taken, permitting the use of very weak sources.

2. Description of the Apparatus

The two core pieces of the magnet, on which the coils are wound, are 37 sq. in. in cross-sectional area and 9 in. high. The yoke is a hollow iron rectangle made of four pieces, $2\frac{1}{2}$ in.$\times$10 in. in cross section, providing a return path for the flux on both sides of the core and windings. The core pieces are mounted inside this rectangle one attached to the top piece and the other to the bottom. The pole pieces and the assembly which holds them in alignment, fit between the core pieces and are easily inserted and removed. The iron parts are all made from Armco Ingot forgings, chosen for their high saturation flux density.

The two pole pieces are trapezoids at the back surfaces ($8\frac{3}{8}$ in. and $12\frac{19}{32}$ in.$\times$3 in.) which fit against the core, and taper down to curving pole faces $1\frac{3}{16}$ in. wide, as indicated in Fig. 1. They are $2\frac{1}{8}$ in. high and tapered at an inclination of 45° to the pole face. Four columns set in holes in the pole pieces as shown in Fig. 1 keep them in alignment. The columns are steel below the surface of the pole pieces and brass above. They were pressed into their holes on the sloping sides of these pieces and the whole face side of each piece, including the tops of the columns, was ground off to the same level. The two pole pieces are clamped together by means of brass rods, threaded at both ends, running through the columns and held by steel nuts in holes countersunk in the back surfaces of these pole pieces.

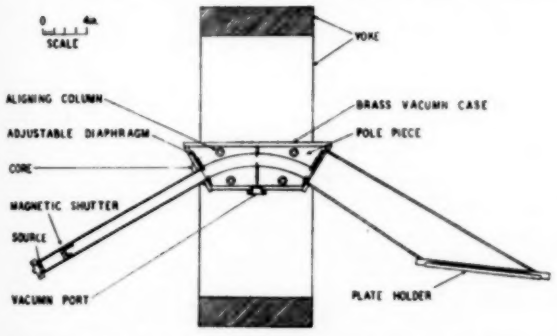

FIG. 1. A horizontal cross section through the spectrograph, taken at the level of the middle of the gap between the poles. The vacuum line and the magnet windings (on the core) are omitted.

[3] R. Herzog, Zeits. f. Physik 89, 447 (1934).

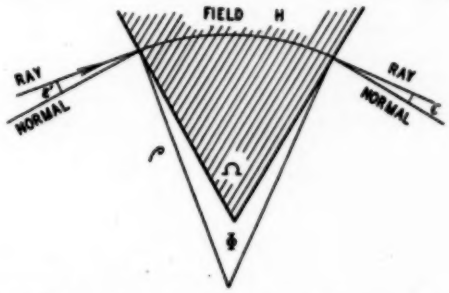

FIG. 2. The path of a charged particle through a magnetic field with the boundaries shown. The direction of the field is perpendicular to the plane of the paper.

The pole pieces are separated from each other by brass washers, $\frac{1}{8}$ in. thick, between their columns. This insures the pole faces being parallel and separated by a constant distance.

The windings consist of 1000 turns of No. 12 wire on each core piece, cooled by copper sheets between every other layer of the windings. This arrangement carries a current of 2 amp. with little heating after an hour's operation. This current was sufficient for the α-particles studied. A current as large as 8 amp. can be safely carried if a desk fan is turned on the coils.

The whole instrument weighs about 1200 pounds and is mounted on a truck so that it may be moved easily.

The magnet current was drawn from a 48-volt battery of lead cells. It was measured by a potentiometer and held constant, to within 1 part in 3000, by varying a rheostat in series with the magnet.

The source and plateholder were designed according to the equations for the focusing of ion beams given by Herzog.[3] The relation between the position of the source and the position of the focus for an ion beam with the central ray incident normally on, and emerging normally from the boundaries of a homogeneous magnetic,

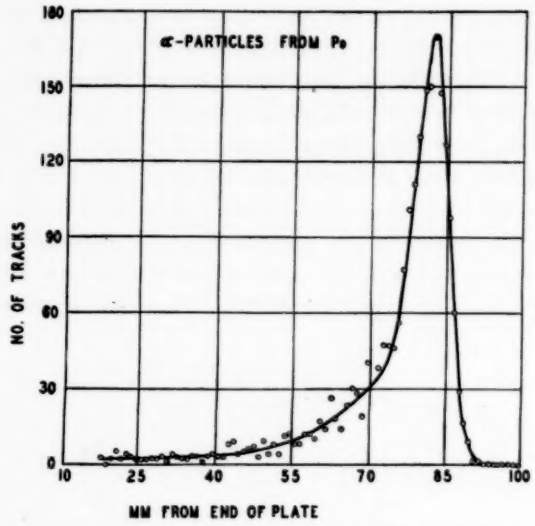

FIG. 3. The number of α-particles from the thicker Po source reaching 0.64 mm² of the plate, plotted against the distance from the low energy end of the plate. In the region of the maximum 1 cm change in position represents 1.5 percent change in energy. The exposure time was 1 hour.

field is

$$(l'-g')(l''-g'')=f^2, \tag{1}$$

where l' is the distance of the source, or object, from the edge of the field, l'' is the distance of the focus, or image, from the other edge, g' is the distance from the edge of the field to the focal point on the source side (i.e., the point where a parallel bundle of rays, incident normally to the edge of the field on the image side, should focus), and g'' is the corresponding distance on the image side. In this case $g'=g''=14.03$ cm and f is the focal length, the distance from the principal plane to the focal point, which for 60° deflection is $2g'$. For the case $l'=l''$, (1) gives $l'=42.09$ cm.

For a particle going through the field in a path whose radius of curvature ρ differs from that of the particles following the middle of the pole faces, the angular deflection and the focal position are different. For this more general case we have from Herzog's paper

$$g'=\rho\frac{\cos\epsilon'\cos(\Phi-\epsilon'')}{\sin\Omega}, \tag{2}$$

$$g''=\rho\frac{\cos\epsilon''\cos(\Phi-\epsilon')}{\sin\Omega}, \tag{3}$$

$$f=\rho\frac{\cos\epsilon'\cos\epsilon''}{\sin\Omega}. \tag{4}$$

Equation (1) holds also. The symbols have the meanings defined above or shown in Fig. 2.

In the instrument under discussion, with $\epsilon'=0$, the maximum radius of curvature of any path which will pass through the diaphragm at the exit from the field, when it is open 1 in., is 25.8 cm and the minimum is 22.9 cm. From this, and Eqs. (1)–(4), we have $l''=36.0$ cm and 51.9 cm in the two cases. By finding the direction of the ray by geometrical construction on a drawing of the pole face, and laying off l'' along it, one obtains the position of the focus for these extreme rays. The plateholder is designed so that the plate passes through the positions of the foci of the rays of maximum, middle and minimum radii.

The source mounting is 42.1 cm from the entrance to the magnetic field so that l' will equal l'' for the rays entering and leaving the field normally. The plateholder is in the position indicated in Fig. 1. It is set at an angle of 21° from the normal to the edge of the field. At this angle of incidence the α-particles leave tracks, each one of which is observed as a row of developed grains on the developed plate but which has sufficient depth to be distinguished from a surface scratch. Because a vacuum of 10^{-3} mm of mercury is sufficient, it is convenient to break the vacuum every time the plate is changed and no special equipment is used for inserting the plates.

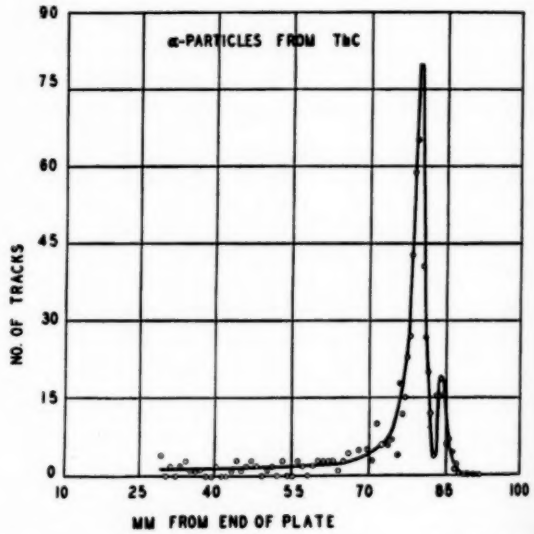

FIG. 4. The number of α-particles from a ThC source on 1 mm² of the plate, plotted against the distance from the low energy end of the plate.

A vacuum good enough to remove the danger of change of charge of the particles during passage through the magnetic field is all that is needed, for scattering is unimportant with such energetic particles. At a pressure of 10^{-3} mm the mean free path for the gain of an electron is 10^5 cm, and for loss of an electron by He^+ particles, which are present in the radiation from even thin natural radioactive sources to the extent of one percent, the mean free path is 10^4 cm.[4] Either process thus is quite unlikely in the 26 cm of path in the field.

The photographic detection of the particles follows a technique recommended by Wilkins.[5] The plates used were Eastman α-particle plates 1 in.$\times$8 in., which were developed 4 min. 30 sec. at 18°C in Eastman x-ray developer. The plates were then cut into three pieces after the separation of fiducial marks on each piece was measured, and examined in a microscope using 450$\times$ magnification and bright field illumination. The distribution of α-particles over the plate is found by counting the number of α-particle tracks in a definite vertical range as the plate is moved along horizontally.

3. Preliminary Observations

The behavior of the spectrograph was first studied with α-particles from polonium and thorium C. The distribution of α-particle tracks after an exposure of one hour to a polonium source, is shown in Fig. 3. The source was a silver wire, 0.3 mm in diameter, which had been dipped in a radium D solution in which polonium was growing. This source emitted 6.7×10^5 α-particles per sec. in all directions. The graph shows the horizontal position on the plate as abscissa and the number of tracks observed in a strip 2 mm high and 0.32 mm wide, at that position as ordinate. Figure 4 shows the number on a strip 3 mm high from a thorium C source emitting approximately 7×10^4 particles per sec. in all directions. The exposure time was two hours. The ThC source was prepared by collecting the active deposit of thoron produced by some radiothorium, on a charged platinum wire 0.2 mm in diameter.

In Fig. 4, the two lines photographed by Rosenblum[1] and referred to as α_0 and α_1, are seen to be separated. The two very faint lines recorded in his photographs, α_2 and α_3, do not show up, probably because of insufficient exposure. Many tracks of particles with velocities less than those of the two main groups appear. Similar tracks of low velocity particles from Po are seen in Fig. 3. These would not have been expected from the clear backgrounds shown in Rosenblum's photographs and their origin will be discussed in Section 6.

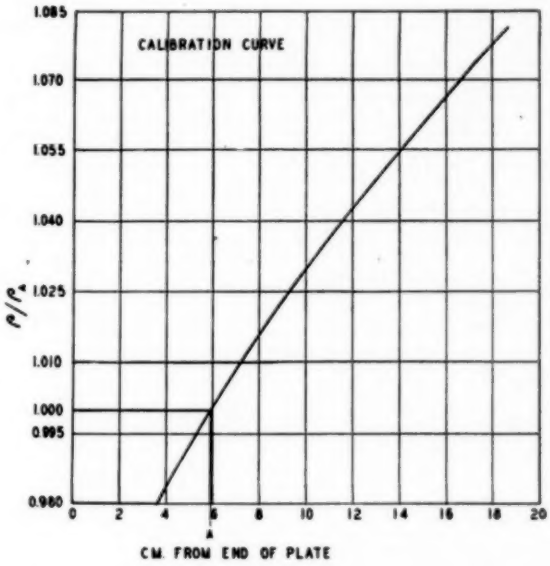

Fig. 5. The ratio of the radius of curvature in the magnetic field, corresponding to a point s on the plate, to the radius of curvature of the particles arriving at A, plotted against the distance from the low energy end of the plate, s. This ratio is equal to the ratio of the momenta of the particles arriving at s to those arriving at A. A is arbitrarily chosen as the point at which the Po α-particles happened to fall on a plate used in drawing the curve.

4. Calibration of the Spectrograph

The strength of the magnetic field was measured by a method of Ellis and Skinner,[6] which was modified slightly. The charge produced by removing a small search coil from the field was balanced against that produced in a search coil in a long solenoid when the current in the solenoid is interrupted. A ballistic galvanometer was used for the balance. The results obtained by this method were checked by measurements of the $H\rho$ of α-particles of known energy. The results from these two methods of the measure-

[4] E. Rutherford, Phil. Mag. **47**, 277 (1924).
[5] T. R. Wilkins, J. App. Phys. **11**, 35 (1940).
[6] C. D. Ellis and H. W. B. Skinner, Proc. Roy. Soc. **A105**, 60 (1924).

ments of H agree within the probable error, which was about two percent, because of stray fields, lack of precision in measuring the angle of deflection and variation in the magnetic field corresponding to one setting of the magnet current. It was found that a current of 1.5 amp. produced a field of 11,900 oersteds between the pole faces, 3 amp. a field of 21,600 oersteds, and 6 amp. one of 25,000 oersteds, at which current the iron was nearly saturated. With a field of 25,000 oersteds, α-particles of energy as large as 19.5 Mev could be brought on the plate.

The dispersion, defined as the separation of particles differing one percent in momentum, was obtained by measuring the distribution of particles from several natural radioactive elements, Po, ThC, ThC′, and RaC′. A wire coated with Po and one coated with the thorium-active deposit were mounted together in the source position and the separation of the α-particle groups measured. The ThC α-particles ($E=6.086$ Mev, $H\rho=3.532\times10^5$) were 103.5 mm from the Po particles ($E=5.303$ Mev,[2] $H\rho=3.302\times10^5$). Hence the average dispersion is 15.3 mm for a one-percent change in momentum.

To each point on the plate, distant S from one end, corresponds a definite radius of curvature (ρ) in the magnetic field. Thus if we plot a curve of the position, S, of tracks of several groups of α-particles of known energy, for some one value, H, of the field, against $K\rho$ for these particles, where K is an arbitrary constant, we may read off the curve, for any two points on the plate, the ratio of the ρ's corresponding to the α-particles that caused the tracks appearing at those two points. Since the momentum of a particle is proportional to ρ, this ratio is also the ratio of the momentum of the two α-particle groups. Such a curve is given in Fig. 5. The ordinate is the ratio $\rho/\rho_A=K\rho$ and the abscissa, the distance S along the plate, A is arbitrarily chosen as the point at which the Po α-particles happened to fall on one exposure.

Two points on the curve in Fig. 5 are given by the results with ThC and Po mentioned above, and the slopes at various points, which are inversely proportional to the dispersions at these points, are given by the separation of the two main groups of the ThC α-particles. The slope is found to be 1.5 times as large at the position of

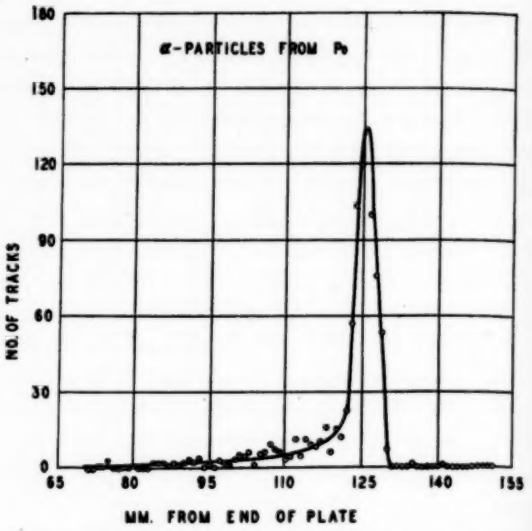

FIG. 6. The number of α-particle tracks from the thinner Po source on 0.64 mm² of the plate, plotted against the distance from the low energy end of the plate. Exposure time was 4 hours.

the Po α-particle tracks as at the position of the most intense ThC α-particle group on the plate on which both are recorded. From these data, the calibration curve which is not far from a straight line, can be drawn as shown in Fig. 5.

In Herzog's theory,[3] the dispersion, D, is given by

$$D=\frac{\rho}{100}\left(1+\frac{f}{l'-g'}\right)$$

($=2\rho/100$ in our case). However this is dispersion in a direction perpendicular to the beam; to get the dispersion along the plate, it is necessary to divide by the sine of the angle between the plate and the beam, 21°. This gives $D=13.6$ mm for one percent change in momentum at the position on the plate where the beam leaving the field normally strikes, that is 8 cm from the left-hand, or low energy end of the plate. This is very near the measured value of 13.7 mm.

In using the calibration curve it is assumed that the dispersion is independent of the absolute value of the field. This is true if the stray field does not change too much in proportion to the field proper as the latter is changed. In this spectrograph with a gap of $\frac{1}{8}$ in. between the pole faces and operating well below the point of saturation of the iron, the change in dispersion due to stray field is negligible. This was checked by the results obtained with ThC′ and RaC′

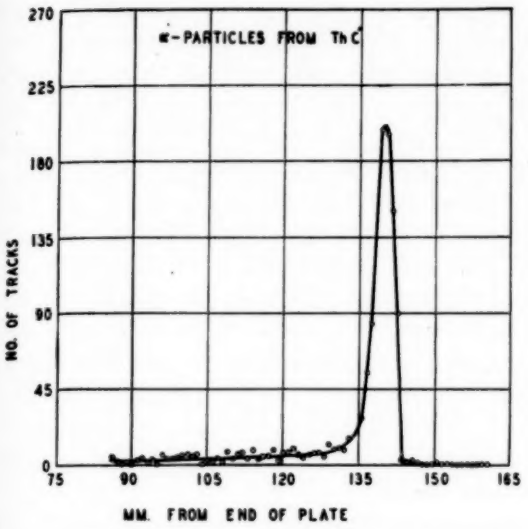

FIG. 7. The number of α-particle tracks from a ThC′ source on 0.64 mm² of the plate plotted against the distance from the low energy end of the plate. Exposure time was 4 hours.

α-particle sources together in the spectrograph. The ThC′ α-particles ($E=8.778$ Mev[2]) reached the plate 15.05 cm from the low energy end and the RaC′ α-particles ($E=7.683$ Mev[2]) 4.96 cm from that end. These values fit the calibration curve.

The resolution obtained so far, is at best barely equal to that theoretically expected with the width of sources used. The width of the lines is in theory[7] equal to $\rho\beta^2 \sin \frac{1}{2}\Phi$ where β is the angle between the normal from the source to the boundary of the field and the path deviating the most from that, which still passes through the diaphragms in the field. The width comes out to be 0.2 mm. This width could not be attained because of the width of the sources, which, being over 0.3 mm, gives images over 1 mm wide. Some lines were obtained whose width at $\frac{1}{2}$ of their maximum was 1 mm. These give a resolution (equal to the dispersion×100/line width) of 1300, but most lines were much broader, probably because of absorption of energy in the source for some particles, and unsteadiness of the magnetic field, which, on the long exposures taken with the thinnest sources, varied by more than 1 part in 1000. For the immediate purpose of calibration and for many measurements this broadening of the lines is not a serious disadvantage however.

[7] W. E. Stephens, Phys. Rev. **45**, 513 (1934).

The fraction of the total of emitted α-particles which gets through this spectrograph at the maximum usable field width of 2 cm, is 1 out of 70,000. This compares with 1 out of 20,000 detected in Rutherford's magnet[2] with a diaphragm 3 cm×1 cm. The theoretical and attained resolutions of Rutherford's magnet were slightly larger than those of this magnet.

5. Energy of the Protoactinium α-Particles

Because of the method of detection employed, this instrument can be used to measure the α-particles from quite weak sources. One such source whose α-particles were measured was a preparation of protoactinium, kindly lent by Dr. A. V. Grosse. It contained seven percent Pa_2O_5 mixed with zirconium and hafnium oxides. A source which emitted 1200 particles per sec. was prepared by depositing this material on a platinum strip 1 mm×5 mm in area. The value for the high energy limit of the α-particles from Pa obtained by comparison with the α-particles from Po, put in the spectrograph at the same time, was 5.053 ± 0.007 Mev. This is to be compared with a value 5.063 Mev, found by using the Pa α-particle range, 3.673 cm, and the Po α-particle range, 3.925 cm, in air at 15 C and 760 mm pressure, given by Geiger,[8] the slope of the Cornell University range-energy curve[9] in this region, and the value 5.303 Mev for the energy of the Po α-particles[2] used with the data from the spectrograph.

The thickness of material necessary to obtain a source of the strength used, caused such a broadening of the line by retardation of the particles in the source that nothing could be told of any possible fine structure. This illustrates an inherent limitation of the apparatus when used on weak or impure radioactive materials.

6. Low Energy α-Particles

In addition to the widening of the peak of the α-particle lines observed, and ascribed in part to loss of energy in escaping from the source, many α-particles of much lower energies are observed (cf. Fig. 4). These have been observed before by

[8] H. Geiger, Zeits. f. Physik **8**, 45 (1921).
[9] M. G. Holloway and M. S. Livingston, Phys. Rev. **54**, 18 (1938).

I. Curie[10] and J. Schintlmeister,[11] and are noticeable on curves published by Rutherford.[2] The results in earlier work were all obtained with sources 100 or more times as thick as the comparable sources used in this work and were generally ascribed to absorption in the sources. The results obtained with this spectrograph are shown in Figs. 3, 6 and 7. The density of deposit on the source producing the spectrum shown in Fig. 3, was 9.93×10^{-8} g per cm^2, equivalent in stopping power to 5.3×10^{-4} mm of air. Figure 6 shows the distribution of α-particles from a Po α-particle source of density 5.29×10^{-9} g per cm^2 or 2.8×10^{-5} mm air equivalent, deposited on a flat strip of silver 1 mm$\times$5 mm$\times$0.1 mm. Figure 7 shows the distribution of particles from a ThC′ α-particle source of 0.5×10^{-11} g per cm^2, deposited on a similar platinum strip.

The Po sources were prepared by precipitation on silver from a RaD solution whose only contamination was believed to be inactive lead. The ThC′ was prepared as was the ThC source described previously (Section 3). The sources all appeared clean when first prepared and used but darkened later, presumably because of oxidation resulting from ionization by radiations from the radioactive materials.

In the case of the thinner Po α-particle source 2.6 percent of the particles were retarded by an amount equivalent to 200 to 300 kev, for the other Po α-particle source, 4.3 percent, and for the ThC′ α-particles, 4.0 percent. To retard the particles by an amount equivalent to 250 kev a path in air approximately 1.8 mm long is required. This means a layer of air 5×10^5 atoms deep or $\frac{1}{10}$ as many atoms of the radio-elements if the ordinary free paths for the α-particles are assumed. Assuming a very favorable case for the absorption in the radioactive material, that it is all concentrated in a small area and forms a cone with base diameter equal to the altitude, we find that such a cone, high enough to account for the retardation observed, would contain 3 times as much material as there is Po on the stronger Po source, 50 times the amount on the other Po source and 5000 times the amount of thorium-active deposit present on the ThC′ α-particle source.

[10] I. Curie, Ann. de physique **3**, 299 (1925).
[11] J. Schintlmeister, Sitz. d. Akad. Wien, Abt. 2a **146**, 389 (1937).

The possibility that the active material might have deposited in clumps, was tested as follows. For a short time, the sources were placed in contact with a photographic plate which was protected from infection by the radioactive material by a thin sheet of collodion. The plate was then developed and examined under a microscope. The α-particle tracks were found to be quite uniformly distributed in the case of the Po; no centers were observed. In the case of the ThC many distinct clusters were seen while more than $\frac{3}{4}$ of the area touched showed very few tracks. However the total amount present here is so small that these clusters, by the argument of the preceding paragraph, cannot account for the retardation observed.

Because the retardation does not depend much on the average density of deposit, an increase of 20 times in the density of Po increased the fraction retarded only 60 percent, and because there are hardly enough atoms present in the most favorable case to account for the retardation observed, it is believed that absorption in the source cannot be held responsible for these low energy particles.

Scattering, on the pole faces, or in air, is excluded as a source of these particles, as it should also cause an appreciable number to appear on the high energy side of the peak, by the alteration in direction it causes, and this region is remarkably free of tracks. However, as a precaution against scattering the pole faces had been coated with Aquadag, and diaphragms inserted, which collimated the beam vertically as well as horizontally, so that the number of particles reaching the pole faces was reduced.

If absorption in the source is also excluded as an explanation of these low energy particles, these experiments then show that there is present among the α-particles of homogeneous velocity, a considerable number, leaving the radioactive atoms, or at most small groups of such atoms, with a continuous distribution of energies going down as low as ten percent below the energy of the high energy limit, or lower. This number may include ten percent of the total number of particles in energy ranges five percent below the maximum.

In conclusion the author wishes to express his gratitude for the advice and guidance of Dr. A. J. Dempster, who suggested this problem.

Note on a Possible Scheme for the Assignment and Prediction of Radioactive Periods

G. R. DICKSON AND E. J. KONOPINSKI
Indiana University, Bloomington, Indiana

(Received October 15, 1940)

Families of odd nuclei differing from each other only by α-units show some evidences of a certain type of regularity in their stability against β-processes. The assumption that a similar regularity holds for all such families permits the unique assignment to the correct isotope of many known radioactive periods and the prediction of many yet unknown lifetimes.

BY assuming the existence of certain regularities among the half-lives of the radioactive nuclei as functions of their atomic numbers, the assignment of discovered half-lives to the proper isotopes may be helped and the periods of yet unknown isotopes may be estimated. The existence of such regularities might be expected because of the well-known regularities among the energies of nuclei, if a unique correspondence between life and energy release could be assumed. Such a uniqueness is, of course, actually destroyed by the possibility of "allowed" and "forbidden" transitions. However, one can hope that the nuclei chosen for comparison with each other (henceforth referred to as a "family") will behave so similarly toward such disturbing factors as to result in a dependence on atomic number smooth enough to be useful. The approach is almost entirely empirical; the known half-lives of a family are compared and whatever regularity is found is extrapolated to predictions about unknown and uncertain members.

The criterion we have adopted for the formation of a family is that the members differ only in the number of α-units (of two protons and two neutrons each) they contain. We have chosen this in preference to other possible criteria[1] because of the fact that the occurrence and even the abundance of the stable isotopes shows great similarity for alternating values of the atomic number, Z, throughout the periodic table and makes promising the extensibility of the scheme even to the heaviest nuclei. It also has as a result that the stable isotopes of each family follow each other consecutively as Z increases.[2] The finite lifetimes of the family should then be expected to fall off smoothly as Z increases or decreases from its stable values.

Our specific procedure was to plot the logarithms of the known half-lives against their atomic numbers. Results are shown in the figure for several families for which the data are most abundant. The families are distinguished by such symbols as $(3e)$ and $(5o)$, in which the number represents the neutron excess (isotopic number) while the letters "e" and "o" denote families with even and odd Z, respectively. The plots show some evidence of the expected behavior, especially among the positron emitters (nuclei with a *larger* than stable Z) of the families $(-1e)$, $(-1o)$, $(7e)$ and among the negatron emitters of $(3e)$. All these are families of odd nuclei. All the families of even nuclei without exception display extreme irregularity, even at the beginning of the periodic table as is demonstrated by the family $(0o)$ in the diagram. We must, therefore, at the outset confine our method to the odd nuclei. The completely random behavior of the even nuclei serves only to make the few definite evidences of regularity among the odd isotopes appear less accidental.

The diagram shows not only the families of odd nuclei giving the best agreement with our expectations but also those containing the most numerous exceptions to the expected behavior. In the case of every such exception, some question concerning the experimental evidence can be raised, as is shown in the following paragraphs.

[1] Our scheme is consistent with Professor E. Wigner's treatment (Phys. Rev. **51**, 106 (1937)) of nuclei differing by four particles as having the same multiplet structure in a first approximation. This may help in maintaining a similarity of behavior with regard to "forbidden" transitions.

[2] This also is true to a large extent of nuclei differing only by one neutron and one proton, but exceptions are frequent (e.g. $I=1$, 3, etc.,). Moreover, whatever advantage the argument of footnote 1 gives would be lost under this criterion.

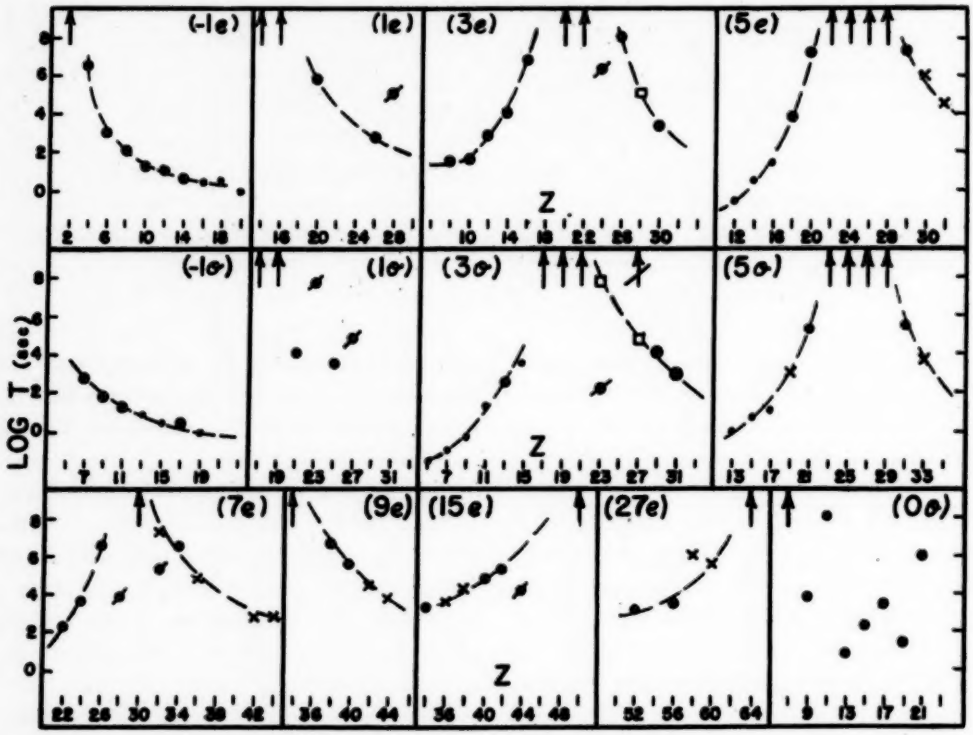

FIG. 1. Logarithms of half-lives, T, as functions of atomic number Z for several families, as denoted by symbols such as $(-1e)$ (i.e. $I=-1$, Z even. To get mass number, double Z and add I). Most of the data are from Livingood and Seaborg's summary (see footnote to Table I). The upward arrows (↑) denote stable isotopes. The full circles (●) represent the best established radioactive isotopes, of classes A and B according to Livingood and Seaborg. The crosses (×) denote isotopes not previously definitely assigned. The assignments best agreeing with our scheme were chosen for these cases (see Table I). The small dots (·) represent estimates from Barkas' masses (Phys. Rev. 55, 691 (1940)) with the assumption that the transition is "allowed." A diagonal dash through a point signifies that the datum has been put in doubt from the standpoint of our scheme as discussed in the text. The squares are new assignments of some of the newly doubted isotopes. The dashed curves were used in making the predictions of Table II. Cr^{55}, of the family $(7e)$, was originally predicted to have a 2- to 3-hour period on the basis of this scheme; the subsequent verification was done at our laboratory by McDaniel and Dickson (Phys. Rev. 57, 351 (1940)) and also by others (Amaki, Iimori and Sugimoto, Phys. Rev. 57, 752 (1940)).

The final decisions must, of course, be left to experimental test.

(1e).—The activity assigned to Ni^{57} fits better in the family $(3e)$ as Ni^{59}. Only the failure to observe it in neutron capture by Ni^{58} seems to have prevented the latter assignment; a low capture cross section may be responsible instead.

(1o) and (3o).—Co^{57} is one of only three exceptions to the rule that stable members of a family follow each other consecutively when ordered according to Z.[3] This makes it desirable to verify further its mass-spectrographic observation,[4] especially since its isobar Fe^{57} is stable. Moreover, the supporting evidence offered by Sampson, Ridenour and Bleakney,[5] that the two negatron periods which arise in Co through neutron capture must be due to *two* stable isotopes, seems now to be nullified. Co^{58} produced in several other ways emits positrons with a totally different period. The existence of Co^{57} as a target of transmutations has, therefore, not yet been proved.

Only the supposition that Co^{57} is stable has prevented the assignment to it of the activity presently given to Co^{58}; the transfer would help the agreement in both the

[3] A second exception is the rare isotope, Rh^{101}, isobaric with Ru^{101}. Only the finding that Ma^{97} is stable would help this case. The third exception among the odd nuclei is due to the absence of Ce^{141} from the stable nuclei of family $(25e)$. This rare earth isotope may yet turn up when the mass-spectrographic investigation of Ce is pushed to the accuracy usual in other parts of the periodic table. A similar exception exists in family $(13o)$ due to the near-stable isotope Rb^{87}. Only the rather farfetched assumption that this long period is isomeric to a much faster decay from the ground state seems able to make it consistent with our scheme. There may be some support for this in the fact that Sr^{87}, which differs from Rb^{87} only in that a proton replaces a neutron, has isomeric states.

[4] M. B. Sampson and W. Bleakney, Phys. Rev. 50, 732 (1936).

[5] Sampson, Ridenour, and Bleakney, Phys. Rev. 50, 382 (1936).

TABLE I. *New or confirmed assignments of known periods.*[1]

ASSIGNMENT	PERIOD	FORMERLY
K^{43}	18 min.	$K^{42,44}$
Ge^{69}	6–10 days	$Ge^{69,71}$
Ge^{71}	195 days	$Ge^{67,69,71}$
Ge^{71*}	37 hr.	Ge^{71}
As^{71}	88 min.	$As^{71,73}$
Se^{81}	19 min.	$Se^{79,81}$
Kr^{79}	~1 day	$Kr^{79,81}$
Rb^{81}	42 min.	$Rb^{79,81,83,(87)}$
Rb^{83}	200 hr.	$Rb^{79,81,83,(87)}$
Sr^{85*}	70 min.	Sr^{85}
Sr^{91}	6 hr.	Class *D*
Zr^{97}	6 min.	Class *F*
Mo^{91}	17 min.	$Mo^{91,93}$
Ru^{97}	90 min.	Class *E*
Ag^{107*}	40 sec.	$Ag^{107,109*}$
Sn^{123}	40 min.	Class *D*
Xe^{133}	9.4 hr.	Class *D*
Er^{169}	12 hr.	$Er^{169,171}$
Er^{171}	7 min.	$Er^{169,171}$
Os^{191}	40 hr.	$Os^{191,193}$
Hg^{203}	25 hr.	$Hg^{203,205}$

[1] See J. J. Livingood and G. T. Seaborg, Rev. Mod. Phys. **12**, 30 (1940).

(3*o*) and (1*o*) families. The agreement would become complete if, further, the activity which has been tentatively assigned to V^{47} were to be attributed to the ground state decay of V^{49} instead. The possibility of this isomerism was recognized by its observers.[6]

(3e) and (7e).—On the basis of our scheme, the ground-state decay of Cr^{51} is expected to be too slow to be easily observed (a period of some decades). That the far shorter period actually observed may be from an isomeric state is supported by the appearance of a highly converted half-million-volt gamma-ray with it. A similar explanation seems also necessary for the too short Ni^{63} period in family (7*e*).

[6] Walke, Williams and Evans, Proc. Roy. Soc. **A171**, 360 (1939). *Note added in proof.*—In agreement with our conclusion is L. A. Turner, Phys. Rev. **58**, 679 (1940).

For most of the families not shown or specifically discussed, the data are not sufficient to make a decision about the validity of our scheme. In four of these families (19*e*, 25*o*, 25*e*, 37*e*) there occur pairs of well established nuclei which in no case conflict with our scheme.

In Table I are listed assignments of known, but previously unassigned, activities made to agree with our assumptions. Table II contains estimates of yet unknown half-lives as obtained from extrapolations and interpolations along curves such as those shown in Fig. 1. Both tables contain values having varying degrees of certainty, depending on the amount of data available concerning the corresponding families. More assignments and predictions will be possible as more information becomes available.

TABLE II. *Approximate half-lives predicted for yet unknown isotopes.*

ISOTOPE	PERIOD	ISOTOPE	PERIOD	ISOTOPE	PERIOD
B^{13}	0.01 sec.	Ca^{39}	1 sec.	Kr^{77}	1 hr.
C^{15}	20 sec.	Ca^{47}	10 sec.	Kr^{81}	10 yr.
N^{17}	0.1 sec.	Ti^{45}	5 hr.	43^{97}	∞
F^{21}	0.5 sec.	Cr^{49}	1 hr.	Ru^{103}	1 min.
Na^{25}	20 sec.	Cr^{51}	20–200 yr.	Ru^{107}	10 sec.
Mg^{29}	0.5 sec.	Mn^{53}	1 min.	Pd^{101}	1 hr.
Al^{25}	10 sec.	Co^{57}	20 hr.	Pd^{113}	1–60 min.
Al^{31}	1 sec.	Ni^{57}	2 min.	Cd^{121}	3 min.
Si^{33}	5 sec.	Ni^{59}	30 hr.	In^{133}	30 min.
P^{29}	5 sec.	Ni^{63}	20 yr.	Sn^{127}	10–50 min.
P^{33}	10 hr.	Cu^{59}	20 min.	Te^{135}	<20 sec.
P^{35}	5 sec.	Zn^{61}	1 min.	Cs^{135}	3 yr.
S^{31}	2 sec.	Ge^{67}	2 min.	Ba^{143}	< 2 min.
S^{37}	10 sec.	Ge^{79}	20 min.	Ce^{141}	∞
Cl^{39}	1 min.	As^{69}	2 min.	Sm^{151}	> 1 yr.
A^{35}	1 sec.	Se^{85}	1 min.	Gd^{161}	40 min.
K^{37}	1 sec.	Br^{75}	5 min.	Os^{195}	2 min.
K^{45}	<20 min.				

Mesons in a Coulomb Field

IG. TAMM
P. N. Lebedev Physical Institute, Academy of Sciences of the USSR, Moscow, USSR

(Received August 18, 1940)

THE theory of charged mesons of spin 1 leads in its present form to divergent or otherwise unreasonable results not only in the majority of nuclear problems, but also in the treatment of the interaction of mesons with the electromagnetic field. The simplest instance is the scattering of mesons by a point charge. Massey and Corben[1] and Oppenheimer, Snyder and Serber[2] have shown that in the Born approximation the cross section for this scattering does not decrease with the energy E of the meson, if $E \gg \mu c^2$, but tends to a finite limit. Still one could hope that the exact solution of the problem would lead to a reasonable result. However, this is not the case.

The meson wave function has 6 independent components which correspond to the components of the vector potential and of the electric intensity of the electromagnetic field. Let us investigate the stationary solutions ($\Psi \sim e^{i\omega t}$) of the Proca equations in a central field of force for $\hbar|\omega| > \mu c^2$ (unbound states). The complete set of these solutions consists of three independent eigenfunctions for any given set of values of ω, j and m, such that $|m| \leq j$ and $j \geq 1$ (for $j=0$ there is only one eigenfunction). Here $j\hbar$ denotes the total angular momentum of the meson and $m\hbar$ its projection on the Z axis. The three eigenfunctions correspond to three possible orientations of the spin s of the meson with respect to its orbital momentum l. However s and l are not constants of the motion: One of the eigenfunctions is of the form

$$\Psi_\lambda = f_\lambda^0(r) \cdot Y_j^{m_\lambda}(\theta, \varphi) \cdot e^{i\omega t}, \quad \lambda = 1, 2 \cdots 6, \quad (1)$$

where $m_\lambda = m$ or $m_\lambda = m \pm 1$, while two others are of the form

$$\psi_\lambda = \{f_\lambda^+(r) \cdot Y_{j+1}^{m_\lambda}(\theta, \varphi) + f_\lambda^-(r)\, Y_{j-1}^{m_\lambda}(\theta, \varphi)\} e^{i\omega t}, \quad (2)$$

where f_λ^+ and f_λ^- are not independent of one another.

If the potential energy $V(r)$ of the meson has no singularity at $r=0$ and if $j \geq 1$, then for fixed ω, j and m there is one regular eigenfunction of the type (1) and two of the type (2). However, in the field of a point charge $e'V = ee'/r$ there is again one regular eigenfunction of the type (1), but the solutions of the equations for f_λ^+ and f_λ^- are of the form:

$$f_\lambda^\pm \sim r^{-7/4} \cdot e^{2\eta\sqrt{s}},$$

where

$$s = \frac{[j(j+1)]^{\frac{1}{2}}}{\mu c^2} \cdot \frac{ee'}{r} \quad \text{and} \quad \eta = 1^{\frac{1}{2}},$$

i.e., $\eta = \pm 1$ or $\eta = \pm i$. Not two, but only one of these four solutions is finite at $r=0$; the three others lead to an infinite value of the energy $E = \int \psi^* H \psi \cdot d\tau$ of the meson.[3]

Thus the regular solutions of the Proca equations in a field of a point charge do not form a complete set of functions and the problem of the Coulomb scattering of mesons has no solution.

The reason for this breakdown of the theory may be sought in the neglect of the finite size of elementary particles. If that is the case, the Coulomb scattering of mesons with energies $E \gtrsim \hbar c/r_0$ must substantially depend on the size r_0 of elementary particles. This will also be true for the bremstrahlung and probably also for the production by mesons of fast β-electrons. Thus the estimates of the cross sections for these processes based on the results of the Born approximation cannot be valid for $E \gtrsim \hbar c/r_0$.

We hope to discuss in a further note some further consequences of the peculiar behavior of mesons in a Coulomb field (in particular the bound states of the mesons).

The present note is a summary of a part of a paper which will appear in the *Journal of Physics*, edited by the Academy of Sciences of the USSR.

[1] H. F. W. Massey and H. C. Corben, Proc. Camb. Phil. Soc. **35**, 463 (1939).
[2] J. R. Oppenheimer, H. Snyder and R. Serber, Phys. Rev. **57**, 75 (1940).

[3] If one calculates the charge density ρ of mesons with the help of the least objectionable nonregular solutions ($\eta = \pm i$) one finds that in the neighborhood of the point charge $e'\rho \sim r^{-5/2}$ and that the sign of ρ is uniquely determined by the sign of e' and is opposite to it. This means, that if e.g. $e' > 0$ an infalling negative meson may be caught by e' in a spiral orbit, whereas an infalling positive meson produces pairs, the negative components of which are caught by e'.

The Electromagnetic Properties of Mesotrons

H. C. CORBEN* AND JULIAN SCHWINGER†
Department of Physics, University of California, Berkeley, California
(Received June 27, 1940)

A general theory describing particles of unit spin and arbitrary magnetic moment is developed and applied to the motion of such particles in a Coulomb field. In the particular case of magnetic moment unity (Proca theory), the exact equations for the radial components of the wave functions possess regular solutions only for those states ($j=l\neq 0$ and $j=0$, $l=1$) in which the orbital angular momentum l is a constant of the motion. For particles possessing a magnetic moment of two mesotron magnetons, the radial equations are free of singularities for all states but two: $j=1$, $l=0$ and $j=0$, $l=1$. The cross section for a fractional energy transfer to electrons by energetic mesotrons is calculated for the various simple possibilities of mesotron spin σ (0, $\frac{1}{2}$, 1) and magnetic moment μ (arbitrary except for zero spin), and it is shown that only for $\sigma=\frac{1}{2}$, $\mu\neq 1$ (in particular, $\mu=0$) and $\sigma=1$, $\mu=1$ is the cross section of the correct magnitude and form (i.e., essentially independent of the mesotron energy) to account for observed burst phenomena at energies greater than 2×10^{10} ev. Criteria for the validity of these formulae indicate that the region of applicability for the theory $\sigma=1$, $\mu\neq 1$ is more limited than that for $\sigma=1$, $\mu=1$ (Proca).

I. INTRODUCTION

THE electromagnetic properties of nuclear systems depend on the interaction of mesotrons both with heavy particles and with the electromagnetic field. Indeed, so simple a quantity as the magnetic moment of the neutron is completely determined only by both of these interactions. Data obtained experimentally from electromagnetic nuclear properties do not therefore determine independently the mesotron-heavy particle coupling and the mesotron-radiation interaction, and it would be of advantage to study each of these forms of interaction directly. Information concerning the influence of the electromagnetic field on mesotrons may be obtained by the investigation of recoil electrons resulting from collisions with the mesotrons forming the penetrating component of cosmic radiation. This process presumably accounts for the fraction of the soft component (apart from secondaries arising from the disintegration of mesotrons in the atmosphere) which is in equilibrium with the hard component. The observed dependence of cosmic-ray bursts on their magnitude and the surrounding material indicates that mesotrons may, with appreciable probability, transfer a large fraction of their energy to the soft component. Phenomena associated with bursts of energy greater than 2×10^{10} ev may be adequately described by assuming that the cross section for a given fractional transfer of energy to the soft component is independent of the mesotron energy. A cross section of this nature possessing the correct magnitude would indeed be obtained[1,2] if the electromagnetic properties of the mesotron were those deduced from the Proca equations[3] by the application of the Born approximation.

To examine the validity of the Born approximation, one may consider the limiting case of scattering by an electron of infinite mass, the process involved then being the scattering of mesotrons by a static Coulomb field. An exact solution of this problem would enable one to judge the reliability of the Born approximation as applied to this type of process. Unfortunately, as will be shown in Section III, when one attempts to follow this program one encounters singular equations which admit of no complete set of regular solutions. This implies either that the theory is wrong or that the model of the scattering of a mesotron by a Coulomb field is too great an abstraction of the physical process to which it purports to approximate.

* Commonwealth Fund Fellow.
† National Research Fellow.

[1] Oppenheimer, Serber and Snyder, Phys. Rev. **57**, 75 (1940).
[2] H. S. W. Massey and H. C. Corben, Proc. Camb. Phil. Soc. **35**, 463 (1939).
[3] A. Proca, J. de phys. et rad. **7**, 347 (1936); N. Kemmer, Proc. Roy. Soc. **A166**, 127 (1938).

The electromagnetic properties of a particle with given charge and mass are essentially determined by its spin and its magnetic moment. One may therefore use the experimental evidence available from cosmic-ray measurements to determine these two characteristics of the mesotron. Of the three simple possibilities for the spin (0, $\frac{1}{2}$, 1) the case of zero spin may be excluded, for the impossibility of associating an intrinsic magnetic moment with a scalar mesotron implies an energy transfer cross section varying inversely with the mesotron energy, thus contradicting the experimental evidence. Were the spin of the mesotron $\frac{1}{2}$, one could exclude the possibility of a magnetic moment of one mesotron magneton, as predicted by the Dirac theory, for this would lead to a cross section of similar character.[4] However, an alteration of the magnetic moment changes the energy dependence of the cross section to that demanded by experiment. On the basis of cosmic-ray evidence, therefore, one cannot exclude the possibility of a mesotron of spin $\frac{1}{2}$ and magnetic moment different from unity (in particular, zero) although such evidence as is available from nuclear phenomena indicates that this is not likely.

The current theory of mesotrons postulates a spin of unity and a magnetic moment of one mesotron magneton. The physical adequacy and the mathematical difficulties of this theory have already been mentioned. The sole remaining simple possibility is that of a mesotron of spin unity and magnetic moment different from that assumed in the Proca theory. The following pages are devoted to the development of a general Lagrangian theory of such particles (Section II) and the application of the theory to the motion of mesotrons in a Coulomb field (Section III) and the problem of electron recoils (Section IV).

II. General Theory

The most general bilinear Lagrangian density which involves only a four-vector ϕ_μ, and the electromagnetic potentials A_ν in the form of the first-order gauge covariant derivative

$$D_\nu\phi_\mu=[\partial_\nu+(ie/\hbar c)A_\nu]\phi_\mu,$$

together with the conjugate complex quantities $\bar{\phi}_\mu$, $\bar{D}_\nu\bar{\phi}_\mu$ is

$$L=A^{\mu\nu}_{\sigma\tau}(\bar{D}_\mu\bar{\phi}^\sigma)(D_\nu\phi^\tau)+\kappa^2\bar{\phi}^\sigma\phi_\sigma, \tag{1}$$

a quantity which automatically satisfies the condition of gauge invariance. Here the $A^{\mu\nu}_{\sigma\tau}$ are numerical tensors which can depend only on the values of the metric

$$\begin{aligned} g_{\mu\nu}&=0 \quad (\mu\neq\nu),\\ &=1 \quad (\mu=\nu=1,2,3),\\ &=-1 \quad (\mu=\nu=4). \end{aligned}$$

A general form of such a tensor is

$$A^{\mu\nu}_{\sigma\tau}=g^{\mu\nu}g_{\sigma\tau}+\beta g^{\mu}_{\tau}g^{\nu}_{\sigma}+\gamma g^{\mu}_{\sigma}g^{\nu}_{\tau}, \tag{2}$$

where β and γ are constants. The choice of unity for the first coefficient on the right-hand side of (2) is not an essential limitation. To guarantee the reality of L, one must impose the condition

$$\bar{A}^{\mu\nu}_{\sigma\tau}=A^{\nu\mu}_{\tau\sigma} \tag{3}$$

which implies that β and γ are real.

The equations of motion derived by variation of (1) are

$$A^{\mu\nu}_{\sigma\tau}D_\mu D_\nu\phi^\tau=\kappa^2\phi_\sigma \tag{4}$$

and the conjugate complex equations. Inserting the form (2) for the $A^{\mu\nu}_{\sigma\tau}$ one obtains

$$D^\mu D_\mu\phi_\sigma+\beta D_\nu D_\sigma\phi^\nu+\gamma D_\sigma D_\nu\phi^\nu=\kappa^2\phi_\sigma$$

or

$$\begin{aligned} D^\mu D_\mu\phi_\sigma+(\beta+\gamma)D_\sigma(D_\nu\phi^\nu)&\\ +(ie/\hbar c)\beta\phi^\nu H_{\nu\sigma}=\kappa^2\phi_\sigma,& \end{aligned} \tag{5}$$

where we have used the commutation relation

$$D_\mu D_\nu-D_\nu D_\mu=(ie/\hbar c)H_{\mu\nu}$$

and the $H_{\mu\nu}$ are the strengths of the electromagnetic field.

Specializing Eqs. (5) to the field-free case one obtains

$$\partial^\mu\partial_\mu\phi_\sigma+(\beta+\gamma)\partial_\sigma(\partial_\nu\phi^\nu)=\kappa^2\phi_\sigma. \tag{6}$$

Solutions of these equations may be written in the form

$$\phi_\sigma=\psi_\sigma+\partial_\sigma\varphi,$$

where ψ^σ satisfies the condition $\partial_\sigma\psi^\sigma=0$ and φ

[4] H. J. Bhabha, Proc. Roy. Soc. **A164**, 257 (1938).

is a scalar. Hence

$$(\partial^\mu\partial_\mu-\kappa^2)\psi_\sigma=0;\quad(\beta+\gamma+1)\partial^\mu\partial_\mu\varphi=\kappa^2\varphi. \tag{7}$$

Writing $\kappa=Mc/\hbar$ we may identify the first of Eqs. (7) as that satisfied by a particle of spin unity and mass M, and the second as that of a scalar particle of mass $M(\beta+\gamma+1)^{-\frac{1}{2}}$. One therefore has a theory of a particle which may exist in two states, with which are associated different spins and different masses. The theory may be restricted to particles of spin 1 by the choice

$$\beta+\gamma+1=0, \tag{8}$$

which implies $\varphi=0$. Were this restriction not imposed, there would be a finite probability for a particle to change its mass and spin in an external electromagnetic field, a phenomenon for which there is no experimental evidence.

With this restriction, the coefficients assume the form

$$A^{\mu\nu}_{\sigma\tau}=(g^{\mu\nu}g_{\sigma\tau}-g^{\mu\ \nu}_{\tau}g_{\sigma})+\gamma(g^{\mu\ \nu}_{\sigma}g_{\tau}-g^{\mu\ \nu}_{\tau}g_{\sigma}), \tag{9}$$

to which corresponds the Lagrangian density

$$L=\tfrac{1}{2}\bar{F}_{\mu\nu}F^{\mu\nu}+\kappa^2\bar{\phi}_\mu\phi^\mu+\gamma\{(\bar{D}_\mu\bar{\phi}^\mu)(D_\nu\phi^\nu)-(\bar{D}_\nu\bar{\phi}^\mu)(D_\mu\phi^\nu)\}, \tag{10}$$

where $F_{\mu\nu}=D_\mu\phi_\nu-D_\nu\phi_\mu$. This Lagrangian may be simplified by noting that the expression in brackets may be rewritten

$$-\partial_\mu(\bar{\phi}^\mu D_\nu\phi^\nu)+\partial_\mu(\bar{\phi}^\mu D_\nu\phi^\nu)-(ie/2\hbar c)H_{\mu\nu}(\bar{\phi}^\mu\phi^\nu-\bar{\phi}^\nu\phi^\mu). \tag{11}$$

The first two terms of (11) may be disregarded, for, possessing the form of divergences, they contribute nothing to the variation of the Lagrangian. We have therefore arrived at a convenient expression for the Lagrangian density,

$$L=\tfrac{1}{2}\bar{F}_{\mu\nu}F^{\mu\nu}+\kappa^2\bar{\phi}_\mu\phi^\mu-(ie/2\hbar c)\gamma H_{\mu\nu}(\bar{\phi}^\mu\phi^\nu-\bar{\phi}^\nu\phi^\mu), \tag{12}$$

which differs from that of current theory by the addition of a term involving the explicit appearance of the electromagnetic field strengths. This term may be interpreted as corresponding to an additional magnetic moment for the mesotron.

The linear equations of motion which follow from (12) are

$$D^\mu F_{\mu\nu}=\kappa^2\phi_\nu+(ie/\hbar c)\gamma\phi^\mu H_{\mu\nu};\quad D_\mu\phi_\nu-D_\nu\phi_\mu=F_{\mu\nu}. \tag{13}$$

The electromagnetic current four-vector of the mesotrons which follows by variation of the Lagrangian with respect to $-A_\mu$ then assumes the form

$$j^\mu=(ie/\hbar c)[\bar{\phi}_\nu F^{\mu\nu}-\bar{F}^{\mu\nu}\phi_\nu+\gamma\partial_\nu(\bar{\phi}^\mu\phi^\nu-\bar{\phi}^\nu\phi^\mu)], \tag{14}$$

which differs from that of the usual theory by the term in γ which is independently conserved. To show the interpretation of this additional term, we rewrite the expression for the current in the form

$$j^\mu=(ie/\hbar c)[(\bar{\phi}_\nu D^\mu\phi^\nu-\phi_\nu\bar{D}^\mu\bar{\phi}^\nu)+(\gamma+1)\partial_\nu(\bar{\phi}^\mu\phi^\nu-\bar{\phi}^\nu\phi^\mu)+\phi^\mu(\bar{D}_\nu\bar{\phi}^\nu)-\bar{\phi}^\mu(D_\nu\phi^\nu)]. \tag{15}$$

The second term represents a polarization current arising from the magnetic moment. Indeed, its coefficient is to be identified as the magnetic moment of the mesotron, which thus has on this theory the value $1+\gamma$ mesotron magnetons. The first term has the appearance of a convection current yet may not receive this interpretation for it is not by itself conserved. It is, in fact, conserved only upon the addition of the terms involving $D_\mu\phi^\mu$—terms which have no simple physical interpretation. The importance of the proposed generalization now becomes apparent, for, by proper choice of γ these terms may be made to vanish under certain conditions.

One may evaluate $D_\nu\phi^\nu$ by applying the operator D_ν to the first of Eqs. (13), with the result

$$\kappa^2D_\nu\phi^\nu=(ie/2\hbar c)(\gamma-1)H_{\mu\nu}F^{\mu\nu}-(4\pi ie/\hbar c^2)\gamma J_\nu\phi^\nu, \tag{16}$$

where J_ν, the current-vector of the external charges, has been introduced by means of the equation

$$\partial^\mu H_{\mu\nu}=-(4\pi/c)J_\nu.$$

Thus in regions outside those occupied by the external charges (i.e., $J_\nu=0$) the choice $\gamma=1$ implies $D_\nu\phi^\nu=0$. It would then appear that the choice of $\gamma=1$, which in the absence of external charges guarantees the subdivision of the current into independently conserved conduction and convection currents and imparts to the particle a gyromagnetic ratio of 2, places the theory in close analogy with the Dirac theory of the electron.

This simplification finds its counterpart in the equations of motion

$$D^\mu D_\mu\phi_\nu - D_\nu(D_\mu\phi^\mu) = \kappa^2\phi_\nu + (ie/\hbar c)(\gamma+1)\phi^\mu H_{\mu\nu}, \tag{17}$$

which are obtained from (5) by writing $\beta=-(\gamma+1)$. In comparison with the rather complicated equations of the current theory ($\gamma=0$) *viz.*:

$$(D^\mu D_\mu-\kappa^2)\phi_\nu = (ie/\hbar c)\phi^\mu H_{\mu\nu} - (ie/2hc)(1/\kappa^2)D_\nu(H_{\mu\sigma}F^{\mu\sigma}) \tag{18}$$

one obtains, for $\gamma=1$,

$$(D^\mu D_\mu-\kappa^2)\phi_\nu = (2ie/hc)\phi^\mu H_{\mu\nu} - (4\pi ie/hc^2\kappa^2)D_\nu(J_\mu\phi^\mu), \tag{19}$$

which in regions external to charge and current distributions reduce to

$$(D^\mu D_\mu-\kappa^2)\phi_\nu = (2ie/\hbar c)\phi^\mu H_{\mu\nu}. \tag{20}$$

To complete the theory, it is necessary to construct the stress-energy-momentum tensor and show that it satisfies all conditions that may be reasonably imposed on it. The real tensor constructed by the recipe

$$T^\mu{}_\nu = 2\{(\partial L/\partial\bar{F}_{\mu\sigma})\bar{D}_\nu\bar{\phi}_\sigma + (\partial L/\partial F_{\mu\sigma})D_\nu\phi_\sigma + (\partial L/\partial H_{\mu\sigma})H_{\nu\sigma}\} - \delta_\nu{}^\mu L \tag{21}$$

satisfies the conservation equation

$$\partial_\mu T^\mu{}_\nu = -j^\mu H_{\mu\nu} \tag{22}$$

and thus may be interpreted as a stress tensor. For the Lagrangian (12), it assumes the explicit form:

$$T_{\mu\nu} = F_{\mu\sigma}\bar{D}_\nu\bar{\phi}^\sigma + \bar{F}_{\mu\sigma}D_\nu\phi^\sigma - (ie/\hbar c)\gamma H_{\nu\sigma}(\bar{\phi}_\mu\phi^\sigma - \bar{\phi}^\sigma\phi_\mu) - g_{\mu\nu}L. \tag{23}$$

In order to guarantee the conservation of angular momentum it is necessary that a theory yield a symmetric stress tensor. Although (23) is not symmetric, it may be replaced by the symmetric tensor[5]

$$\Theta_{\mu\nu} = \bar{F}_{\mu\sigma}F_\nu{}^\sigma + \bar{F}_{\nu\sigma}F_\mu{}^\sigma + \kappa^2(\bar{\phi}_\mu\phi_\nu + \bar{\phi}_\nu\phi_\mu) + (ie/\hbar c)\gamma\{H_{\sigma\mu}(\bar{\phi}_\nu\phi^\sigma - \bar{\phi}^\sigma\phi_\nu) + H_{\sigma\nu}(\bar{\phi}_\mu\phi^\sigma - \bar{\phi}^\sigma\phi_\mu)\} - g_{\mu\nu}L, \tag{24}$$

which also satisfies the conservation equation

$$\partial_\mu\Theta^\mu{}_\nu = -j^\mu H_{\mu\nu}$$

since

$$\Theta^\mu{}_\nu = T^\mu{}_\nu - \partial_\sigma\{F^{\mu\sigma}\bar{\phi}_\nu + \bar{F}^{\mu\sigma}\phi_\nu\}. \tag{25}$$

Although the energy density derived from this stress tensor is not positive definite, it does become so in the absence of an external electromagnetic field, which is all that may reasonably be required of the energy density derived from a theory of particles with integral spin.

III. Stationary States in a Coulomb Field

The importance of a rigorous treatment of the equations representing the mesotron in a Coulomb field has been stressed in the Introduction. An attempt to construct exact solutions of these equations forms the basis of this section.

The spherical symmetry of the Coulomb problem introduces the possibility of defining conserved

[5] This symmetric tensor may be also derived directly from the Lagrangian by the prescription

$$\Theta^\mu{}_\nu = 2\{(\partial L/\partial\bar{F}_{\mu\sigma})\bar{F}_{\nu\sigma} + (\partial L/\partial\bar{\phi}_\mu)\phi_\nu + (\partial L/\partial F_{\mu\sigma})F_{\nu\sigma} + (\partial L/\partial\phi_\mu)\phi_\nu + (\partial L/\partial H_{\mu\sigma})H_{\nu\sigma}\} - \delta_\nu{}^\mu L.$$

angular momentum integrals. Appropriate definitions, in terms of the stress tensor $\Theta_{\mu\nu}$ are:

$$M_{jk}=\frac{1}{c^2}\int(x_j\Theta_{k4}-x_k\Theta_{j4})d\tau, \tag{26}$$

which, by employing the definition (24) of $\Theta_{\mu\nu}$ may be written

$$M_{jk}=(i/c^2)\int\{\bar{F}_{4l}(-i)(x_j\partial_k-x_k\partial_j)\phi^l-F_{4l}\,i(x_j\partial_k-x_k\partial_j)\bar{\phi}^l\}d\tau$$
$$+(i/c^2)\int\{(-i)(\bar{F}_{4j}\phi_k-\bar{F}_{4k}\phi_j)-i(F_{4j}\bar{\phi}_k-F_{4k}\bar{\phi}_j)\}d\tau. \tag{27}$$

The first term, with its associated operator

$$L_{jk}=-i(x_j\partial_k-x_k\partial_j)$$

is obviously to be interpreted as the orbital angular momentum, thus endowing the additional term with the properties of spin angular momentum. The operator representing the total angular momentum may therefore be defined by the equation

$$J_{jk}\phi^l=L_{jk}\phi^l-i(\delta_j{}^l\delta_{km}-\delta_k{}^l\delta_{jm})\phi^m, \tag{28}$$

from which one infers the operational definition of J^2, the square of the total angular momentum, *viz.*:

$$J^2\phi_l=(L^2+2)\phi_l-2iL_{lj}\phi^j. \tag{29}$$

To express these formulae in a more amenable form, we may introduce space-vector notation, representing the space-components of ϕ^μ by the vector $\mathbf{\Phi}$ and the time-component ϕ^4 by the scalar function $i\varphi$. The angular momentum definitions thus assume the guise of vector formulae:

$$J_z\mathbf{\Phi}=L_z\mathbf{\Phi}+i\mathbf{e}_z\times\mathbf{\Phi},\quad\text{etc.},\quad J^2\mathbf{\Phi}=(L^2+2)\mathbf{\Phi}+2i\mathbf{L}\times\mathbf{\Phi}, \tag{30}$$

wherein $\mathbf{e}_z$ denotes a unit vector in the z direction. The analogous definitions involving operations on the scalar φ are simply

$$J_z\varphi=L_z\varphi;\quad J^2\varphi=L^2\varphi. \tag{31}$$

Stationary states of the system may be characterized by m and $j(j+1)$, the proper values of J_z and J^2, respectively, and by the parity, the eigenvalue of the reflection operator R which is defined by

$$R\mathbf{\Phi}(\mathbf{r})=\mathbf{\Phi}(-\mathbf{r});\quad R\varphi(\mathbf{r})=-\varphi(-\mathbf{r}). \tag{32}$$

This latter equation is a consequence of the opposite behavior of vector and scalar functions under spatial reflection. The construction of stationary state wave functions is facilitated by the consideration of auxiliary $\mathbf{\Phi}$-functions which are also eigenfunctions of L^2 associated with the proper value $l(l+1)$. By virtue of Eq. (30), such auxiliary wave functions satisfy the condition:

$$(j(j+1)-l(l+1)-2)\mathbf{\Phi}=2i(\mathbf{L}\times\mathbf{\Phi}). \tag{33}$$

The detailed consideration of this equation is deferred to the Appendix, wherein it is shown that there exist three types of auxiliary $\mathbf{\Phi}$-functions which may be symbolically expressed in the form:

$$\begin{aligned} &l=j: && \mathbf{\Phi}=\mathbf{L}F(r)P_j{}^m,\\ &l=j+1: && \mathbf{\Phi}=\{(j+1)(\mathbf{r}/r)+i(\mathbf{r}/r)\times\mathbf{L}\}F^{(1)}(r)P_j{}^m,\\ &l=j-1: && \mathbf{\Phi}=\{-j(\mathbf{r}/r)+i(\mathbf{r}/r)\times\mathbf{L}\}F^{(2)}(r)P_j{}^m, \end{aligned} \tag{34}$$

involving three arbitrary radial functions. The general solution associated with the eigenvalue j is obtained by linear combination of these auxiliary $\mathbf{\Phi}$-functions. The existence of the parity quantum number permits a further classification of these solutions, for the parity associated with a state of

orbital angular momentum l is $(-1)^l$, thus assigning to the state $l=j$ a parity opposite to that of the state $l=j\pm1$. The state $l=j$ and a linear combination of the states $l=j\pm1$ therefore constitute independent stationary states. No further sub-division will be possible in general, for the spin-orbit coupling introduced by relativistic requirements destroys the constancy of orbital angular momentum. Turning to the scalar function φ, we observe from (31) that

$$\varphi=G(r)P_j^m,$$

introducing an additional arbitrary radial function $G(r)$. For $l=j$ the requirement that φ and Φ have opposite reflection characteristics can be made compatible with the equal parities of these two functions only by demanding that $\varphi\equiv0$. These remarks find their complete expression in the following formulae for the two distinct types of admissible solutions:

$$l=j:\ \begin{cases}\Phi=\mathbf{L}F(r)P_j^m,\\ \varphi=0,\end{cases}\qquad l=j\pm1:\ \begin{cases}\Phi=\{(\mathbf{r}/r)F_1(r)+i[(\mathbf{r}/r)\times\mathbf{L}]F_2(r)\}P_j^m,\\ \varphi=G(r)P_j^m,\end{cases}\tag{35}$$

which are written in terms of the linear combinations

$$F_1(r)=(j+1)F^{(1)}(r)-jF^{(2)}(r),\quad F_2(r)=F^{(1)}(r)+F^{(2)}(r).\tag{36}$$

These formulae express all the information available from the general symmetry properties of the system; to proceed further we must resort to the specific dynamical equations. The equations (18) of current theory, specialized to represent the motion of a mesotron with energy W in a static field described by a scalar potential $V(r)$, read

$$\begin{aligned}&\left\{\nabla^2+\left(\frac{W+eV}{\hbar c}\right)^2-\left(\frac{Mc}{\hbar}\right)^2\right\}\Phi=-\frac{e}{\hbar c}\frac{\mathbf{r}}{r}\frac{dV}{dr}\varphi+\frac{e\hbar}{M^2c^3}\nabla\left[\frac{dV}{dr}\left\{\frac{W+eV}{\hbar c}\frac{\mathbf{r}}{r}\cdot\Phi-\frac{\partial\varphi}{\partial r}\right\}\right],\\ &\left\{\nabla^2+\left(\frac{W+eV}{\hbar c}\right)^2-\left(\frac{Mc}{\hbar}\right)^2\right\}\varphi=\frac{e}{\hbar c}\frac{dV}{dr}\frac{\mathbf{r}}{r}\cdot\Phi+\frac{e\hbar}{M^2c^3}\frac{W+eV}{\hbar c}\frac{dV}{dr}\left\{\frac{W+eV}{\hbar c}\frac{\mathbf{r}}{r}\cdot\Phi-\frac{\partial\varphi}{\partial r}\right\},\end{aligned}\tag{37}$$

when translated into vector notation. These equations must be supplemented by the subsidiary condition contained in (16), *viz.*:

$$\nabla\cdot\Phi+\frac{W+eV}{\hbar c}\varphi=\frac{e\hbar}{M^2c^3}\frac{dV}{dr}\left\{\frac{W+eV}{\hbar c}\frac{\mathbf{r}}{r}\cdot\Phi-\frac{\partial\varphi}{\partial r}\right\}.\tag{38}$$

This set of equations then yields the radial equations appropriate to the two types of solutions (35). The treatment of the state $l=j$ affords no difficulty, for $\varphi=0$, $(\mathbf{r}/r)\cdot\Phi=0$, $\nabla\cdot\Phi=0$ $(\mathbf{L}=-i\mathbf{r}\times\nabla)$, thus effectively reducing the set of Eqs. (37), (38) to

$$\left\{\nabla^2+\left(\frac{W+eV}{\hbar c}\right)^2-\left(\frac{Mc}{\hbar}\right)^2\right\}\Phi=0,$$

or, in radial form

$$\left\{\frac{d^2}{dr^2}+\frac{2}{r}\frac{d}{dr}-\frac{l(l+1)}{r^2}+\left(\frac{W+eV}{\hbar c}\right)^2-\left(\frac{Mc}{\hbar}\right)^2\right\}F(r)=0.\tag{39}$$

This is simply the canonical form of the Klein-Gordon equation, which requires no further attention. The radial equations for the second type of solution $(l=j\pm1)$ are readily derived with the aid of a few elementary lemmata. The gradient operator finds its most convenient expression in the form:

$$\nabla=\frac{\mathbf{r}}{r}\frac{\partial}{\partial r}-i\frac{\mathbf{r}\times\mathbf{L}}{r^2}\tag{40}$$

with the derivative relation

$$\nabla^2=\frac{\partial^2}{\partial r^2}+\frac{2}{r}\frac{\partial}{\partial r}-\frac{L^2}{r^2}. \tag{40a}$$

Further

$$L^2\Phi=\left\{\frac{\mathbf{r}}{r}(j(j+1)F_1+2F_1+2j(j+1)F_2)+i\left(\frac{\mathbf{r}}{r}\times\mathbf{L}\right)(j(j+1)F_2+2F_1)\right\}P_j^m,$$

which is most easily obtained by reverting to the original expression of Φ in terms of eigenfunctions of L^2. It is now possible to write the terms of the first of Eqs. (37) as linear combinations of the two angular functions $(\mathbf{r}/r)P_j^m$ and $i[(\mathbf{r}/r)\times\mathbf{L}]P_j^m$, the coefficients of which yield the desired radial equations for F_1 and F_2. The radial equation corresponding to the latter part of (37) may be written down by inspection, while to perform a similar operation for (38) requires only the observation that

$$\nabla\cdot\Phi=\left\{\nabla\cdot\frac{\mathbf{r}}{r}F_1+i\nabla\cdot\frac{\mathbf{r}}{r}\times\mathbf{L}F_2\right\}P_j^m=\left\{\left(\frac{\partial}{\partial r}+\frac{2}{r}\right)F_1+\frac{j(j+1)}{r}F_2\right\}P_j^m.$$

The complete set of radial equations thus obtained is:

$$\begin{gathered}\Omega F_1=\frac{2}{r^2}(F_1+j(j+1)F_2)-\frac{e}{\hbar c}\frac{dV}{dr}G-\frac{e}{\hbar c}\frac{d}{dr}\left(Q\frac{dV}{dr}\right),\\ \Omega F_2=\frac{2}{r^2}F_1+\frac{e}{\hbar c}\frac{1}{r}Q\frac{dV}{dr},\quad \Omega G=\frac{e}{\hbar c}\frac{dV}{dr}F_1-\frac{e}{\hbar c}\frac{W+eV}{\hbar c}Q\frac{dV}{dr},\\ \frac{dF_1}{dr}+\frac{2}{r}F_1+\frac{j(j+1)}{r}F_2+\frac{W+eV}{\hbar c}G=-\frac{e}{\hbar c}Q\frac{dV}{dr},\end{gathered} \tag{41}$$

where Ω symbolizes the Klein-Gordon operator

$$\Omega=\frac{d^2}{dr^2}+\frac{2}{r}\frac{d}{dr}-\frac{j(j+1)}{r^2}+\left(\frac{W+eV}{\hbar c}\right)^2-\left(\frac{Mc}{\hbar}\right)^2 \tag{42}$$

and Q is defined by

$$\left(\frac{Mc}{\hbar}\right)^2Q=\frac{dG}{dr}-\frac{W+eV}{\hbar c}F_1. \tag{43}$$

It should be noted that if $j=0$ the second equation of the set (41) disappears, for this equation was inferred from the coefficients of $i[(\mathbf{r}/r)\times\mathbf{L}]P_j^m$, which identically vanishes for zero angular momentum.

In order that regular solutions of these equations exist for the Coulomb field, $V=Ze/r$, it is necessary that the functions F_1, F_2 and G vanish at the origin at least as rapidly as some power of r, e.g., r^l, so that, from Eqs. (41), Q must exhibit a radial dependence proportional to r^{l+1}. To test the consistency of these requirements with the definition of Q, we may employ the equations obtained by substituting the fourth member of (41) into the first and third members, namely:

$$\begin{gathered}-\frac{W+eV}{\hbar c}Q=F_1+\left(\frac{\hbar}{Mc}\right)^2\frac{j(j+1)}{r^2}\left\{F_1+\frac{d}{dr}(rF_2)\right\},\\ \frac{dQ}{dr}+\frac{2}{r}Q=G+\left(\frac{\hbar}{Mc}\right)^2\frac{j(j+1)}{r^2}\left\{G+\frac{W+eV}{\hbar c}(rF_2)\right\}.\end{gathered} \tag{44}$$

In states of nonvanishing angular momentum ($j\neq 0$), the second terms of these expressions for Q are dominant near the origin, thus imparting to Q a radial dependence two powers of r less than that of the functions F_1, F_2, and G, contrary to the mathematical regularity requirements. Therefore, no regular solutions exist for states possessing finite angular momentum. Whether *any* solutions compatible with the physical requirements exist remains an open question. For $j=0$, these Eqs. (44) become simply

$$F_1=-\frac{W+eV}{\hbar c}Q;\quad G=\frac{dQ}{dr}+\frac{2}{r}Q, \tag{45}$$

which, coupled with the definition (43) of Q, imply that

$$\frac{d^2Q}{dr^2}+\frac{2}{r}\frac{dQ}{dr}-\frac{2}{r^2}Q+\left\{\left(\frac{W+eV}{\hbar c}\right)^2-\left(\frac{Mc}{\hbar}\right)^2\right\}Q=0, \tag{46}$$

the Klein-Gordon equation for a state of unit angular momentum. This result is quite satisfactory, for a state of zero total angular momentum is rigorously a state of unit orbital angular momentum. The general conclusion to be drawn from these considerations based on the Proca theory may be summarized by the statement that regular solutions exist for the Coulomb field only for those states in which the orbital angular momentum is a rigorous constant of the motion, namely $l=j\neq 0$ and $l=1$, $j=0$.

The technique developed for the expression of the Proca equations in radial form is immediately applicable to the equations of the modified theory ($\gamma=1$). In vectorial notation these equations comprise the following set:

$$\begin{gathered}\left\{\nabla^2+\left(\frac{W+eV}{\hbar c}\right)^2-\left(\frac{Mc}{\hbar}\right)^2\right\}\boldsymbol{\Phi}=-\frac{2e}{\hbar c}\frac{\mathbf{r}}{r}\frac{dV}{dr}\varphi-\frac{4\pi e\hbar}{M^2c^3}\nabla(\Gamma(r)\varphi),\\ \left\{\nabla^2+\left(\frac{W+eV}{\hbar c}\right)^2-\left(\frac{Mc}{\hbar}\right)^2\right\}\varphi=\frac{2e}{\hbar c}\frac{dV}{dr}\frac{\mathbf{r}}{r}\cdot\boldsymbol{\Phi}-\frac{4\pi e}{M^2c^4}(W+eV)\Gamma(r)\varphi,\\ \nabla\cdot\boldsymbol{\Phi}+\frac{W+eV}{\hbar c}\varphi=-\frac{4\pi e\hbar}{M^2c^3}\Gamma(r)\varphi,\end{gathered} \tag{47}$$

wherein $\Gamma(r)=J^4/c$ denotes the density of the static, spherically symmetric charge distribution under whose influence the mesotron moves. The treatment of the state $l=j$ need not detain us, the Klein-Gordon equation being obtained as before. The radial equations describing the coupled states $l=j\pm 1$, *viz.*:

$$\begin{gathered}\Omega F_1=\frac{2}{r^2}(F_1+j(j+1)F_2)-\frac{2e}{\hbar c}\frac{dV}{dr}G-\frac{4\pi e\hbar}{M^2c^3}\frac{d}{dr}(\Gamma(r)G),\\ \Omega F_2=\frac{2}{r^2}F_1+\frac{4\pi e\hbar}{M^2c^3}\frac{1}{r}\Gamma(r)G,\quad \Omega G=\frac{2e}{\hbar c}\frac{dV}{dr}F_1-\frac{4\pi e}{M^2c^4}(W+eV)\Gamma(r)G,\\ \frac{dF_1}{dr}+\frac{2}{r}F_1+\frac{j(j+1)}{r}F_2+\frac{W+eV}{\hbar c}G=-\frac{4\pi e\hbar}{M^2c^3}\Gamma(r)G,\end{gathered} \tag{48}$$

may be obtained, *mut. mutand.*, from the previous set (41). A complete solution of these equations can be effected in regions of space unoccupied by external charges ($\Gamma(r)=0$). Within such domains,

the radial equations assume a particularly simple aspect:

$$\Omega F_1=(2/r^2)[F_1+j(j+1)F_2+Z\alpha G],\quad \Omega F_2=(2/r^2)F_1,\quad \Omega G=(2/r^2)(-Z\alpha F_1),$$
$$\frac{dF_1}{dr}+\frac{2}{r}F_1+\frac{j(j+1)}{r}F_2+\frac{W+eV}{\hbar c}G=0 \tag{49}$$

when the Coulomb field ($eV=Ze^2/r=Z\alpha\hbar c/r$) is introduced explicitly. A process of diagonalization reduces these equations to a canonical form.

The linear combination

$$\lambda F_1+j(j+1)F_2+Z\alpha G \tag{50}$$

provides a solution of the differential equation

$$\Omega\mathfrak{F}=(2\lambda/r^2)\mathfrak{F}$$

if λ is chosen to represent one of the roots of the eigenvalue equation

$$\lambda(\lambda-1)=j(j+1)-Z^2\alpha^2 \tag{51}$$

viz.:

$$\lambda_1=\tfrac{1}{2}+[(j+\tfrac{1}{2})^2-Z^2\alpha^2]^{\frac{1}{2}};\quad \lambda_2=\tfrac{1}{2}-[(j+\tfrac{1}{2})^2-Z^2\alpha^2]^{\frac{1}{2}}. \tag{52}$$

Associated with these roots, therefore, are two functions:

$$(\lambda_1-\lambda_2)\mathfrak{F}_1=\lambda_1F_1+j(j+1)F_2+Z\alpha G,\quad (\lambda_2-\lambda_1)\mathfrak{F}_2=\lambda_2F_1+j(j+1)F_2+Z\alpha G, \tag{53}$$

which satisfy the differential equation

$$\left\{\frac{d^2}{dr^2}+\frac{2}{r}\frac{d}{dr}+\frac{W^2-M^2c^4}{\hbar^2c^2}+\frac{2W}{\hbar c}\frac{Z\alpha}{r}-\frac{\lambda(\lambda+1)}{r^2}\right\}\mathfrak{F}_\lambda=0$$
$$(\mathfrak{F}_1=\mathfrak{F}_{\lambda_1},\quad \mathfrak{F}_2=\mathfrak{F}_{\lambda_2}), \tag{54}$$

the form assumed by the Klein-Gordon equation in a Coulomb field. The two Eqs. (53), supplemented by the fourth member of (49), *viz.:*

$$F_1=\mathfrak{F}_1+\mathfrak{F}_2,\quad j(j+1)F_2+Z\alpha G=-(\lambda_2\mathfrak{F}_1+\lambda_1\mathfrak{F}_2)$$
$$G=-\frac{\hbar c}{W}\left\{\frac{d}{dr}\mathfrak{F}_1+\frac{1+\lambda_1}{r}\mathfrak{F}_1+\frac{d}{dr}\mathfrak{F}_2+\frac{1+\lambda_2}{r}\mathfrak{F}_2\right\}, \tag{55}$$

constitute a complete solution of the problem in terms of $\mathfrak{F}_1$ and $\mathfrak{F}_2$.

In states of nonvanishing angular momentum, there exist two linearly independent solutions associated with $\mathfrak{F}_1$ and with $\mathfrak{F}_2$, which we label by a quantum number "l"$=j+1$, $j-1$, respectively. In the nonrelativistic limit, "l" becomes the orbital quantum number. $\mathfrak{F}_1$ and $\mathfrak{F}_2$ may not be considered as independent in states of zero angular momentum, for a relation between them is implied by the Eqs. (55) specialized to the state $j=0$. The last two equations—equations for G—now serve to determine the arbitrary constants in $\mathfrak{F}_2$ in terms of those in $\mathfrak{F}_1$ thus providing only one independent solution. To show this in detail, we observe that, if $\mathfrak{F}_\lambda$ is a solution of (54),

$$\mathfrak{F}_{\lambda-1}=\frac{d}{dr}\mathfrak{F}_\lambda+\frac{1+\lambda}{r}\mathfrak{F}_\lambda-\frac{W}{\hbar c}\frac{Z\alpha}{\lambda}\mathfrak{F}_\lambda, \tag{56}$$

whence

$$-\frac{\hbar c}{W}\left\{\frac{d}{dr}\mathfrak{F}_1+\frac{1+\lambda_1}{r}\mathfrak{F}_1+\frac{d}{dr}\mathfrak{F}_2+\frac{1+\lambda_2}{r}\mathfrak{F}_2\right\}=-\frac{1}{Z\alpha}(\lambda_2\mathfrak{F}_1+\lambda_1\mathfrak{F}_2)-\frac{\hbar c}{W}(\mathfrak{F}_{\lambda_1-1}+\mathfrak{F}_{\lambda_2-1}), \tag{57}$$

in which the relation $\lambda_1\lambda_2=Z^2\alpha^2$ $(j=0)$ has been utilized. Since $\lambda_1(\lambda_1-1)=\lambda_2(\lambda_2-1)$, $\mathfrak{F}_{\lambda_1-1}$ and $\mathfrak{F}_{\lambda_2-1}$ satisfy the same differential equation, thus enabling one to impose consistently the condition

$$\mathfrak{F}_{\lambda_1-1}+\mathfrak{F}_{\lambda_2-1}\equiv 0, \tag{58}$$

which exhibits the relation between $\mathfrak{F}_1$ and $\mathfrak{F}_2$ demanded by the coexistence of Eqs. (55) for $j=0$.

Although the equations of the modified theory $(\gamma=1)$ are completely soluble in regions devoid of external charges, a comparable situation does not exist within charge distributions $(\Gamma(r)\neq 0)$. While the equations presumably possess regular solutions in regions of smoothly varying charge density, no serious attempt has been made to obtain them. In the limiting case of a point charge, the presence of the singular terms in $\Gamma(r)$ imposes boundary conditions, which may be inferred from the requirement of the existence of physically admissible charge distributions. According to Eqs. (15) and (16), the mesotron charge density ρ is given by

$$\rho=-\frac{2e}{\hbar c^2}\left\{\frac{W+eV}{\hbar c}(\bar{\mathbf{\Phi}}\cdot\mathbf{\Phi}+\bar{\varphi}\varphi)-(\mathbf{\Phi}\cdot\nabla)\bar{\varphi}-(\bar{\mathbf{\Phi}}\cdot\nabla)\varphi+\frac{4\pi e\hbar}{M^2c^3}\Gamma(r)\bar{\varphi}\varphi\right\},$$

which would predict an amount of charge

$$-2Z\alpha(e\hbar/M^2c^4)G^2(0) \tag{59}$$

to be contained within an arbitrarily small neighborhood of a point charge Ze. For solutions of the type $j=$"l"$+1$, $G(r)\sim r^{\lambda_1-2}$ in the vicinity of the origin, while for those of type $j=$"l"-1, $G(r)\sim r^{\lambda_1-1}$ Since λ_1 is not an integer, $G(r)$ tends to either zero or infinity as r is diminished. In the latter case, which occurs for $j=0$, "l"$=1$, and $j=1$, "l"$=0$, the amount of charge (59) in the immediate neighborhood of the origin, and hence also the total charge of the system, becomes infinite. This meaningless situation implies that these two states are completely forbidden.

It is of some interest to note that the energy levels of the allowed discrete states are represented by the Sommerfeld formula, all states of given total angular momentum and principal quantum number coalescing as in the Dirac theory. This result is inexplicable on the basis of the formula derived from the Larmor and Thomas precessions, which would predict in addition a dependence on the orbital angular momentum quantum number l. The origin of this discrepancy is to be sought in the inadequacy of considering the spin as a simple vector, for the coupling energy between spin and orbit consists not only of the usual Larmor-Thomas terms but in addition terms which are nonlinear in the spin. The equivalence between the Larmor-Thomas formula and the corresponding prediction of the Dirac theory is to be attributed to the necessary linearity of the spin terms for a particle of spin $\frac{1}{2}$.

The general program of this section has been an attempt to obtain rigorous solutions of the equations for a particle of unit spin in a Coulomb field. While for the equations describing Proca particles this attempt has been abortive, the modified theory discussed in this paper provides regular solutions for all states save two, these being completely forbidden. The net result of the modification has been, therefore, the concentration rather than the removal of the singularities. The lack of a complete set of regular solutions thus compels us to have resort to the Born approximation in order to give meaning to these two theories.

IV. Electron-Mesotron Collisions

Information concerning the electromagnetic properties of mesotrons may be obtained by the study of various scattering processes. However, it would be difficult to infer such information from processes such as mesotron-proton scattering and radiative emission induced by mesotrons, which involve in addition the mesotron-heavy particle coupling. For collisions between mesotrons and electrons, however, this latter type of coupling is presumably absent, and the energy transfer is dependent only on the electromagnetic interaction between the particles. Using various mesotron

models, we shall calculate the cross section for this energy transfer, developing a general analysis, based on the Born approximation, without use of the explicit form of the mesotron charge and current densities. The results are applied to mesotrons of spin $\sigma=0$, magnetic moment $\mu=0$, $\sigma=\frac{1}{2}$, μ arbitrary (in particular $\mu=0$) and $\sigma=1$, μ arbitrary (in particular $\mu=1$ and $\mu=2$).

Let us consider a transition of the mesotron from a state of energy W^0 and momentum $\mathbf{P}^0$ to a state of energy W and momentum $\mathbf{P}$. With this transition are associated charge and current densities

$$\rho=\rho_{if}\exp\{i[(\mathbf{P}^0-\mathbf{P})\cdot\mathbf{r}-(W^0-W)t]/\hbar\},\quad \mathbf{j}=\mathbf{j}_{if}\exp\{i[(\mathbf{P}^0-\mathbf{P})\cdot\mathbf{r}-(W^0-W)t]/\hbar\} \tag{60}$$

which produce a transition electromagnetic field

$$\mathbf{A}=\frac{4\pi\hbar^2}{c}\mathbf{j}_{if}\frac{\exp\{i[(\mathbf{P}^0-\mathbf{P})\cdot\mathbf{r}-(W^0-W)t]/\hbar\}}{|\mathbf{P}^0-\mathbf{P}|^2-c^{-2}(W^0-W)^2},\quad V=4\pi\hbar^2\rho_{if}\frac{\exp\{i[(\mathbf{P}^0-\mathbf{P})\cdot\mathbf{r}-(W^0-W)t]/\hbar\}}{|\mathbf{P}^0-\mathbf{P}|^2-c^{-2}(W^0-W)^2}. \tag{61}$$

This field induces transitions of the electron from a state of energy and momentum E^0, $\mathbf{p}^0$ to the state E, $\mathbf{p}$. The spin direction of the electron in these positive energy states may be characterized by the indices λ^0, $\lambda=1, 2$. If the electron wave functions are taken to be

$$\text{initially: } u_{\mathbf{p}^0\lambda^0}\exp[i(\mathbf{p}^0\cdot\mathbf{r}-E^0t)/\hbar],\quad \text{finally: } u_{\mathbf{p}\lambda}\exp[i(\mathbf{p}\cdot\mathbf{r}-Et)/\hbar], \tag{62}$$

the condition $(u_{\mathbf{p}^0\lambda^0}, u_{\mathbf{p}^0\lambda^0})=(u_{\mathbf{p}\lambda}, u_{\mathbf{p}\lambda})=1$ corresponds to one electron per unit volume. The transition probability per unit time from the state $(\lambda^0, \mathbf{p}^0)$ to the state $(\lambda, \mathbf{p})$ of the electron is then given by

$$\frac{2\pi}{\hbar}\left[\frac{4\pi\hbar^2e}{|\mathbf{P}^0-\mathbf{P}|^2-c^{-2}(W^0-W)^2}\right]^2\left|\left(u_{\mathbf{p}\lambda},(\rho_{if}-\frac{1}{c}\boldsymbol{\alpha}\cdot\mathbf{j}_{if})u_{\mathbf{p}^0\lambda^0}\right)\right|^2\cdot\delta(W+E-W^0-E^0)\delta_{\mathbf{P}+\mathbf{p},\,\mathbf{P}^0+\mathbf{p}^0}. \tag{63}$$

To find the total electron transition probability, we sum over the final spin and momentum states of the electron. The summation over the final momentum states has merely the effect of imposing the condition of momentum conservation. Summing over the final spin directions, one has

$$\sum_{\lambda=1,2}\left|\left(u_{\mathbf{p}\lambda},(\rho_{if}-\frac{1}{c}\boldsymbol{\alpha}\cdot\mathbf{j}_{if})u_{\mathbf{p}^0\lambda^0}\right)\right|^2=\frac{1}{E^0E}\Big[(E^0\rho_{if}-\mathbf{p}^0\cdot\mathbf{j}_{if})(E\rho_{if}-\mathbf{p}\cdot\mathbf{j}_{if})$$
$$-\tfrac{1}{2}(E^0E-c^2\mathbf{p}^0\cdot\mathbf{p}-m^2c^4)(\rho_{if}^2-\frac{1}{c^2}\mathbf{j}_{if}\cdot\mathbf{j}_{if})\Big], \tag{64}$$

which is independent of the initial spin of the electron. To calculate the cross section for a given incident mesotron, we sum the transition probability (63) over all relevant final states of the mesotron and divide by the product of the mesotron particle density and the relative velocity of the electron and mesotron. The cross section thus defined is relativistically invariant and is most easily computed in the center of mass system ($\mathbf{P}^0+\mathbf{p}^0=0$), since in this system the energy of either particle does not change during the collision. The resulting cross section for the scattering of mesotrons through an angle ϑ into a solid angle $d\omega$ is

$$d\sigma=\frac{e^2}{4c^4P^{0^4}}\left(\frac{W^0}{W^0+E^0}\right)^2\left[(E^0\rho_{if}+\mathbf{P}^0\cdot\mathbf{j}_{if})^2-c^2P^{0^2}\sin^2\tfrac{1}{2}\vartheta(\rho_{if}^2-\frac{1}{c^2}\mathbf{j}_{if}\cdot\mathbf{j}_{if})\right]\frac{d\omega}{\sin^4\frac{1}{2}\vartheta} \tag{65}$$

if the mesotron particle density is also normalized to represent one particle per unit volume. Here we have used the facts that the relative velocity is $(c^2P^0/W^0)+(c^2P^0/E^0)$ in this coordinate system and that the number of mesotron states per unit volume and per unit total energy range is

$$\frac{P^0}{8\pi^3\hbar^3c^2}\frac{E^0W^0}{E^0+W^0}d\omega.$$

For a particle of spin one-half and magnetic moment unity the charge and current densities are given, according to the usual Dirac theory, by the four-vector

$$j^\mu = -(e\hbar/2M)\{(\phi\partial^\mu\psi - (\partial^\mu\phi)\psi) + \tfrac{1}{2}\partial_\nu(\phi(\gamma^\mu\gamma^\nu - \gamma^\nu\gamma^\mu)\psi)\}. \tag{66}$$

Here ϕ is defined by $\phi = \psi^+\gamma^4$, and γ^μ is given in terms of the more familiar Dirac matrices α, β by $\gamma^4 = -i\beta$, $\gamma^i = -i\beta\alpha^i$. The two terms on the right-hand side of (66) are independently conserved and correspond, respectively, to a convection current and a polarization current arising from the magnetic moment. In close analogy with the theory for particles of spin unity, outlined in Section II, one may develop a theory for which the coefficient of the polarization current is arbitrary, corresponding to a particle of spin $\frac{1}{2}$ and of arbitrary magnetic moment. We consider here the particular case for which this magnetic moment is zero. The charge-current four-vector then assumes the simple form

$$j^\mu = (ie\hbar/2M)[\psi^+\beta\partial^\mu\psi - (\partial^\mu\psi^+)\beta\psi], \tag{67}$$

an expression which differs from the corresponding result for particles of spin zero only by the presence of the matrix β. Using plane waves for the mesotron wave functions, *viz.*:

$$\psi_i = u_{\mathbf{P}^0\lambda^0}\exp[i(\mathbf{P}^0\cdot\mathbf{r} - W^0t)/\hbar], \quad \psi_f = u_{\mathbf{P}\lambda}\exp[i(\mathbf{P}\cdot\mathbf{r} - Wt)/\hbar],$$

one finds that the transition charge and current densities corresponding to a mesotron of spin $\frac{1}{2}$ and magnetic moment zero are

$$\rho_{if} = -e(W^0/Mc^2)(u_{\mathbf{P}\lambda}, \beta u_{\mathbf{P}^0\lambda^0}), \quad \mathbf{j}_{if} = -e\frac{c^2(\mathbf{P}^0+\mathbf{P})}{2W^0}\frac{W^0}{Mc^2}(u_{\mathbf{P}\lambda}, \beta u_{\mathbf{P}^0\lambda^0}). \tag{68}$$

The wave functions are normalized by the condition

$$(u_{\mathbf{P}^0\lambda^0}, u_{\mathbf{P}^0\lambda^0}) = (u_{\mathbf{P}\lambda}, u_{\mathbf{P}\lambda}) = 1,$$

which corresponds to one mesotron per unit volume.

Using the relation

$$\sum_{\lambda=1,2}|(u_{\mathbf{P}\lambda}, \beta u_{\mathbf{P}^0\lambda^0})|^2 = \frac{M^2c^4}{W^{0^2}}\left(1+\frac{P^{0^2}}{M^2c^2}\sin^2\tfrac{1}{2}\vartheta\right) \tag{69}$$

and substituting (68) in (65), one finds that the cross section for the scattering of a mesotron through an angle ϑ into a solid angle $d\omega$ is

$$d\sigma = \frac{e^4}{4c^4P^{0^4}}\left(\frac{W^0}{W^0+E^0}\right)^2\frac{d\omega}{\sin^4\frac{1}{2}\vartheta}\left[\left(E^0+\frac{c^2P^{0^2}}{W^0}\right)^2 - c^2P^{0^2}\sin^2\tfrac{1}{2}\vartheta\left\{\frac{2}{W^0}\left(E^0+\frac{c^2P^{0^2}}{W^0}\right)+\frac{M^2c^4}{W^{0^2}}\right\}\right]\cdot\left[1+\frac{P^{0^2}}{M^2c^2}\sin^2\tfrac{1}{2}\vartheta\right]. \tag{70}$$

The corresponding cross section for a particle of zero spin—and hence zero magnetic moment—differs from the above expression only by the absence of the last factor, which, for the case of spin $\frac{1}{2}$, arises from the spin summation. It is to be noted that at high energies this factor entirely alters the dependence of the cross section on the mesotron energy.

To obtain from (70) the cross section for Coulomb scattering it is only necessary to consider the limiting case of infinite E^0, which yields

$$d\sigma = \frac{1}{4}\left(\frac{e^2}{Mc^2}\right)^2\frac{\epsilon^2}{(\epsilon^2-1)^2}[1+(\epsilon^2-1)\sin^2\tfrac{1}{2}\vartheta]\frac{d\omega}{\sin^4\frac{1}{2}\vartheta}, \tag{71}$$

in which we have set $W^0=\epsilon Mc^2$. At high mesotron energies (71) becomes

$$d\sigma=\frac{1}{4}\left(\frac{e^2}{Mc^2}\right)^2\frac{d\omega}{\sin^2\frac{1}{2}\vartheta}, \tag{72}$$

which differs from the corresponding formula deduced from the Proca theory[6] by the absence of a factor $\frac{2}{3}\cos^2\frac{1}{2}\vartheta$.

The above formulae represent the angular scattering cross section in the barycentric system; we are primarily interested in the cross section for a given fractional energy transfer to an initially stationary electron. It is therefore expedient to introduce the ratio, f, of the kinetic energy gained by the electron to $W_0=\epsilon Mc^2$, the total energy of the incident mesotron, measured in the laboratory system. The relation between f and the angle of scattering in the center of mass system is simply

$$f=f_{\max}\sin^2\tfrac{1}{2}\vartheta, \quad \text{where} \quad f_{\max}=\frac{2\omega(\epsilon^2-1)}{\epsilon(1+\omega^2+2\omega\epsilon)} \quad (\omega=m/M) \tag{73}$$

represents the maximum fraction of the mesotron energy which may be transferred to an electron by impact. Employing the relation between W_0 and the electron and mesotron energies in the barycentric system, *viz.*:

$$E^0=\frac{\omega(\epsilon+\omega)}{(1+\omega^2+2\omega\epsilon)^{\frac{1}{2}}}Mc^2, \quad W^0=\frac{1+\omega\epsilon}{(1+\omega^2+2\omega\epsilon)^{\frac{1}{2}}}Mc^2, \tag{74}$$

we may rewrite the cross section as follows:

$$d\sigma=\pi\left(\frac{e^2}{Mc^2}\right)^2\frac{\epsilon^2}{\epsilon^2-1}\frac{df}{f^2}\left[f(1-f)+\frac{2}{\omega\epsilon}(1-f-\tfrac{1}{4}f^2)-\frac{1}{\omega^2\epsilon^2}f\right]. \tag{75}$$

At high energies this is independent of the energy of the incident mesotron. For a mesotron of arbitrary magnetic moment $\mu\neq 1$ and spin $\frac{1}{2}$ the leading term of this expression is multiplied by a factor $(\mu-1)^2$. The corresponding result for mesotrons of spin zero is obtained by omitting the last factor in (70):

$$d\sigma=\pi\left(\frac{e^2}{Mc^2}\right)^2\frac{\epsilon^2}{\epsilon^2-1}\frac{df}{f^2}\left[\frac{2}{\omega\epsilon}(1-f)-\frac{1}{\omega^2\epsilon^2}f\right], \tag{76}$$

which for high mesotron energies ϵ decreases inversely with ϵ.

For mesotrons of spin unity, one again uses plane waves for the mesotron wave functions, *viz.*:

$$\Phi_i=\hbar c\left(\frac{c}{2W^0}\right)^{\frac{1}{2}}\mathbf{e}^0\exp\left[i(\mathbf{P}^0\cdot\mathbf{r}-W^0t)/\hbar\right], \quad \varphi_i=-i\hbar c\left(\frac{c}{2W^0}\right)^{\frac{1}{2}}\frac{c\mathbf{P}^0\cdot\mathbf{e}^0}{W^0}\exp\left[i(\mathbf{P}^0\cdot\mathbf{r}-W^0t)/\hbar\right]$$

with similar expressions for the final state. The normalizing condition

$$\mathbf{e}^0\cdot\mathbf{e}^0-(c\mathbf{P}^0\cdot\mathbf{e}^0/W^0)^2=1$$

then corresponds to one mesotron per unit volume.

The transition current and charge densities are given by

$$\begin{aligned}\rho_{if}&=-e\left\{\left(\mathbf{e}^0\cdot\mathbf{e}-\frac{c\mathbf{P}^0\cdot\mathbf{e}^0}{W^0}\frac{c\mathbf{P}\cdot\mathbf{e}}{W^0}\right)+\tfrac{1}{2}(\gamma+1)\left(\frac{c\mathbf{P}\cdot\mathbf{e}}{W^0}\frac{c(\mathbf{P}^0-\mathbf{P})\cdot\mathbf{e}^0}{W^0}-\frac{c\mathbf{P}^0\cdot\mathbf{e}^0}{W^0}\frac{c(\mathbf{P}^0-\mathbf{P})\cdot\mathbf{e}}{W^0}\right)\right\},\\ \mathbf{j}_{if}&=-e\frac{c^2}{2W^0}\left\{(\mathbf{P}^0+\mathbf{P})\left(\mathbf{e}^0\cdot\mathbf{e}-\frac{c\mathbf{P}^0\cdot\mathbf{e}^0}{W^0}\frac{c\mathbf{P}\cdot\mathbf{e}}{W^0}\right)+(\gamma+1)(\mathbf{e}^0\times\mathbf{e})\times(\mathbf{P}^0-\mathbf{P})\right\},\end{aligned} \tag{77}$$

[6] O. Laporte, Phys. Rev. **54**, 905 (1938).

TABLE I. *Values of $f\kappa(f)$ for particles with various spins and magnetic moments which collide with the electron.*

TYPE	SPIN	MAGNETIC MOMENT	$f\kappa(f)$
I	0	0	$2\eta^{-1}(1-f)$
II	$\frac{1}{2}$	1	$2\eta^{-1}(1-f+\frac{1}{2}f^2)$
III	$\frac{1}{2}$	$\mu\neq 1$	$(\mu-1)^2(1-f)$
IV	1	1	$\frac{2}{3}(1-f+\frac{1}{2}f^2)$
V	1	$\mu\neq 1$	$\frac{2}{3}(\mu-1)^2\eta(1-f)$

and on substitution in (65) one may obtain the cross section. For general γ and ϵ the expression obtained is complicated but for large ϵ and $\gamma\neq 0$ the major contribution to the cross section arises from the terms proportional to γ^2 which correspond to longitudinal-longitudinal transitions. One finds, for $f\omega\epsilon\gg 1$, $f<f_{\max}\doteq 1-(1/2\omega\epsilon)$, and $\gamma\neq 0$,

$$d\sigma=\tfrac{2}{3}\pi(e^2/Mc^2)^2\gamma^2\omega\epsilon(1-f)df, \qquad (78)$$

which is to be compared with the corresponding cross section for $\gamma=0$

$$d\sigma=\tfrac{2}{3}\pi(e^2/Mc^2)^2(1-f+\tfrac{1}{2}f^2)df. \qquad (79)$$

It is to be noted that for $\gamma\neq 0$ the cross section increases linearly with the energy of the incident mesotron.

Writing

$$d\sigma=\sigma_0\kappa(f)df, \quad \sigma_0=\pi(e^2/Mc^2)^2 \qquad (80)$$

for the cross section for a particle of energy ϵMc^2 and mass M to transfer energy $f\epsilon Mc^2$ to an electron of mass $m=\omega M$, we may summarize the above results for $\eta=f\epsilon\omega\gg 1$ in Table I.

Only cases III and IV lead to cross sections essentially independent of the mesotron energy, as required by experiment. In addition, it has been shown[1] that in order to account for the observed size[7] of bursts of energy $>2\times 10^{10}$ ev it is necessary for the cross section to be such that

$$\kappa=\int_0^1\kappa(f)f^{1.8}df\sim\tfrac{1}{2}.$$

For the case of spin $\frac{1}{2}$ and magnetic moment $\mu\neq 1$

$$\kappa=0.2(\mu-1)^2,$$

which is of the correct order for $|\mu-1|<2$. Because of the uncertainty in the experimental evidence the value of μ cannot be assigned more definitely, but it is to be noted that, for the particular case $\mu=0$ the value of κ is 0.2, which is very close to the corresponding value (0.22) obtained from the Proca theory. It is therefore impossible to distinguish between cases III and IV from cosmic-ray evidence alone.

All these results having been obtained by use of the Born approximation, it is important to examine the conditions under which they may be expected to have validity. A necessary condition for the validity of the Born approximation is the smallness of the coupling between the mesotron and the fields arising from both the electron and the zero-point fluctuations of the electromagnetic field. A previous investigation of these questions by Oppenheimer, Snyder and Serber[1] has disclosed that the more incisive condition arises from the requirement that the coupling between the mesotron and the zero-point fluctuations be small. To express this requirement in quantitative form, we consider the mesotron-electron collision in the center of mass system, employing wave packets of approximate linear dimensions $\hbar/P$. The kinetic energy density $\sim Pc(P/\hbar)^3$ must then be large compared with the coupling energy density $-(1/c)\mathbf{j}\cdot\mathbf{A}$. The potential $\mathbf{A}$ describes the zero-point fluctuations of wave-length $\sim\hbar/P$ and possessses the order of magnitude $P(c/\hbar)^{\frac{1}{2}}$. The form of the current density $\mathbf{j}$ depends on the assumed mesotron model and is of the order of magnitude $ec(P/\hbar)^3\times(P/Mc)^n$, where n assumes the value zero for particles of type I, II of Table I, $n=1$ for types III, IV, and $n=2$ for type V. This varied momentum dependence of the current density is of course intimately related to the different energy dependence of the cross sections for these several types of particles. The condition of smallness of the coupling energy density compared with the kinetic energy density is then expressed quantitatively by

$$\alpha^{\frac{1}{2}}(P/Mc)^n\ll 1.$$

For the various types of particles this condition assumes the form

$$\begin{aligned}&\text{(I, II):}\quad && \alpha^{\frac{1}{2}}\ll 1,\\ &\text{(III, IV):}\quad && W_0\ll M^2c^2/\alpha m\doteq 2\times 10^{12}\text{ ev},\\ &\text{(V):}\quad && W_0\ll M^2c^2/\alpha^{\frac{1}{2}}m\doteq 2\times 10^{11}\text{ ev}\end{aligned} \qquad (81)$$

[7] M. Schein and P. S. Gill, Phys. Rev. **55**, 1111 (1939); M. Schein and V. C. Wilson, Rev. Mod. Phys. **11**, 292 (1939); H. Carmichael and C. N. Chou, Nature **144**, 325 (1939); Bhabha, Carmichael and Chou, Proc. Ind. Acad. Sci. **A10**, 221 (1939).

in its limitation on the mesotron energy W_0. The domain of validity of the modified theory (case V) is thus more limited than that of the Proca theory, but it is still of sufficient extent to include most of the experimental region.

The authors wish to express their gratitude to Professor J. R. Oppenheimer for his continued advice and encouragement.

Appendix

The basic equation determining the simultaneous eigenfunctions of L^2 and J^2, Eq. (33) of the text:

$$((j(j+1)-l(l+1)-2)\mathbf{\Phi}=2i(\mathbf{L}\times\mathbf{\Phi}), \tag{A1}$$

may be readily solved by elementary quantum algebra. The operations of scalar and vector multiplication with $\mathbf{L}$ yield, respectively,

$$\begin{aligned}&(j(j+1)-l(l+1))\mathbf{L}\cdot\mathbf{\Phi}=0,\\ &l(l+1)\mathbf{\Phi}-\mathbf{L}(\mathbf{L}\cdot\mathbf{\Phi})=\tfrac{1}{4}(j(j+1)-l(l+1))\\ &\qquad\times(j(j+1)-l(l+1)-2)\mathbf{\Phi},\end{aligned} \tag{A2}$$

from which one obtains the characteristic equation

$$(j(j+1)-l(l+1))((j(j+1)-l(l+1))^2-2j(j+1)-2l(l+1))=0 \tag{A3}$$

by elimination of $\mathbf{L}\cdot\mathbf{\Phi}$. The admissible values of the orbital angular momentum are thereby restricted to

$$l=j-1,\ j,\ j+1, \tag{A4}$$

a not altogether unexpected result.

Sufficient information is available from the relations (A2) to determine the properties of the solution $l=j$. The equation thus obtained:

$$j(j+1)\mathbf{\Phi}=\mathbf{L}(\mathbf{L}\cdot\mathbf{\Phi}), \tag{A5}$$

when reformulated in terms of the scalar function u, defined by

$$\mathbf{L}\cdot\mathbf{\Phi}=j(j+1)u \tag{A6}$$

yields the general form of $\mathbf{\Phi}$, *viz.*:

$$\mathbf{\Phi}=\mathbf{L}u,\quad L^2u=j(j+1)u. \tag{A7}$$

The second equation of the set (A7) implies that u is a spherical harmonic of order j, P_j^m, multiplied by an arbitrary radial function $F(r)$. The spherical harmonics are assumed normalized to provide the conventional matrix representation of angular momenta. One therefore obtains

$$l=j:\ \mathbf{\Phi}=\mathbf{L}F(r)P_j^m. \tag{A8}$$

The choice of the spherical harmonic P_j^m guarantees that J_z shall have the eigenvalue m, for

$$J_z\Phi_z=L_z\Phi_z=m\Phi_z. \tag{A9}$$

The relations thus far developed (A2) provide only the information that

$$\mathbf{L}\cdot\mathbf{\Phi}=0 \tag{A10}$$

when restricted to the states $l=j\pm1$. To proceed further one may utilize the equations

$$\begin{aligned}&(j(j+1)-l(l+1)+2)(\mathbf{r}/r)\cdot\mathbf{\Phi}=-2i\mathbf{L}\cdot((\mathbf{r}/r)\times\mathbf{\Phi}),\\ &(j(j+1)-l(l+1))(\mathbf{r}/r)\times\mathbf{\Phi}=2i\mathbf{L}((\mathbf{r}/r)\cdot\mathbf{\Phi}),\end{aligned} \tag{A11}$$

obtained by applying the operations of scalar and vector multiplication with $\mathbf{r}/r$ to the basic equation (A1). The introduction of the scalar function v, defined by

$$(\mathbf{r}/r)\cdot\mathbf{\Phi}=-\tfrac{1}{2}(j(j+1)-l(l+1))v, \tag{A12}$$

permits a more convenient expression of Eq. (A11), namely $(\mathbf{r}/r)\times\mathbf{\Phi}=-i\mathbf{L}v$,

$$\begin{aligned}L^2v&=\tfrac{1}{4}(j(j+1)-l(l+1))\\ &\qquad\times(j(j+1)-l(l+1)+2)v\\ &=j(j+1)v.\end{aligned} \tag{A13}$$

The relations (A12) and (A13) suffice to determine the general form of $\mathbf{\Phi}$, for

$$\begin{aligned}\mathbf{\Phi}&\equiv(\mathbf{r}/r)((\mathbf{r}/r)\cdot\mathbf{\Phi})-(\mathbf{r}/r)\times[(\mathbf{r}/r)\times\mathbf{\Phi}]\\ &=\{\tfrac{1}{2}(l(l+1)-j(j+1))(\mathbf{r}/r)+i((\mathbf{r}/r)\times\mathbf{L})\}v.\end{aligned} \tag{A14}$$

In virtue of the second of Eqs. (A13), the scalar function v may be represented as the product of the spherical harmonic P_j^m with an arbitrary radial function which is independently assignable for the two states $l=j\pm1$. As before, the choice of the harmonic P_j^m guarantees that J_z shall have the eigenvalue m. The $\mathbf{\Phi}$-functions associated with these two states, expressed in terms of the two arbitrary functions $F^{(1)}(r)$, $F^{(2)}(r)$ then assume the symbolic form

$$\begin{aligned}&l=j+1:\ \mathbf{\Phi}=\{(j+1)(\mathbf{r}/r)+i(\mathbf{r}/r)\times\mathbf{L}\}F^{(1)}(r)P_j^m,\\ &l=j-1:\ \mathbf{\Phi}=\{-j(\mathbf{r}/r)+i(\mathbf{r}/r)\times\mathbf{L}\}F^{(2)}(r)P_j^m.\end{aligned} \tag{A15}$$

To exhibit clearly the angular dependence of the $\mathbf{\Phi}$-functions for the several states, we shall write in detail the behavior of the components

$$\begin{aligned}&\begin{Bmatrix}\Phi_x+i\Phi_y\\ \Phi_x-i\Phi_y\\ \Phi_z\end{Bmatrix},\\ &l=j:\quad\begin{Bmatrix}[(j-m)(j+m+1)]^{\frac{1}{2}}P_j^{m+1}\\ [(j+m)(j-m+1)]^{\frac{1}{2}}P_j^{m-1}\\ m\qquad\qquad P_j^m\end{Bmatrix}F(r),\\ &l=j+1:\quad\left(\frac{2j+1}{2j+3}\right)^{\frac{1}{2}}\begin{Bmatrix}-[(j+1+m)(j+2+m)]^{\frac{1}{2}}P_{j+1}^{m+1}\\ [(j+1-m)(j+2+m)]^{\frac{1}{2}}P_{j+1}^{m-1}\\ [(j+1)^2-m^2]^{\frac{1}{2}}\qquad P_j^m\end{Bmatrix}F^{(1)}(r),\\ &l=j-1:\quad\left(\frac{2j+1}{2j-1}\right)^{\frac{1}{2}}\begin{Bmatrix}[(j-m)(j-m-1)]^{\frac{1}{2}}P_{j-1}^{m+1}\\ -[(j+m)(j+m-1)]^{\frac{1}{2}}P_{j-1}^{m-1}\\ [j^2-m^2]^{\frac{1}{2}}\qquad P_{j-1}^m\end{Bmatrix}F^{(2)}(r).\end{aligned} \tag{A16}$$

These results are not completely novel, being intimately related to the angular representation of electromagnetic multipole fields.[8] The electromagnetic equations are identical with the field-free Proca equations in the limit of zero rest mass, the quantities $\mathbf{\Phi}$ and $i\varphi$ being identified with the vector and scalar potentials in this limit. The vector $\mathbf{\Phi}$ satisfies the differential equation

$$(\nabla^2+k^2)\mathbf{\Phi}=0\quad(k=W/\hbar c), \tag{A17}$$

[8] W. Heitler, Proc. Camb. Phil. Soc. **32**, 112 (1936); W. W. Hansen, Phys. Rev. **47**, 139 (1935); S. M. Dancoff and P. Morrison, Phys. Rev. **55**, 122 (1939).

which, for our purposes, is more conveniently expressed as

$$\left(\frac{d^2}{dr^2}+\frac{2}{r}\frac{d}{dr}-\frac{L^2}{r^2}+k^2\right)\Phi=0,$$

employing Eq. (40a) of the text. All three possible types of radial functions associated with a given orbital angular momentum l thus satisfy the differential equation

$$\left\{\frac{d^2}{dr^2}+\frac{2}{r}\frac{d}{dr}+k^2-\frac{l(l+1)}{r^2}\right\}f_l(r)=0. \tag{A18}$$

The solution Φ_j for $l=j$ (or more exactly the real part of $\Phi_j e^{-ikct}$):

$$\Phi_j=\mathbf{L}f_j(r)P_j^m$$

represents a transverse wave field ($\nabla\cdot\Phi_j=0$) which is to be identified as the vector potential describing the radiation emitted by a magnetic multipole of order $2j$. Appropriate linear combinations of the solutions for $l=j\pm1$

$$\Phi_{j+1}=\{(j+1)(\mathbf{r}/r)+i((\mathbf{r}/r)\times\mathbf{L})\}f_{j+1}P_j^m,$$
$$\Phi_{j-1}=\{-j(\mathbf{r}/r)+i((\mathbf{r}/r)\times\mathbf{L})\}f_{j-1}P_j^m,$$

may be found to represent the longitudinal and transverse parts of the vector potential associated with an electric multipole of order $2j$. Using the recursion relations

$$f_{j+1}+f_{j-1}=(2j+1/kr)f_j, \tag{A19}$$
$$(j+1)f_{j+1}-jf_{j-1}=-(2j+1/k)(d/dr)f_j,$$

one may verify that

$$\Phi_1=\Phi_{j+1}+\Phi_{j-1}=-\frac{2j+1}{k}\left\{\frac{\mathbf{r}}{r}\frac{d}{dr}f_j-i\frac{\mathbf{r}\times\mathbf{L}}{r^2}f_j\right\}P_j^m \tag{A20}$$
$$=-(2j+1/k)\nabla f_jP_j^m,$$

by Eq. (40) of the text. Similarly

$$\Phi_2=\frac{j}{2j+1}\Phi_{j+1}-\frac{j+1}{2j+1}\Phi_{j-1}$$
$$=\left\{\frac{j(j+1)}{kr}\frac{\mathbf{r}}{r}f_j-i\frac{\mathbf{r}\times\mathbf{L}}{r}\frac{1}{kr}\frac{d}{dr}(rf_j)\right\}P_j^m \tag{A21}$$
$$=-(i/k)\nabla\times(\mathbf{L}f_jP_j^m).$$

These functions therefore satisfy

$$\nabla\times\Phi_1=0,\quad \nabla\cdot\Phi_2=0,$$

and are thus to be identified as the longitudinal and transverse fields of an electric $2j$-pole.

DECEMBER 1, 1940 PHYSICAL REVIEW VOLUME 58

On the Theory of Recombination

GEORGE JAFFÉ
Louisiana State University, University, Louisiana

(Received October 5, 1940)

In Section I a general formula for α, the coefficient of recombination of ions in gases, is developed. It covers all ranges of pressures and temperatures and can be made to include all types of recombination (preferential, initial and volume ionization). The evaluation of the general formula, (1.1), depends on the relative values of three linear quantities: the mean free path of the ions λ, the mean distance between ions of different signs $\bar{r}$ and the well-known parameter $a_0=e^2/(kKT)$. In Section II the case $\lambda\ll a_0$ is treated. The mechanism of recombination then depends on the ratio $a_0/\bar{r}$. If $a_0/\bar{r}$ is large the migration of the ions under their mutual attraction prevails and (1.1) leads to Langevin's formula; in the opposite case, $a_0/\bar{r}\ll1$, diffusion is the decisive feature and 1.1 leads to a formula which is practically identical with that of Harper. In Section III the case $\lambda\gg a_0$ is treated by a method previously developed by the author. Under certain restrictions (1.1) reduces to Thomson's formula, but in general α depends on the concentration of the ions. In Section IV it is shown that (1.1) is in fair agreement with such experimental data as are available for the region of transition between the cases treated in Sections II and III.

THE problem of recombination of ions in gases under varying conditions of ionization, pressure and temperature has proved to be much more complex than was originally anticipated. Various types, such as preferential, initial and volume recombination are involved.[1] It has been recognized in recent years that the two most important theoretical formulae for the coefficient of recombination, that of Langevin and that of Thomson, have separate domains of applicability. Harper[2] and Loeb[3] have given formulae which bridge the expressions of Langevin and Thomson in a formal way, but it

[1] For the definition of these types and a survey of the whole subject see the excellent treatment in: L. B. Loeb, *Fundamental Processes of Electrical Discharge in Gases* (John Wiley and Sons, New York, 1939).

[2] W. R. Harper, Phil. Mag. **18**, 97 (1934); **20**, 740 (1935).
[3] L. B. Loeb, Phys. Rev. **51**, 1110 (1937).

seems desirable to establish a general theoretical expression from which either of them, and eventually others, can be derived. It is the object of the following paper to give a theory that covers the whole range of physical conditions and that can be made to include the various types of recombination.

I. The General Formula

We start by defining three probabilities. Let n_+ and n_- be the instantaneous average volume densities of positive and negative ions, respectively. The ionization is considered to be homogeneous in a macroscopic sense and no preferential directions are assumed to exist. Still, in order to include preferential and initial recombination, we shall admit microscopic inhomogeneities. Then let $p_1(r)n_-d\tau$ be the probable number of negative ions which are located in an element of volume $d\tau$ at a distance r (irrespective of direction) from a positive ion.

By $p_2(r)dr$ we define the probability that the nearest neighbor to a positive ion is to be found at distances between r and $r+dr$. Evidently we have to have

$$\int_{r_m}^{\infty} p_2(r)dr=1,$$

if r_m is the nearest distance of approach for two ions of different signs.

Further, let $p_3(r)$ signify the probability of recombination. That is, of dN_r pairs of nearest neighbors of different signs which are at distances between r and $r+dr$, $p_3(r)dN_r$ are supposed to recombine on the average. This probability concept replaces the strict criterion for recombination which other authors[4] have tried to establish.

Finally, we have to define the velocity of approach of two nearest neighbors of different signs. If they are at a distance r apart, $u(r)$ is to signify the average component, in the direction of r (from the negative to the positive ion), of the relative velocity. This is supposed to be the resultant of all acting influences, i.e., diffusion and electrostatic attraction. It might also be made to include the action of an external field, but we limit ourselves to the case where there is no such external field.

The expressions of n_+, n_-, p_1 and p_2 will, in general, be functions of the time, as it is our object only to calculate the instantaneous coefficient of recombination, α.

With these definitions it is easy to write down a general expression for α by generalizing Langevin's argument. In doing so we first fix our attention on such positive ions as have their nearest negative neighbors at distances between r and $r+dr$. There are $p_2(r)n_+dr$ positive ions of this class per cc. We consider each of them surrounded by a sphere of radius r. The number of negative ions crossing one of these spheres during a time interval Δt will be given by $4\pi r^2p_1(r)n_-u(r)\Delta t$. But not all these ions will ultimately move up to the positive center and recombine, but only the fraction $p_3(r)$ of them. Hence

$$4\pi r^2n_+n_-p_1(r)p_2(r)p_3(r)u(r)dr\Delta t$$

is the number of pairs (per cc) of the specified class which are to be considered as lost by recombination during Δt. Adding over all distances r and dividing by $n_+n_-\Delta t$ we obtain

$$\alpha=4\pi\int_{r_m}^{\infty} p_1(r)p_2(r)p_3(r)u(r)r^2dr \qquad (1.1)$$

as our general expression for the coefficient of recombination.

Before we try to evaluate (1.1) for special cases, a few words must be said regarding the physical significance of the various functions of r. First of all, the probabilities $p_1(r)$ and $p_2(r)$ determine the particular type of recombination. They are not independent of each other.

If the distribution is homogeneous also in the microscopic sense, i.e. if $p_1(r)=1$, and, furthermore, if the diameter of the ions can be neglected, the probability $p_2(r)$ is known. P. Hertz[5] has shown that, in a random distribution of points without extension (n per cc), $p_2(r)$ is given by

$$p_2(r)dr=4\pi nr^2\exp(-4\pi nr^3/3)dr. \qquad (1.2)$$

This law is modified, though only slightly, if, instead of points without extension, ions of

[4] (a) J. J. Thomson, Phil. Mag. **47**, 337 (1924); (b) L. B. Loeb and L. C. Marshall, J. Frank. Inst. **208**, 371 (1929); W. R. Harper, Proc. Camb. Phil. Soc. **28**, 219 (1932); **31**, 430 (1935).

[5] P. Hertz, Math. Ann. **67**, 387 (1909).

finite diameter have to be considered. It is, however, evident that this modification will be insignificant if the average separation of the ions is very large compared with their diameter, as in all cases of gaseous ionization. Then, also, r_m can be replaced by 0.

If $p_1(r)$ is a given variable function of r, it can be shown by an argument which is exactly analogous to that of Hertz that $p_2(r)$ will be determined by

$$p_2(r)dr = 4\pi r^2 n_- p_1(r) \exp(-n_- P(r))dr, \quad (1.3)$$

where

$$P(r) = \int_{r_m}^{r} 4\pi r^2 p_1(r)dr. \quad (1.4)$$

Thus when $p_1(r)$ is determined the probability $p_2(r)$ may be calculated. Bradbury[6] has recently determined $p_1(r)$ for the cases of preferential and initial recombination and, therefore, it would not be difficult to evaluate α for these types of recombination. However, we shall limit ourselves to the fundamental case of volume ionization with $n_+ = n_- = n$. Not even then is it permissible, in the strict sense, to replace $p_1(r)$ by 1. Owing to the electrostatic attraction there is a greater probability of finding a negative ion in an element $d\tau$ near a positive ion than in an equal element at a greater distance. This is conclusively shown by the theory of ionic atmospheres as developed by Debye and Hückel.[7] This theory is applicable to our case, but for all cases of gaseous ionization the characteristic distance of the Debye theory is so large in comparison with the mean distance between two ions that this inhomogeneity may be disregarded.

For these reasons we shall, in all that follows, take $p_1(r) = 1$ and shall also replace r_m by 0 which amounts to determining $p_2(r)$ by (1.2).

The functions $p_3(r)$ and $u(r)$ depend on the mechanism of recombination which is effective under given circumstances. Their determination constitutes the specific difficulty of the problem. Before starting to effectuate this determination for particular cases we wish to emphasize that these evaluations are only approximate. Whereas our formula (1.1) claims to be exact and to cover the whole ground, the following calculations are only intended to give a survey of possible cases.

II. Special Case: λ Small in Comparison with a_0

The mechanism of recombination depends upon the relative importance of Brownian movement and migration under the mutual attraction of the ions. Whether the one or the other process is prevalent can be inferred from the ratio of two linear quantities: $\bar{r}$, the mean distance between an ion and its nearest neighbor of opposite sign, and a characteristic length defined by

$$a_0 = e^2/(KkT), \quad (2.1)$$

where e is the elementary charge, K the dielectric coefficient and k the Boltzmann constant. If $a_0/\bar{r}$ is large, migration is decisive, while, if $a_0/\bar{r}$ is small, Brownian movement predominates. This fact has been pointed out by Loeb and Harper and will be shown by our treatment in a somewhat different way.

A further distinction has to be introduced according to whether Brownian movement can be adequately described by the differential equation of diffusion or not, and this distinction depends upon whether the mean free path of the ions, λ, is small or large in comparison with a_0.

Boltzmann's fundamental equation must be considered the basis for every rigorous kinetic deduction. The author[8] has shown that the solution of Boltzmann's equation has to proceed along entirely different lines if the mean free path λ is small and if it is large compared with the linear dimensions concerned in the problem. The decisive length, in our case, is a_0. If, then, λ is small compared with a_0 the usual treatment by the differential equations of transport is adequate, though it represents only a first approximation.

From the study of the differential equation of *relative* Brownian movement Onsager[9] has deduced the following expression for the probability $p_3(r)$:

$$p_3(r) = 1 - \exp(-a_0/r). \quad (2.2)$$

[6] N. E. Bradbury, J. App. Phys. **11**, 267 (1940).
[7] P. Debye and E. Hückel, Physik. Zeits. **24**, 185 (1923).
[8] G. Jaffé, Ann. d. Physik **6**, 195 (1930).
[9] L. Onsager, Phys. Rev. **54**, 554 (1938).

It follows that a_0 is, in a certain way, the length which decides the fate of a pair of ions. Though there is no definite critical distance, the pair will recombine if $a_0/r \gg 1$ and will not recombine if $a_0/r \ll 1$.

To these two limiting cases correspond two entirely different mechanisms of motion. To show this we shall calculate the time which the one ion takes to travel the distance $\bar{r}$ relative to the other, upon the assumption that either migration in their mutual field or diffusion alone is effective.

If k_+ and k_- are the mobilities of the ions and if $r_m \ll \bar{r}$, the time required under the mutual attraction alone will be[10]

$$t_k = \bar{r}^3 K/[3e(k_+ + k_-)]. \tag{2.3}$$

If, on the other hand, diffusion alone were effective the corresponding time would be[11]

$$t_D = \bar{r}^2/[2(D_+ + D_-)], \tag{2.4}$$

D_+ and D_- being the coefficients of diffusion.

If t_D is very much shorter than t_k diffusion will be prevalent and vice versa. Hence the ratio

$$t_D/t_k = 3a_0/2\bar{r} \quad \text{(by 2.17)} \tag{2.5}$$

is decisive, as stated above.

The probability function (1.2) has a strong maximum for

$$r_0 = [1/(2\pi n)]^{\frac{1}{2}}. \tag{2.6}$$

Hertz has pointed out that this "most probable value" is numerically very little different from the "mean value"

$$\bar{r} = \Gamma(4/3) \cdot [3/(4\pi n)]^{\frac{1}{3}}, \tag{2.7}$$

and that both are well approximated by the value $5/9n^{\frac{1}{3}}$ which ought to replace the value $(1/n)^{\frac{1}{3}}$ usually adopted. For reasons which will become evident we shall use r_0 instead of $\bar{r}$.

Now we are prepared to treat the subsidiary limiting cases. If, besides $\lambda \ll a_0$, the ratio a_0/r_0 is large, migration will be prevalent. Then we have

$$u_k(r) = e(k_+ + k_-)/(Kr^2), \tag{2.8}$$

and for all significant values of r, namely those in the neighborhood of the maximum r_0, (2.2) yields

$$p_3(r) = 1. \tag{2.9}$$

Inserting these expressions into (1.1) and making use of (1.2), we find

$$\alpha_k = 4\pi e(k_+ + k_-)/K, \quad \lambda \ll a_0, \quad r_0 \ll a_0, \tag{2.10}$$

which is Langevin's formula.

If, on the other hand, a_0/r_0 is small diffusion prevails and we find from (2.2)

$$p_3(r) = a_0/r. \tag{2.11}$$

We still have to calculate $u(r)$ and it is this calculation which introduces a certain ambiguity. Because, according to the usual treatment of Brownian movement, a velocity in the proper sense does not exist, we must define $u(r)$ by some mean value. In doing so we start from the point-source solution for relative Brownian movement, i.e.,[12]

$$p(r, t) = \frac{1}{[4\pi(D_+ + D_-)t]^{\frac{3}{2}}} \times \exp\left(-\frac{r^2}{4(D_+ + D_-)t}\right). \tag{2.12}$$

Arguing in the usual way we might deduce from (2.12) the relation

$$\langle r^2 \rangle_{Av} = 6(D_+ + D_-)t, \tag{2.13}$$

but it must be remembered that this is the mean square of the distance traveled in time t. What is required in our case is the mean time required for a given displacement. This is found from (2.12) to be

$$\bar{t} = r^2/[2(D_+ + D_-)]. \tag{2.14}$$

By differentiating this expression we obtain an approximative value for $u(r)$. As, however, there remains a certain ambiguity regarding the numerical coefficient, we shall write

$$u_D(r) = f_1(D_+ + D_-)/r, \tag{2.15}$$

[10] In deducing (2.3) we have tacitly assumed that the mobilities are not affected by the very intense fields in the immediate neighborhood of the ions, but it must be remembered that we are only making an estimate.

[11] For an explanation of the numerical factor see paragraph containing Eq. (2.14).

[12] We have normalized (2.12) in such a way that $\int_0^\infty 4\pi r^2 p\,dr = 1$, i.e., $4\pi r^2 p$ represents the probability of finding two ions at time t at a distance r if, at time $t=0$, they are both at $r=0$. The solution (2.12) can be verified either directly as the point-source solution of the differential equation of *relative* Brownian movement (see for instance L. Onsager, J. Chem. Phys. 2, 599 (1934)), or it can be derived by multiplying the point-source solutions for a positive and a negative ion (relative to a fixed system of coordinates) and subsequent suitable transformation and integration.

where f_1 represents a numerical factor which is likely to be equal to 1 and certainly is of the order 1.

Introducing (2.11) and (2.15) into (1.1) we obtain

$$\alpha_D = f_1 4\pi(D_+ + D_-)a_0, \quad \lambda \ll a_0, \quad r_0 \gg a_0, \quad (2.16)$$

which is, but for the numerical factor, an equation previously deduced by Harper.[13]

Making use of Townsend's relation in the form

$$(D_+ + D_-)/(k_+ + k_-) = kT/e, \quad (2.17)$$

the expression (2.17) can be transformed into

$$\alpha_D = f_1 \alpha_k. \quad (2.18)$$

This shows the remarkable fact, previously observed by Harper, that the coefficient of recombination is practically (exactly, for $f_1 = 1$) the same, whether migration in the field or diffusion is alone effective, though, of course, the mechanisms are far different.

We shall see in Section IV that the case where r_0 and a_0 are comparable is of no practical significance. It is, however, easy to obtain an approximate solution which bridges the two limiting cases treated so far. As a first, rough, approximation it will be legitimate to assume that $u(r)$ will then be a simple superposition of the expressions (2.8) and (2.15). Introducing this superposition and the general expression (2.2) into (1.1) we obtain

$$\alpha = 4\pi \int_0^\infty (1 - e^{-a_0/r}) \times (e(k_+ + k_-)/K + f_1(D_+ + D_-)r)p_2(r)dr, \quad (2.19)$$

where $p_2(r)$ is given by (1.2). As the function (1.2) has a strong maximum for $r = r_0$ we obtain a good approximation for (2.19) by using the saddle-value method. Remembering (2.17) we can write the result in the form:

$$\alpha = 4\pi(D_+ + D_-)a_0(1 - e^{-z})(1 + f_1/z), \quad \lambda \ll a_0, \quad (2.20)$$

where we have put

$$z = a_0/r_0. \quad (2.21)$$

It will be noticed that in the limiting cases $z \gg 1$ and $z \ll 1$ formula (2.20) leads back to (2.10) and (2.16), but that in all other cases α is dependent on z, i.e., on the concentration of the ions.

[13] W. R. Harper, reference 4(*b*).

III. Special Case: λ Large in Comparison with a_0

With this restriction conditions are analogous to those prevailing in "molecular flow." The solution of problems of this type can be developed[8] into a series which progresses with powers of λ^{-1}.

We shall split the probability $p_3(r)$ into two factors, the probability $p_3'(r)$ that two neighboring opposite ions which are at a distance r will be caught into related closed orbits, and the probability p_3'' that, subsequently, actual recombination takes place. The probability $p_3'(r)$ could be calculated rigorously by successive approximations and even the curvature of the paths could be taken into account (reference 8, §4). The problem offers a comparatively simple application of the method developed by the author since no boundaries have to be considered. Still, some law of interaction between the ions and the neutral molecules would have to be accepted and the evaluations would be very involved.

For these reasons we shall adopt an approximative procedure which is based on the analogy with the theory of heat radiation. In the zero approximation collisions are altogether disregarded and the ions are considered to be "emitted" from each element of volume isotropically with their mean velocity.

We start again by considering a positive ion A which is supposed to be at rest and has its nearest negative neighbor B at a distance between r and $r+dr$. The two ions will, on the average, form closed orbits if B approaches A within a distance less than[4]

$$d = 2e^2/(3KkT) = 2a_0/3. \quad (3.1)$$

We are only interested in the case $d \ll r$. Then we shall have in our present approximation

$$p_3'(r) = (1/4\pi)(d^2\pi/r^2) = d^2/4r^2 \quad (3.2)$$

and

$$u(r) = c_{12}, \quad (3.3)$$

where c_{12} is the average relative velocity.

Assuming provisionally $p_3'(r) = p_3(r)$ and inserting (3.2) and (3.3) into (1.1) we find as zero

approximation

$$\alpha_\lambda^{(0)} = \pi d^2 c_{12}. \tag{3.4}$$

This is, of course, the usual formula of the kinetic theory (for a cross section of radius d), and it becomes identical with the limiting value of Thomson's theory if we take

$$c_{12} = (\bar{c}_+^2 + \bar{c}_-^2)^{\frac{1}{2}}. \tag{3.5}$$

If, now, collisions occur, each of them is considered an act of "absorption" and "re-emission," the re-emission being equally probable in all directions and the velocity remaining, on the average, unaltered. Since the probability of a collision along an element of path ds is given by ds/λ, the reciprocal of the mean free path must be considered the "coefficient of absorption."

Let us again assume that a negative ion B is emitted at a distance r from its nearest positive neighbor A at an angle ϑ_1 with the line joining them. We obtain a first approximation by assuming that one, and only one, collision occurs outside the sphere of radius d around A. If the collision occurs at a distance r_1 from the starting point of B, at a point which is at a distance ρ_1 from A, B will have to travel a distance $r_1+\rho_1-d \sim r_1+\rho_1$ before being caught, and its average radial velocity (as required for (1.1)) will be $u(r)=c_{12}r/(r_1+\rho_1)$.

It simplifies matters to calculate in one step $\langle u(r)p_3'(r)\rangle_{Av}$, i.e., the average of the product for all possible loci of the collision. We obtain[14]

$$\langle u(r)p_3'(r)\rangle_{Av} = \frac{c_{12}d^2}{8\lambda}\int_0^\infty \frac{e^{-r_1/\lambda}dr_1}{r_1}\int_{\rho_{10}}^{\rho_{11}} \frac{d\rho_1}{\rho_1(r_1+\rho_1)}, \tag{3.6}$$

where

$$\rho_{11} = r+r_1, \quad \rho_{10} = [(r'-r_1)^2+d^2]^{\frac{1}{2}}, \quad r' = (r^2-d^2)^{\frac{1}{2}}. \tag{3.7}$$

The first integration in (3.6) is immediate, the second can be carried out to a good approximation since the function $r_1^2 \exp(-r_1/\lambda)$ has a pronounced maximum for $r_1=\lambda$. We thus find

$$\langle u(r)p_3'(r)\rangle_{Av} = \frac{c_{12}d^2}{8\lambda^2}\left\{\log\frac{r+\lambda}{r+2\lambda} - \log\frac{[(r'-\lambda)^2+d^2]^{\frac{1}{2}}}{[(r'-\lambda)^2+d^2]^{\frac{1}{2}}+\lambda}\right\} \tag{3.8}$$

$$= \frac{c_{12}d^2}{8\lambda^2}\varphi_1\left(\frac{d}{\lambda}, \frac{d}{r}\right).$$

In order to calculate α, we must remember that it consists now of two parts, the one being due to ions which are caught without having undergone a collision, and the second to ions which have made one collision. The first part we obtain by multiplying (3.4) by $\exp(-r_0/\lambda)$, the second by inserting (3.8) and (1.2) into (1.1) and evaluating by the saddle-value method. Thus we finally obtain

$$\alpha_\lambda^{(1)} = \pi d^2 c_{12}\left\{e^{-r_0/\lambda} + \frac{r_0^2}{2\lambda^2}\varphi_1\left(\frac{d}{\lambda}, \frac{d}{r_0}\right)\right\}$$

$$= \pi d^2 c_{12}\psi_1\left(\frac{d}{\lambda}, \frac{d}{r_0}\right). \tag{3.9}$$

The function ψ_1 approaches unity for small and large values of λ/r_0. Neglecting terms of the order $(d/r_0)^2$ we find

$$\alpha_\lambda^{(1)} = \pi d^2 c_{12}\left\{e^{-r_0/\lambda} + \frac{1}{2}\left(\frac{r_0}{\lambda}\right)^3 + \cdots\right\}, \quad \lambda/r_0 \gg 1, \tag{3.10}$$

and

$$\alpha_\lambda^{(1)} = \pi d^2 c_{12}\left\{1 - \frac{\lambda}{r_0} + \cdots\right\}, \quad \lambda/r_0 \ll 1. \tag{3.11}$$

For the latter case, however, our present approximation is not adequate. The author, therefore, has carried through the next approximation taking account of those ions B which reach A after two collisions. The result is too lengthy to be quoted *in extenso*. In the limiting case $\lambda/r_0 \ll 1$

[14] It must be pointed out that, in establishing (3.6), we have made use of (3.2) (with ρ_1 replacing r) for the probability of capture after the collision. However, this is not quite correct because it is not true that $d \ll \rho_1$ in the whole space of integration. The correct value of the solid angle determining capture would be $\Omega = 2\pi[1-(1-d^2/\rho_1^2)^{\frac{1}{2}}]$ rather than $\pi d^2/\rho_1^2$. We have carried out the calculations with this value and verified that the result is not noticeably different from (3.6).

In determining the region of integration we have omitted the whole solid angle Ω' subtended at B by the sphere of radius d. This means omitting the negligible probability of cases in which the ion remains inside Ω' in spite of a collision. The space inside Ω' behind the sphere has to be omitted.

Finally it must be remarked that (3.6) is not a symmetrical function of the ions A and B unless λ is taken as the average value for positive and negative ions. In a somewhat more rigorous deduction (3.6) would have to be replaced by its arithmetic mean for λ_+ and λ_-.

it is found

$$\alpha_\lambda^{(2)} = \pi d^2 c_{12}\left\{1 - \frac{2\lambda}{r_0} + 6\left(\frac{\lambda}{r_0}\right)^2 + \cdots\right\},$$

$$\lambda/r_0 \ll 1. \quad (3.12)$$

The comparison with (3.11) shows that the convergence of our procedure for this limiting case may be slow, though the essential feature, convergence towards $\pi d^2 c_{12}$ for $\lambda/r_0 \to 0$, is preserved.

So far we have identified $p_3'(r)$ with $p_3(r)$, i.e., we have assumed that each pair of ions which is caught into closed orbits will ultimately recombine. It is, however, evident from J. J. Thomson's well-known argument that this need not be the case. Therefore the α so far calculated has still to be multiplied by the probability p_3'' as defined above.

A rigorous calculation of this p_3'' would have to be based on a quantum-mechanical study of the interaction between ions and neutral molecules on the one hand and ions of different signs on the other. Such a study does not seem feasible at the present time. We may, however, accept Thomson's treatment as a first approximation, though it cannot hold down to zero pressure, as was pointed out by Loeb.[15]

The probability p_3'' as calculated by Thomson is given with sufficient accuracy by [16]

$$p_3'' = \varphi_2(d/\lambda) = 2\omega - \omega^2, \quad (3.13)$$

where

$$\omega = \left[1 - \frac{\lambda^2}{2d^2}\left\{1 - e^{-2d/\lambda}\left(\frac{2d}{\lambda} + 1\right)\right\}\right]. \quad (3.14)$$

Hence our final expression for α_λ becomes

$$\alpha_\lambda = \pi d^2 c_{12} \psi_1(d/\lambda,\ d/r_0)\varphi_2(d/\lambda), \quad \lambda \gg d. \quad (3.15)$$

This result, though intimately connected with Thomson's, is distinguished from it by two essential features: It depends upon d/r_0, i.e., upon the concentration of the ions, and it gives a marked maximum for α_λ at $r_0 = \lambda$, as can be shown from the form of $\varphi_1(d/\lambda,\ d/r_0)$. Sufficiently above pressures where $r_0 \sim \lambda$, and for ionizations sufficiently weak to make d/r_0 a small number, ψ_1 can be approximated by 1 (see (3.11) and (3.12)) and our formula reduces to Thomson's

$$\alpha_\lambda = \pi d^2 c_{12}\varphi_2(d/\lambda), \quad \lambda \gg d, \quad d \ll r_0. \quad (3.16)$$

IV. Discussion and Comparison with Experiment

We have seen that our general expression (1.1) reduces, for well-defined special conditions, to the formulae of Langevin, Harper and Thomson. However, it must be emphasized that only under the restrictions specified by (2.10), (2.16), and (3.16) does the coefficient of recombination become independent of the ionic density, n. The transitional formulae, (2.20) and (3.15), involve the parameter

$$q = d/r_0 = 2a_0/3r_0 = d(2\pi n)^{\frac{1}{2}}. \quad (4.1)$$

It seems to be generally accepted that the Langevin formula holds with adequate accuracy for sufficiently high pressures. As pointed out by Harper, this does not prove the correctness of the mechanism by which Langevin deduced his formula, as shown by the formal similarity between the expressions for α_k and α_D (see (2.18)).

It is pretty certain that in no direct experiments on volume recombination is the migration of the ions under their mutual attraction the predominant feature. The highest observed values of n are of the order 10^7 ions per cc. Even in liquid dielectrics (which behave in this regard like very dense gases) n never rises above 2×10^8. The corresponding values of r_0 are 2.5×10^{-3} and 0.92×10^{-3}. As $d = 4.05\times10^{-6}273/T$, q is never larger than about 4×10^{-3} and in most cases is considerably smaller. Under these circumstances diffusion prevails and the agreement of experimental data with Langevin's formula really proves the diffusion formula (2.16).

There is, however, indirect evidence for the correctness of Langevin's formula, including its mechanism. The theory of columnar ionization, as developed by the author, seems to be generally accepted for the ionization with heavy particles. The fundamental concept of this theory is that, inside the columns, recombination (and diffusion) take place according to the usual laws and with the same coefficients as in cases of more homogeneous ionization.

[15] See reference 1, p. 130.
[16] See reference 1, p. 119. The function φ_2 is found tabulated there.

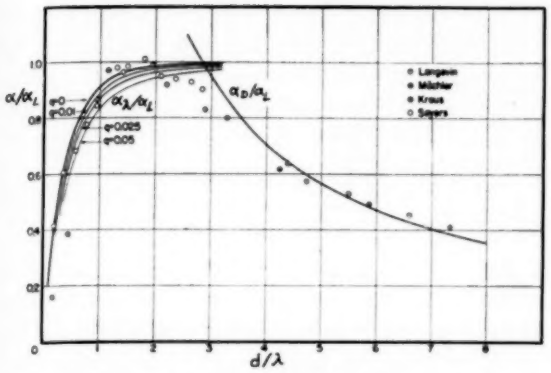

FIG. 1. The diagram represents α/α_L as a function of d/λ. The curves for α_λ/α_L are calculated from (3.16) and (3.12) for various values of q, and the curve for α_D/α_L is calculated from (4.3) with $f_1=f_2=1$. The observational points are reduced values.

The initial concentration in the axis of a column[17] is of the order of 5×10^9 in air of atmospheric pressure and rises in liquid hexane to 2.50×10^{18}, giving values of q from 1.2×10^{-2} to 9.5. This brings columnar ionization in dense gases within the scope of formula (2.20)[18] and for liquid dielectrics even of (2.10). Thus the agreement of the columnar theory with experimental facts indirectly confirms Langevin's theory.

At low pressures, say up to 1 atmos., Thomson's theory seems to give an adequate representation of experimental facts. That is to be expected from our theory as long as λ is somewhat larger than d and, at the same time the pressure is sufficiently high to make λ smaller than r_0.

In the region where λ becomes comparable with d neither the formula for α_D nor that for α_λ is a sufficiently good approximation for our general formula (1.1), as they are only first steps in the evaluation for $\lambda/d\ll1$ and $\lambda/d\gg1$, respectively. Theoretically, it would be possible to carry the two approximations on until they meet, but practically, that is out of the question. The failure is, however, not due to a breakdown of the fundamental concepts (as in the case of Langevin's or Thomson's theory beyond their domains of applicability) but to our inability to evaluate the general formula (1.1). Conditions are thus exactly the same as in the transition from Poiseuille's "frictional flow" to Knudsen's "molecular flow."

As is well known, the critical region is in the neighborhood of atmospheric pressure, since $\lambda=1\times10^{-5}\,(760/p)(\lambda/\lambda_a)$ where λ/λ_a is the ratio of the mean free path of the ion to that of a molecule in air at NTP.[19] For this region of transition it must be tested whether the two approximations approach each other sufficiently to make a graphical interpolation possible.

According to (3.16) α_λ is given as a function of d/λ, whereas α_D is represented by (2.16) as a function of $(D_+ + D_-)$. To reduce the two representations to common terms we must represent D_+ and D_- by atomic data and this reduction introduces a further ambiguity. For our purpose it will suffice to introduce a mean coefficient of diffusion, defined by $D=(D_+ + D_-)/2$, a mean velocity $\bar{c}=(\bar{c}_+ + \bar{c})/2$, and write

$$D=f_2\bar{c}\lambda/3, \tag{4.2}$$

where λ is also the average value for positive and negative ions and f_2 a numerical factor. According to the usual elementary theory f_2 is unity, but we insert the factor f_2 of order 1 to leave room for the improvements of the more elaborate theories.

Making use of (4.2) and (3.1) and remembering that $c_{12}=2^{\frac{1}{2}}\bar{c}$, we find

$$\alpha_D=\pi d^2 c_{12}\cdot f_1 f_2 2^{\frac{1}{2}}\lambda/d. \tag{4.3}$$

If we introduce the limiting value $\alpha_L=\pi d^2 c_{12}$ we see that both α_D/α_L and α_λ/α_L, the latter given by (3.16), are universal functions of d/λ. We have represented these two functions by the heavy lines of Fig. 1, choosing $f_1=f_2=1$. It will be seen that a fair representation of α/α_L for all values of d/λ can be gained by the two approximations from either side, though, of course, we have no quantitative criterion to show at which particular values of d/λ the deviations become noticeable.

As to the agreement with empirical data we are of the opinion that neither the present state of experimental research nor our evaluations of Sections II and III would justify a comparison of absolute values. Therefore we have adopted a procedure of testing relative values. As α/α_L

[17] G. Jaffé, Ann. d. Physik **32**, 152 (1910); H. J. van der Byl, Ann. d. Physik **39**, 170 (1912).

[18] According to (2.20) the coeff. of rec. does not vary much with q. Assuming $f_1=1$, α has a maximum, for $a_0/r_0\sim2$, which is about 30 percent higher than the values at the extremes.

[19] L. B. Loeb, reference 1, p. 118.

should be a universal function of d/λ, we have tried to reduce the α-scale, as well as the p scale, in such a way that the experimental values fit the theoretical curves. This, of course, amounts to taking c_{12} (or the mass of the ion) and λ as two constants which are to be determined experimentally.

All measurements of α in air in the interval between 1 and 8 atmos. have been included. These are the measurements of Langevin, Mächler, Kraus and Sayers.[20] The values adopted for $\alpha_L \cdot 10^6$ are, respectively, 1.83, 1.71, 1.70 and 2.35 and the values for λ/λ_a 0.40, 0.41, 0.33, 0.26, respectively.[21]

It will be seen that the points thus determined seem to confirm the theoretical curve, but we do not want to stress this kind of agreement. Measurements in the indicated interval which include the determination of α and the mobilities in the same sample of gas are an urgent desideratum. The differences among the values of α_L and of λ/λ_a, as assumed above, are probably due to the fact that different observers have been dealing with ions of different age and nature.

So far we have limited our discussion to the case where the parameter q is very small, which reduces the more general expressions (2.20) and (3.15) to the simple forms (2.16) and (3.16). To illustrate the influence of q we have calculated α_λ/α_L from (3.12) for the values $q=0.01$, 0.025 and 0.05 and inserted the curves into the diagram.

It will be seen that α_λ/α_L decreases with increasing q and that means with increasing n.[22] A dependence of α on the concentration of the ions signifies that the simple law $dn/dt=-\alpha n^2$ ceases to hold, but the change of α predicted by theory is so slow that it seems adequate to retain the formal law and to speak of a variation of α with concentration. This procedure has always been adopted by experimenters.

It is well known that the coefficient of recombination, as determined experimentally, is not constant. Even after the stage of initial recombination is over, α goes on changing for a considerable time. This lack of constancy has been explained[23] by a gradual change in the nature of the ions and there can hardly be a doubt that this is the correct interpretation. The aging of ions will generally tend to decrease α with time and, therefore, with decreasing ionic density, as is also confirmed by the corresponding effect on the mobilities. Apart from this aging effect, however, all recent observers[23] have noticed that α is *larger* for lower values of the ionic concentration. The author is of the opinion that this dependence, which coincides in direction with that predicted by the present theory, is a genuine effect not due to secondary causes. The few quantitative data which are available indicate that the observed effect is considerably larger than the effect foreseen by our theory. This, however, is only true as long as the ionization is supposed to be homogeneous in all cases. The effect would be much stronger if, for the lower ionic densities, the initial inhomogeneity became more marked, an effect for which there are distinct indications.[24] The dependence of α on ionic density is the second point where an extension of experimental evidence is desirable.

We do not want to dwell here on the question of recombination at very low pressures. We have observed (p. 974), however, that, under conditions where $\lambda \sim r_0$, something like selective recombination should occur according to Eq. (3.15).[25] This fact shows how careful one ought to be in extending Thomson's formula to very low pressures, whether in the atmosphere or the discharge tube. This point requires further study, but the study will, no doubt, be complicated by the fact that in the same interval of pressures the carriers of electricity change character.

The author wishes to express his gratitude to the Department of Physics of the University of Colorado for courtesies extended.

[20] P. Langevin, Ann. Chim. Phys. **28**, 289, 433 (1903); W. Mächler, Zeits. f. Physik **104**, 1 (1936); P. Kraus, Ann. d. Physik **29**, 449 (1937); J. Sayers, Proc. Roy. Soc. **A169**, 83 (1938).

[21] All measurements refer to "room-temperature," but the exact values are not given in some cases. As d depends on the temperature this ought to be known for a more exact evaluation. We have chosen $t=18°$. Furthermore, Sayers' values had to be taken from his diagram.

[22] A change for α_D is hardly to be expected for realizable values of n, as long as volume ionization only is considered.

[23] L. C. Marshall, Phys. Rev. **34**, 618 (1929); O. Luhr, Phys. Rev. **35**, 1394 (1930); M. E. Gardner, Phys. Rev. **53**, 75 (1938); J. Sayers, reference 20.

[24] A. D. Power, J. Frank. Inst. **196**, 327 (1923).

[25] The maximum indicated by 3.15 is *not* erased by the next approximation, but a second minor maximum is added for $r_0=2\lambda$.

The Magnetic Properties of the Iron Group Anhydrous Chlorides at Low Temperatures

I. Experimental*

C. STARR, F. BITTER AND A. R. KAUFMANN
Massachusetts Institute of Technology, Cambridge, Massachusetts

(Received October 11, 1940)

The magnetic susceptibility of the anhydrous chlorides of the iron group have been studied as a function of field strength up to 32,000 gauss and as a function of temperature down to 13.9°K. Those compounds whose room temperature susceptibility characteristic indicates a positive Curie temperature, also show a field strength dependence of the susceptibility at 13.9°K and 20.4°K. Chromic chloride has a very steep magnetization curve at these low temperatures, with a large initial susceptibility increasing with decreasing temperature. Ferrous, cobaltous, and nickelous chlorides have an S-type magnetization curve characterized by a small initial susceptibility which decreases with decreasing temperature, followed by a very large susceptibility and eventual approach to saturation, both increasing with decreasing temperature. The susceptibility of many of the compounds reaches a maximum at temperatures which do not appear to be correlated with the presence of field dependence, but these temperatures do correspond to the temperatures of known specific heat anomalies.

INTRODUCTION

THE behavior of the magnetic susceptibility of most paramagnetic substances at ordinary temperatures is adequately described by the Curie-Weiss law, $\chi(T-\Theta)=C$, where χ is the susceptibility, T is the absolute temperature, Θ is the Curie temperature, and C is a constant. Theoretical considerations indicate that the value of Θ is determined by the nature and magnitude of the interaction within the magnetic atoms (spin-orbit coupling) and between the magnetic atoms and their surrounding atoms. This latter interaction may be either between the magnetic atoms themselves, both dipole-dipole and exchange effects, or between the magnetic atoms and the crystalline (electric) field produced by the neighboring ions in the substance. When all interactions become negligible, as in a gas of free carriers of magnetic moment, Θ reduces to zero, and the susceptibility follows Curie's law, $\chi T=C$. A magnetic carrier may be considered as free when the energy required to rotate it against interaction forces is small compared to kT. Thus the deviations from Curie's law are sufficiently enhanced at low temperatures to be a valuable source of information concerning the interaction effects.

The anhydrous chlorides of the elements of the first transition series, the iron group, are of particular interest because the magnetic atoms are sufficiently concentrated to produce large interaction effects. In addition, the crystal structures of this group of compounds appears to be isomorphic, although crystal structure studies have not been made for all the compounds. This facilitates comparison between the atoms of varying magnetic moment. Finally, there seems to be no indication of any metallic or semiconducting behavior in these compounds, so the complication that electrical conductivity introduces into magnetic properties does not have to be considered.

The cryomagnetic anomalies associated with some of these compounds have been studied at the Kamerlingh Onnes Laboratory of the University of Leiden, with many interesting results. The present investigation is an elaboration of this work.

METHOD OF MEASUREMENT

The measurements were made with a Bitter type high field solenoid (magnet No. 1 of the M. I. T. magnet laboratory)[1] which permitted investigation up to 32,000 gauss. A nonhomo-

* Contribution No. 457 from the Research Laboratory of Physical Chemistry.

[1] F. Bitter, Rev. Sci. Inst. **10**, 373 (1939).

geneous field method (Curie) described by Bitter and Kaufmann[2] was used for the determination of the susceptibilities. The specimens consisted of the powdered compound sealed off in a thin-walled Pyrex ampoule. The lower part of the ampoule was shaped as a cylinder, 8 mm O.D. and 1 cm high, and this joined to a long tubular neck, 3 mm O.D. and 5 cm long. The cylindrical part of the ampoule was filled with the powder under inevstigation and a short glass-wool plug was placed in the neck to keep the powder in place. The ampoule was then filled with helium gas and sealed off at the top.

The experiments were carried on in a long Dewar flask (2 cm I.D.) which fitted in the magnet. A cylindrical copper working chamber, connected to and supported by a long, 9 mm supernickel tube, was placed within the Dewar at a suitable region of the magnetic field. The specimen tube hung within the copper chamber and was supported by a gold chain connected to one arm of an analytical balance. This arrangement permitted independent control of the atmosphere surrounding the specimen tube and of the refrigerant contained in the Dewar flask. The following fixed temperatures were used in the measurements: solid CO_2 (193°K), boiling N_2 (77.3°K), freezing N_2 (63.1°K), boiling H_2 (20.4°K), and freezing H_2 (13.9°K). For the liquid N_2 temperatures and above, H_2 gas was slowly passed out of the neck of the supernickel tube to prevent condensation of water and air on the specimen tube. For the temperatures made available by liquid H_2, helium gas was used in the working chamber.

Preparation of Specimens[3]

As a result of the extremely hygroscopic nature of the anhydrous chlorides of the iron group, all preparations and transfers were made in glass vessels, in vacuum or dry inert gases, and the final specimen tubes were sealed off with dry helium. The helium was used to insure rapid temperature equilibrium throughout the specimen at all the temperatures used.

$NiCl_2$, $CoCl_2$, $FeCl_2$, $MnCl_2$.—These compounds were all made from the C.P. hydrates. The hydrates were dehydrated in vacuum at 100 to 200°C. The resultant product, containing an appreciable quantity of oxychloride, was then heated in vacuum to about 650°C. The pure chlorides sublime and condense in characteristic crystals on the cold portions of the tube, the oxide impurities remaining behind. The sublimed crystals have a very high purity, and in the case of ferrous chloride, less than 0.1 percent of ferric ion was present.

$FeCl_3$, $CrCl_3$.—These were made from commercially available C.P. anhydrous sublimed material. They were resublimed in vacuum, the $FeCl_3$ at 250°C, the $CrCl_3$ at 650°C.

VCl_3.—Made by decomposition of VCl_4 at 160°C in dry CO_2. The VCl_4 was produced by reacting Cl_2 with V metal at 500°C.

VCl_2.—Made by reduction of VCl_3 at 500°C with H_2.

$TiCl_3$.—Made by reduction of $TiCl_4$, commercially available, at 650°C with H_2 and condensing the $TiCl_3$ on a cold surface.

$TiCl_2$.—Made by vacuum decomposition of $TiCl_3$ at 475°C.

$CuCl_2$.—Made by reacting Cl_2 with Cu at 400°C.

Results

The results of the measurements are shown in Figs. 1 and 2 and in Tables I and II, where χ is the susceptibility per gram mole and σ is the magnetization per gram mole in c.g.s. units. H is the field strength in gauss, and T is the absolute temperature in °K, unless otherwise specified. Figure 1 shows the reciprocal susceptibility as a function of temperature. Figure 2 shows the magnetization as a function of field strength for those compounds which exhibited a dependence of the susceptibility upon the field strength. For these latter compounds, the initial differential susceptibility, $\chi = d\sigma/dH$, is used in the reciprocal susceptibility plots.

The susceptibility constants given in Table I have all been corrected for the diamagnetism of the cation and anion. The susceptibility values used in the graphs are the total measured values, except in the case of the titanium compounds where the corrected values are used. The values

[2] F. Bitter and A. R. Kaufmann, Phys. Rev. **56**, 1044 (1939).

[3] The compounds were prepared by Professor R. C. Young of the M.I.T. Chemistry Department in collaboration with the first author.

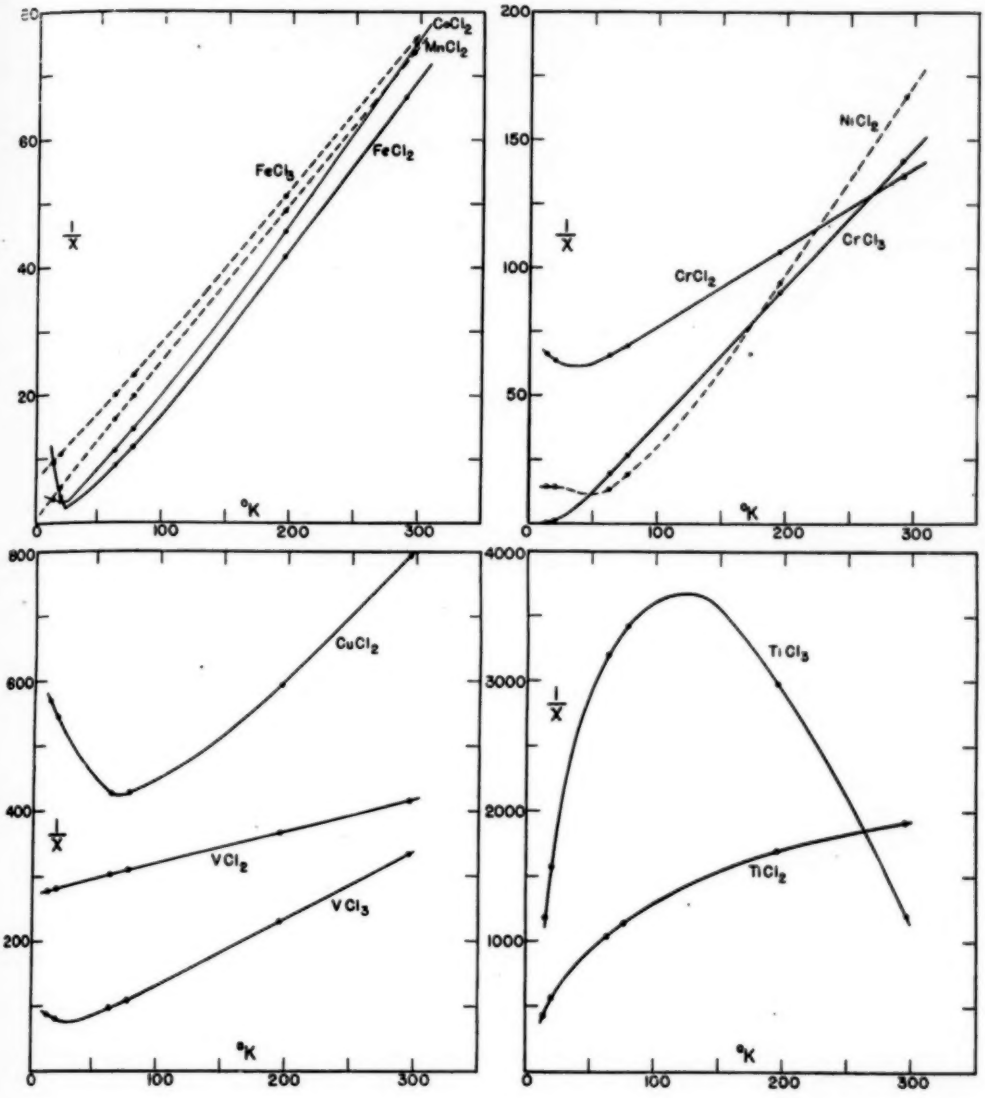

FIG. 1. The reciprocal susceptibility per gram mole as a function of the absolute temperature for $FeCl_3$, $FeCl_2$, $MnCl_2$, $CoCl_2$, $CrCl_3$, $CrCl_2$, $NiCl_2$, VCl_3, VCl_2, $CuCl_2$, $TiCl_3$ and $TiCl_2$. The correction for the diamagnetism of the cation and anions in $TiCl_3$ and $TiCl_2$ has been applied.

given in Table I for the diamagnetic susceptibility per gram mole, χ_d, have been calculated for the complete compound (cation plus anion) by the method of Angus[4] for modifying Slater's[5] formula for ionic diamagnetic susceptibilities. This modification is used since the empirical agreement is improved, although the theoretical basis of Slater's method is better.

The value of the Curie temperature* was determined from the slope of the reciprocal susceptibility *vs.* temperature curve at room temperature, corrected for the diamagnetic susceptibility. The effective number of Bohr magnetons, p, was calculated by means of the formula $p=2.84[\chi(T-\Theta)]^{\frac{1}{2}}$. The temperature of the maximum susceptibility given in Table I corresponds to the temperature of the reciprocal susceptibility minima (where such exist) in Fig. 1.

Specific heat studies of the nickel, cobalt, ferrous, manganous and chromic chlorides have

[4] W. R. Angus, Proc. Roy. Soc. **A136**, 569 (1932).
[5] J. C. Slater, Phys. Rev. **36**, 57 (1930).
* In this paper the term "Curie temperature" refers to the value of Θ found from the extrapolation of measurements made at comparatively high temperatures. The term "Curie point" refers to the actual temperature at which the magnetic behavior sharply changes in character, as determined by actual measurements in this temperature range. This distinction is similar to the usual distinction between the paramagnetic and ferromagnetic Curie point.

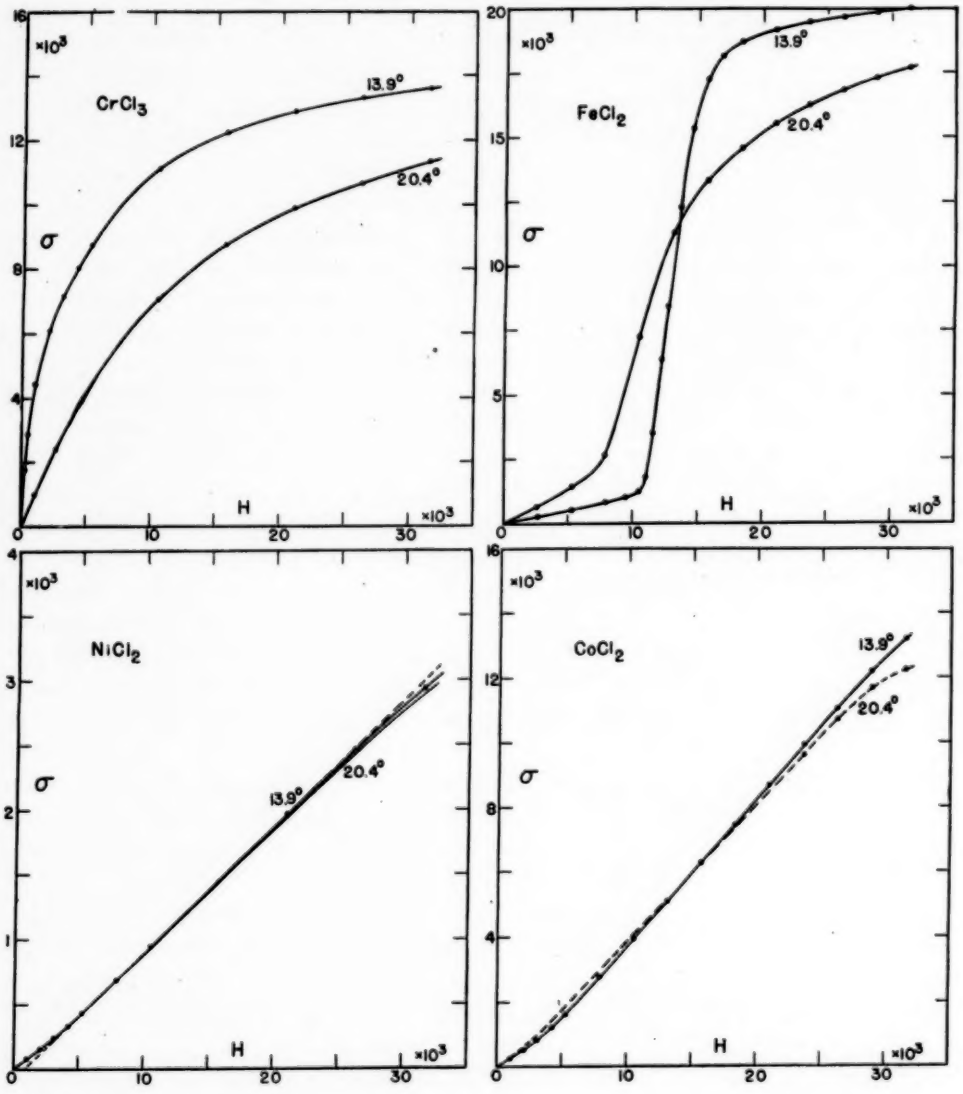

FIG. 2. The magnetization per gram mole as a function of the field strength at 20.4°K and 13.9°K of $CrCl_3$, $FeCl_2$, $NiCl_2$, and $CoCl_2$. In the case of $NiCl_2$ the dotted line represents the straight line continuation of the maximum slope of the curve. In order to maintain the clarity of the figure most of the experimental points on the 20.4° magnetization curve for $CoCl_2$ are not shown.

been made by Trapeznikowa and Schubnikow,[6] and their results, tabulated in Table I, show that the anomalies in the specific heats occur at temperatures which correspond closely to the temperatures of maximum susceptibility.

In Table II, the magnetization data are listed for the compounds, which showed a field dependence of the susceptibility at H_2 temperatures. The differential susceptibility (slope of the magnetization curve) is given for the temperature of boiling H_2, 20.4°, and freezing H_2, 13.9°, and both the initial and maximum values are presented. As can be seen in Fig. 2, the magnetization curves for 20.4° and 13.9° cross each other in the case of $FeCl_2$ and $CoCl_2$. The magnetization and field strength of this point of intersection is shown in Table II.

The precision of the results was not the same for all the specimens, and depended chiefly upon the magnitude of the forces involved. The analytical balance could detect changes of 0.1 milligram force, but this sensitivity could only be used with great difficulty because of the disturbance created by the gas escaping from the specimen chamber. This reduced the working sensitivity of the balance to about 1 milligram.

[6] O. Trapeznikowa and L. Schubnikow, Phys. Zeits. Sowjetunion 7, 66 and 255 (1935); O. Trapeznikowa, L. Schubnikow and G. Miljutin, Phys. Zeits. Sowjetunion 9, 237 (1936); O. Trapeznikowa and G. Miljutin, Phys. Zeits. Sowjetunion 11, 55 (1937).

The forces were usually between 1 gram and 100 grams for the highest field strengths. Generally, the accidental error in any measurement was about 0.1 percent. The sources of systematic errors were as follows: (1) calibration of the field and field gradient, (2) change of position of the specimen in the field caused by the stretching of the gold chain or thermal contractions, (3) errors in the weight of the compound in the specimen tube, and (4) error in the diamagnetic susceptibility correction for the Pyrex specimen tube and gold chain. These errors were probably of the order of magnitude of 1 percent. For specimens of very small susceptibility, such as the titanium compounds, the forces are very small and the correction (4) is relatively large, so that the systematic error may be 10 percent or more.

Another source of error was found in compounds with very large susceptibilities at liquid H_2 temperatures, such as $FeCl_2$. In these cases the forces on the individual crystals are sufficiently large to pack the crystals together. This causes the density of the specimen to be increased slightly, when the magnetic field is applied, in a manner not completely reversible. This packing effect results in an apparently increased magnetization of the specimen when the field is being decreased from its maximum value, as compared to the magnetizations at the same fields when the field is being increased to its maximum value. After repeated magnetizations at the highest fields, the measurements follow a reproducible hysteresis loop in which the difference between increasing and decreasing field points is about 1 percent. This difference could be greatly increased by shaking the specimen tube and loosening the cystals. Repeated magnetizations re-established the small hysteresis loop. For this reason, the curves in Fig. 2 have been plotted from measurements taken in the direction of decreasing field strength after stabilization by repeated magnetizations.

It is of interest that most of these compounds form layer lattice crystals, so that the individual crystal particles take the form of flat flakes. When packed into the specimen ampoule, the flakes tend to lie parallel to the base of the ampoule (i.e., at right angles to the direction of the field) Since the individual crystals are undoubtedly anisotropic, this results in a small anisotropy of the specimen. Serres[7] has found that this specimen anisotropy is about 1 percent at room temperature for $CrCl_3$ crystals. This type of specimen anisotropy was probably present in all the compounds studied.

The correction for the demagnetizing field has not been made, since it is not certain whether the specimen is behaving as a whole or each individual flat crystal is demagnetizing itself. The true magnetic field inside the crystals is $H_i = H_a - DI$, where H_a is the applied field, D is the demagnetizing coefficient, and I is the magnetization per unit volume. This leads to the formula $1/\chi_i = 1/\chi_a - D\rho/M$, where χ_i and χ_a are the gram mole differential susceptibility $(d\sigma/dH)$ true and apparent, respectively, ρ is the density, and M is the molecular weight of the compound. The maximum correction would apply when the flat crystals are demagnetizing themselves individually; $D = 4\pi$ and ρ is the crystal density, and $D\rho/M = 0.3$ to 0.2 approximately. The minimum correction would apply when the specimen ampoule is demagnetizing as a whole; $D = 4$ and ρ is the specimen density (approximately $\frac{1}{2}$ the

TABLE I. *Susceptibility data for the anhydrous chlorides of the elements of the first transition series.*

Compound	$-\chi_g \times 10^6$	$\chi(T-\theta)$	p	θ	Temp. of Max. χ	Temp. Spec. Ht. Anomaly
$TiCl_3$	80.4	0.25	1.42			
$TiCl_2$	66.7	0.521	2.05	−702		
VCl_3	82.3	1.005	2.85	− 30.1	30	
VCl_2	66.9	2.13	4.15	−565		
$CrCl_3$	82.9	1.89	3.90	27.0	~20	16.8
$CrCl_2$	66.1	3.26	5.13	−149	~40	
$MnCl_2$	65.0	4.07	5.73	− 3.3		None
$FeCl_3$	82.5	4.07	5.73	− 11.5		
$FeCl_2$	63.9	3.59	5.38	48.0	24	23.5
$CoCl_2$	62.8	3.46	5.29	38.1	25	24.9
$NiCl_2$	61.8	1.36	3.32	68.2	~50	49.6
						57.0
$CuCl_2$	60.8	0.536	2.08	−109	~70	

TABLE II. *Magnetization data for the compounds whose susceptibility is a function of magnetic field strength.*

Compound	Differential Susceptibility Initial 20.4°	Initial 13.9°	Maximum 20.4°	Maximum 13.9°	Intersection Point σ	Intersection Point H
$CrCl_3$	0.947	6.75				
$FeCl_2$	0.248	0.102	1.88	4.27	11,700	13,500
$CoCl_2$	0.294	0.272	0.422	0.456	5900	14,800
$NiCl_2$	0.0700	0.0700	0.0961	0.0981		

[7] A. Serres, Ann. de physique 17, 5 (1932).

crystal density) and $D\rho/M=0.05$ to 0.03, which is about $\frac{1}{8}$ as much as in the maximum case. The demagnetizing correction is largest for the initial susceptibility of $CrCl_3$ at 13.9°, $\chi_a=6.75$. The maximum assumption would be more than sufficient to make this initial susceptibility infinite. The minimum assumption would make the true initial susceptibility about 9.0. At 13.9°, $FeCl_2$ has a maximum differential susceptibility, $\chi_a=4.27$. The maximum demagnetization assumption would make this differential susceptibility infinite. The minimum assumption would raise it to $\chi_i=5.1$. These demagnetization corrections are so very large as compared with the usual correction for paramagnetics because the above molar susceptibility for $CrCl_3$ is about 50 times as large as the value for dilute chromic compounds (spin-only value), and for $FeCl_2$ is about 20 times as large as the value for dilute ferrous compounds.

No remanences were observed in any of the specimens, within the sensitivity of the apparatus. The magnetizations were measured with the field first in one direction and then reversed. Any remanence would appear as a difference between the two sets of measurements. No such difference was observed. The recent Leiden measurements,[8] however, indicate that some of these compounds exhibit remanence. Inasmuch as the apparatus used for the Leiden work had a very high sensitivity their results may not be at variance with the present work.

Discussion and Comparison of Results

$CuCl_2$.—The specimen used contained sufficient impurity in the form of CuCl to invalidate the absolute values of the measured susceptibility. The relative values agreed very well with the Leiden measurements,[9] so the absolute values of the results were adjusted to agree with the Leiden susceptibility at room temperatures. The CuCl contributes only a diamagnetic correction. No field dependence of the susceptibility was found. The adjusted results are shown in Fig. 1.

$NiCl_2$.—The room temperature value of the susceptibility agrees very closely with that found by Serres[10] who reports a Curie temperature of 95°K. The field dependence at hydrogen temperatures agrees qualitatively with that found at Leiden.[11] The Leiden measurements show no dependence upon the temperature from H_2 temperatures to He temperatures, but their investigations went only to 20,000 gauss.

$CoCl_2$.—The room temperature value of the susceptibility agrees reasonably well with that of Fehrenbach[12] who found a Curie temperature at 26.6°. The recent measurements of deHaas and Schultz[8] do not agree with the older Leiden measurements,[11] but are in good qualitative agreement with the present work. They find a Curie temperature of 19°. They also report that the magnetization curves at boiling and freezing H_2 cross at a field of 6500 gauss, as compared with the 14,800 gauss in the present work. Their ratio of initial susceptibilities is about the same, although their values are lower.

$FeCl_2$.—The Leiden measurements[13] on this compound are very unsatisfactory as they used an incomplete Gouy method, and the results do not permit simple interpretation in terms of magnetization. They found indications of a maximum in the susceptibility at H_2 temperatures, the maximum decreasing and shifting to higher field strengths with decreasing temperature. The present results are at variance with this.

$FeCl_3$.—The room temperature results of Lallemand[14] agree very well with the present work. No field dependence was found at any temperature. The susceptibility deviates slightly at low temperatures from the Curie-Weiss law.

$MnCl_2$.—The present work agrees qualitatively with the Leiden measurements[15] on this compound, and is in good quantitative agreement with the room temperature results of Lallemand[14] and Fehrenbach.[12] At the temperature of freezing H_2 (13.9°) the expected beginning of paramagnetic saturation could be observed. No other field dependence of susceptibility was found.

[8] W. J. de Haas and B. H. Schultz, Physica **6**, 481 (1939); W. J. de Haas, B. H. Schultz and J. Koolhaas, Physica **7**, 57 (1940).

[9] W. J. de Haas and C. J. Gorter, Leiden Comm. 215a (1931).

[10] A. Serres, Ann. de physique **20**, 441 (1933).

[11] H. R. Woltjer, Leiden Comm. 173b (1925); H. R. Woltjer and H. Kamerlingh Onnes, Leiden Comm. 173c (1925).

[12] C. Fehrenbach, J. de phys. et rad. (7) **8**, 11 (1937).

[13] H. R. Woltjer and E. C. Wiersma, Leiden Comm. 201a (1929).

[14] A. Lallemand, Ann. de physique **3**, 97 (1935).

[15] H. Kamerlingh Onnes and E. Oosterhuis, Leiden Comm. 129b (1912).

$CrCl_2$.—The work of Serres[7] at room temperature agrees very well with the present work. Serres reports a Curie temperature of $-115.5°$. Lips[16] studied this compound down to 55°K, and his values, which indicate a Curie temperature of $-128°$, are in excellent agreement with the present ones. No field dependence of the susceptibility was found.

$CrCl_3$.—The Leiden results[11] are in good agreement with the present work on this compound. It is of interest that this compound was the only one that exhibited simple, steep magnetization curves. In this connection it should be noted that the Curie point indicated by the specific heat measurements is 16.8°, although the field dependence of the susceptibility occurs above this temperature as well as below.

VCl_2, VCl_3.—The previous work of Klemm and Hoschek[17] down to 90°K is in good quantitative agreement with the present results. No field dependence of the susceptibility was found at any temperature.

$TiCl_2$, $TiCl_3$.—These compounds have not been investigated before, probably because of the chemical difficulties involved in their production. The dependence of their susceptibility upon temperature is completely different from that of the other compounds. No field dependence of the susceptibility was found. The values shown in Table I for $TiCl_3$ were calculated from the room temperature value of the susceptibility, with Θ assumed equal to zero.

Summary

The salient features of the experimental results may be summarized as follows:

(1) None of the compounds showed any dependence of the susceptibility upon field strength at temperatures above 63°K.

(2) At H_2 temperatures (13.9° and 20.4°) a dependence of the susceptibility upon field strength was found for $NiCl_2$, $CoCl_2$, $FeCl_2$, and $CrCl_3$. These compounds are the only ones which exhibit positive Curie temperatures (Θ) at room temperature.

(3) In the case of $CrCl_3$ the specific heat anomaly indicates a Curie point of 16.8°K. A field dependence of the susceptibility was found above this temperature, as well as below. The initial susceptibility increases with decreasing temperature and may be infinite, or very large, at 13.9° if the demagnetization correction is applied.

(4) $FeCl_2$ exhibits an S-type magnetization curve at H_2 temperatures. This magnetization curve is characterized by a very small initial susceptibility which decreases with decreasing temperature, followed by a very large differential susceptibility and eventual approach to magnetic saturation, both increasing with decreasing temperature. $CoCl_2$ and $NiCl_2$ exhibit this S-type magnetization curve in lesser degree.

(5) $MnCl_2$ exhibits no deviations from the Curie-Weiss law, although its crystal structure is very similar to that of the other anhydrous dichlorides.

(6) Many of the compounds exhibit a minimum in the reciprocal susceptibility *vs.* temperature curve, but apparently this is not necessarily connected with any field dependence of the susceptibility.

The authors express their appreciation for the encouragement and cooperation given by Professor F. G. Keyes, and their thanks for the aid rendered by Professor R. C. Young in the chemical preparation of the compounds.

[16] E. Lips, Helv. Phys. Acta **7**, 537 (1934).
[17] W. Klemm and E. Hoschek, Zeits. f. anorg. allgem. Chemie **226**, 359 (1936).

The Magnetic Properties of the Iron Group Anhydrous Chlorides at Low Temperatures

II. Theoretical*

C. STARR
Massachusetts Institute of Technology, Cambridge, Massachusetts
(Received October 11, 1940)

A theoretical study is made of the experimental results reported in Part I. The predictions of paramagnetic theory are compared with the room-temperature results, and an attempt is made to explain some of the departures from theory in terms of the crystalline field. The low temperature experimental anomalies require the development of a theory of metamagnetism. The assumption is made that at temperatures below the Curie point neighboring atoms behave as groups, which are spontaneously formed at the Curie point. The atomic magnetic moments within each group are assumed to be either parallel or antiparallel to each other, and the antiparallel arrangement is assumed to have the lowest energy. The theory developed on these assumptions satisfactorily explains the general behavior of the metamagnetic chlorides ($CrCl_2$, $FeCl_2$, $CoCl_2$, and $NiCl_2$), and also gives a qualitative explanation of the behavior of the other anhydrous chlorides which exhibit a minimum in the reciprocal susceptibility *vs.* temperature curve but do not show any field dependence of the susceptibility.

INTRODUCTION

THE results of the experimental investigation of the magnetic properties of all the anhydrous chlorides of the first transition series, the iron group, have been reported in the preceding paper, Part I.[1] It is the purpose of this paper to present a qualitative theoretical analysis of these results, especially the anomalous magnetization characteristics which are associated with the lowest temperatures used in the investigation. In order to facilitate the discussion of the results a brief review of present paramagnetic theory will be given. For a detailed treatment of this subject reference should be made to Van Vleck[2] and Stoner.[3]

The paramagnetic susceptibility of atoms in a given j state results from the statistical distribution of the atoms among the various energy levels which are associated with the removal of the degeneracy of the j state by the applied magnetic field. The determination of the various energy levels and the removal of their degeneracy by applied fields or interaction effects is the basic problem in determining the susceptibility of paramagnetic compounds. The normal or "ground" state of an atom is determined by the Hund stability rules. These rules specify that in the lowest term the spin momenta combine to give the maximum resultant value of s consistent with the Pauli exclusion principle, and then the orbital momenta combine to give the maximum resultant value of l; for an incomplete shell of electrons the lowest term $j=l-s$ when the shell is less than half full, and $j=l+s$ when the shell is more than half full. As a result of the various possible combinations of a given resultant s and l, j can assume the values $l+s$, $l+s-1$, $\cdots|l-s|$. This results in a natural multiplet of energy levels, in which the difference in energy between different j values is determined by the strength of the interaction between l and s. In the case of wide multiplets, the energy of transition between successive j states is very large compared to kT, the ls coupling is strong, and nearly all the atoms are in their ground state. In the case of narrow multiplets the energy of transition between successive j states is very small compared to kT, the ls coupling is very weak so that the orbital and spin momenta are quantized separately. It has been shown that the presence of an asymmetrical electrostatic field surrounding an atom may render the l moment partially or completely

* Contribution No. 458 from the Research Laboratory of Physical Chemistry.
[1] See preceding paper "Part I, Experimental."
[2] J. H. Van Vleck, *The Theory of Electric and Magnetic Susceptibilities* (Oxford University Press, New York, 1932).
[3] E. C. Stoner, *Magnetism and Matter* (Methuen and Company, London, 1934).

ineffective by producing a preferred orientation electrostatically, and thus hinder the response to an applied magnetic field. This is similar to the Stark effect. The s moment is unaffected directly by the electrostatic field. In the case of paramagnetic solids the electrostatic "crystalline" field, due to the atoms surrounding the one under consideration, may thus be responsible for the "quenching" of the orbital moment, so that only the spin moment contributes to the magnetic susceptibility.

The theoretical limiting cases for the susceptibility of paramagnetic atoms may be given by the following formulae. The susceptibility per gram mole $\chi_m=(N\mu_B^2p^2/3kT)$, where N is Avogadro's number, μ_B is the magnetic moment of one Bohr magneton, k is the Boltzmann constant, T is the absolute temperature, and p is the effective number of magnetons per atom.

Wide multiplets: $h\nu(jj')\gg kT$

$$p=g[j(j+1)]^{\frac{1}{2}},$$

where g is the Landé splitting factor.

Narrow multiplets: $h\nu(jj')\ll kT$

$$p=[l(l+1)+4s(s+1)]^{\frac{1}{2}}.$$

Spin only: $p=[4s(s+1)]^{\frac{1}{2}}$.

In the case of wide multiplets, a temperature-independent susceptibility term should be added to the above susceptibility. If the multiplet width is very wide this term is negligible. When the multiplet width is comparable with kT, the statistical distribution of the atoms over all the j states must be considered and more detailed formulae must be used. These are presented in the detailed references.

Table I contains the tabulation of the above limiting p values for the iron group ions. These may be compared with the experimental values found in Part I. The experimental p values are determined from the characteristics of the reciprocal susceptibility *vs.* temperature curve at room temperature. Excluding the uncertain p values for the titanium ions, several generalizations may be drawn from Table I. The Mn^{2} and Fe^{3} ions have a ^6S ground state and, theoretically, they should exhibit the spin-only value. The experimental p value is actually less than the spin-only value. This result cannot be attributed to experimental error. The excellent agreement of the experimental p values of the Mn^{2} and Fe^{3} ions is a strong indication of the validity of the results. There is also no question concerning the chemical purity of the compounds (see Part I). Table I also shows that in the trichlorides, Cr^{3} and V^{3} have experimental p values that agree very well with the spin-only values, while in their corresponding dichlorides the experimental p values are considerably larger than the spin-only values. It would thus appear that the orbital magnetic moment is almost completely quenched in the trichlorides and only partially quenched in the dichlorides. When considering the effect of the number of electrons in the $3d$ orbit, it is of interest that although the theoretical spin-only values are symmetrical about the half-filled shell (5 electrons), the experimental p values are larger for the ions in the second half of the shell (5–9 electrons) than in the corresponding ions (same s values) of the first half (1–5 electrons).

Crystalline Field Effects

The theoretical treatment of the effects of the electrostatic crystalline field upon the orbital magnetic moment has been developed by Van Vleck.[2] The action of the crystalline field may be described as a removal of the degeneracy of the resultant orbital moment of the ion. As in the case of narrow multiplets separate quantization of the orbital and spin moments is assumed, since the crystalline field acts directly only on the orbital moment. If the decomposition of the

Table I. *Calculated and observed magneton numbers effective in the ions of the first transition series. N is the number of electrons in the 3d orbit.*

N	Ground State	l	s	j	Effective Number of Bohr Magnetons: Wide Multiplets	Narrow Multiplets	Spin Only	Exp.	Ion
1	$^2D_{3/2}$	2	½	3/2	1.55	3.00	1.73	(1.42)	Ti^{3}
2	$^3F_2$	3	1	2	1.63	4.47	2.83	(2.05)	Ti^{2}
								2.85	V^{3}
3	$^4F_{3/2}$	3	3/2	3/2	0.77	5.20	3.87	4.15	V^{2}
								3.90	Cr^{3}
4	$^5D_0$	2	2	0	0.00	5.48	4.90	5.13	Cr^{2}
5	$^6S_{5/2}$	0	5/2	5/2	5.92	5.92	5.92	5.73	Mn^{2}
								5.73	Fe^{3}
6	$^5D_4$	2	2	4	6.70	5.48	4.90	5.38	Fe^{2}
7	$^4F_{9/2}$	3	3/2	9/2	6.64	5.20	3.87	5.29	Co^{2}
8	$^3F_4$	3	1	4	5.59	4.47	2.83	3.32	Ni^{2}
9	$^2D_{5/2}$	2	½	5/2	3.55	3.00	1.73	2.08	Cu^{2}

orbital energy levels is very large, the ions will mainly reside in the lowest orbital level, and an applied magnetic field will not appreciably change the distribution among the levels. Since the susceptibility is determined by the change in the average energy per ion due to the applied magnetic field, the contribution of the orbital moment is thus effectively quenched. The spin moments remain effective although the freedom of the spins is hindered by the spin-orbit coupling. The magnitude of the deviation of the susceptibility from the spin-only value depends, to a first approximation, upon the ratio of the spin-orbit interaction energy (as determined from the free ion multiplet width) to the crystalline field splitting.

The detailed calculations have been made by Schlapp and Penney[4] for the ions Cr^3, Co^2, and Ni^2, which are all in F states ($l=3$). The crystalline field was assumed to consist of a strong field of cubic symmetry and a superimposed weak field of rhombic symmetry. As will be shown later, this type of field would be expected in the anhydrous chlorides. The effect of the cubic field upon the F state (7-fold orbital degeneracy) is to split it into one singlet level and two triply degenerate levels, the two latter being resolved completely by the rhombic field. In the case of Ni^2 and Cr^3 the singlet level is lowest, and since the splitting due to the strong cubic field is large, the susceptibility approaches the spin-only value. In the case of Co^2 the triplet level is lowest, and since the splitting due to the weak rhombic field is small, the effects are more complicated and large deviations from the spin-only value would be expected. The Hamiltonian function in a magnetic field H was assumed to be of the form

$$D(x^4+y^4+z^4)+AX^2+By^2-(A+B)z^2 +\lambda(l\cdot s)+\mu_B H(l+2S),$$

where A, B, D are constants specifying the crystalline field, the cubic term D predominating, and λ is the constant of spin-orbit interaction. The theoretical analysis resulted in susceptibilities for Ni^2 and Cr^3 equal to the spin-only susceptibility multiplied by a factor depending on λ/D. If p is the actual effective magneton number, p_s the spin-only value, and q is a positive constant, then this multiplying factor is

$$(p/p_s)=(1-4\lambda/5Dq) \text{ for } Ni^2, \text{ and}$$
$$(p/p_s)=(1-2\lambda/5Dq)^2 \text{ for } Cr^3.$$

The value of λ, as determined from the free ion multiplet width, is equal to -335 cm^{-1} for Ni^2, and $+87$ cm^{-1} for Cr^3. From the experimental p values in Table I, Dq is equal to 710 cm^{-1} for Ni^2, and -4700 cm^{-1} for Cr^3. These values of Dq are widely different from those found by Schlapp and Penney[4] and Janes[5] on more magnetically dilute salts. The value for Cr^3 also has the wrong sign, since Gorter[6] has shown that if a metal ion is surrounded by an octahedron of negative charges (as is the case here), D should be positive.

Theoretical studies of the crystalline field effect in other ions of the iron group have been carried out by Jordahl[7] and Siegert.[8] The inversion of the splitting of the orbital levels due to a cubic field for pairs of ions with the same l value, as in Ni^2 and Co^2, has been shown by Van Vleck[9] to be characteristic of any pair of ions for which the number of $3d$ electrons adds up to 5, 10, or 15, such as (Co^2, Ni^2), (Fe^2, Cu^2), (Co^2, Cr^3), (V^3, Ni^2); and the splitting is such that the quenching of the orbital moment should be largest for the second member of each pair provided the spin-orbit interaction is the same. However, for a given l and s, the multiplet width is proportional to the j value, and is, therefore, largest for the ions in the second half of the iron group. The larger spin-orbit interaction may account for the fact that the experimental p values for the ions in the second half of the group deviate very much more from the spin-only values than those of the first half.

In the above treatment of the crystalline field effects, the possible influence upon the susceptibility of the dipole-dipole and exchange effects has been neglected. Since the crystalline field cannot account for the low temperature anomalies observed in the anhydrous chlorides (see Part I), and as the concentration of magnetic ions in these

[4] R. Schlapp and W. G. Penney, Phys. Rev. **42**, 666 (1932).

[5] R. B. Janes, Phys. Rev. **48**, 78 (1935).
[6] C. J. Gorter, Phys. Rev. **42**, 437 (1932).
[7] O. M. Jordahl, Phys. Rev. **45**, 87 (1934).
[8] A. Siegert, Physica **3**, 85 (1936); **4**, 138 (1937).
[9] J. H. Van Vleck, Phys. Rev. **41**, 208 (1932).

compounds is very large, it is probable that the neglected interactions must be considered even at room temperatures.

Van Vleck and Penney[10] have discussed the fact that Mn^{2} and Fe^{3} show less than spin-only values. Although they attribute this discrepancy to experimental error they suggest a number of possible causes of such an effect. As has been mentioned above, this is not a case of experimental error. Dipole-dipole and exchange interactions are considered too small to be a satisfactory explanation. The most probable suggested explanation assumes the presence of incipient *jj* coupling (arising from the coupling between the spin moment of each electron and its own orbital moment). Under such circumstances it is not sufficient to consider only the Russell-Saunders coupling (between the resultant s and l of the ion), and the Hund rule is not valid. Van Vleck[11] has pointed out that the energy of the ion in the crystalline field is a minimum when the resultant spin has its lowest possible value. The internal energy of the ion is a minimum when the resultant spin has its maximum value, i.e., when the Hund rule is valid. Therefore, the combined action of the crystalline field and the incipient *jj* coupling would result in decreased effective spin for the ion, and the experimental p value would be less than the spin-only value. The observed low temperature curvature of the reciprocal susceptibility *vs.* temperature curve of $FeCl_3$ (Fig. 1, Part I) may be a consequence of this crystalline field effect. As has been suggested above the crystalline field in the trichlorides is apparently very much more effective than in the dichlorides. This may account for the fact that $MnCl_2$ does not show the same curvature as $FeCl_3$. The difference between the dichlorides and trichlorides may also be due in part to the difference in exchange effects between the magnetic ions. In the trichlorides each metal ion has three metal-ion near neighbors, and in the dichlorides there are six near neighbors.

Crystal Structures

The crystal structure of about half of the iron group anhydrous chlorides have been determined from x-ray studies.[12] These crystal structures are all of the layer lattice type; each layer of metal atoms is separated by two layers of chlorine atoms from the next metal atom layer. The dichlorides have the typical $CdCl_2$ structure, each metal atom layer forming a two-dimensional hexagonal network in which every metal atom has six near neighbors. The trichlorides are similar, except that a metal atom is missing from the center of each hexagon so that every metal atom has three near neighbors. The dimensions of these structures are given in Table II. $CrCl_3$ and $FeCl_3$ differ slightly, in that the layers of Cl atoms are so stacked as to produce cubic close packing of the Cl atoms in $CrCl_3$, and hexagonal close packing in $FeCl_3$.

Each metal atom in these structures is surrounded by six Cl atoms at the corners of an octahedron. Three of these Cl atoms are in the layer above the metal atom layer, and three are below, so that the axes of the octahedron do not coincide with the hexagonal axes of the crystal as a whole. The octahedra are distorted slightly by the crystal forces, and the distortion is probably greater in the trichlorides than in the dichlorides. It can thus be seen that the crystalline potential surrounding each metal atom is adequately described by a large cubic (octahedral) term and a small rhombic term.

Theory of Metamagnetism

The iron group anhydrous chlorides which have a positive Curie temperature (Θ) at room temperature exhibit a typically anomalous low temperature magnetic behavior (see summary, Part I). This behavior is characterized by (1) a large dependence of the susceptibility upon the field strength, (2) no apparent spontaneous magnetization, and (3) no large hysteresis effects. The first characteristic is not typical of paramagnetism, and the second and third are not typical of ferromagnetism. For this reason it has been suggested[13] that the magnetic behavior of these compounds should be classified as "metamagnetism." No adequate explanation of

[10] J. H. Van Vleck and W. G. Penney, Phil. Mag. **17**, 961 (1934).
[11] J. H. Van Vleck, J. Chem. Phys. **3**, 807 (1935).
[12] R. W. G. Wyckoff, *The Structure of Crystals* (1931) and *Strukturbericht*, [II] (Akademische Verlagsgesellschaft, Leipzig, 1937).
[13] J. Becquerel and J. van den Handel, J. de phys. et rad. **10**, 10 (1939).

metamagnetism has been presented. Landau[14] suggested that some of the properties of metamagnetics are due to the presence of spontaneously magnetized metal atom layers, oppositely oriented. This is similar to the theories of antiferromagnetism suggested by Néel[15] and others.[16] These suggestions, in a modified form, are developed in this paper into a theory which is applicable to the metamagnetic chlorides ($CrCl_3$, $FeCl_2$, $CoCl_2$, and $NiCl_2$).[17]

The specific heat characteristics of the metamagnetic chlorides (Part I, reference 7) indicate a Curie point anomaly of the cooperative type. Such an anomaly would result from a spontaneous arrangement of magnetic moments either parallel, as in ferromagnetism, or antiparallel. This ordering process may occur either throughout the crystal as a whole (long range order) or in small groups, or clusters, of neighboring atoms (short range order). The fact that no spontaneous magnetization occurs below the Curie point temperature may be explained by assuming a group behavior, with either (1) a haphazard orientation of atom groups, each group having a permanent moment due to parallel alignment of the atomic magnetic moments within it, or (2) a zero resultant moment for each atom group due to some antiparallel alignment of the atomic magnetic moments. Because of the complexity of the problem it is not practically feasible to calculate the energies of all the possible magnetic moment configurations in a crystal, and thus to determine theoretically which of the above explanations is most likely. The answer to this question is suggested by the fact that the initial susceptibility of $FeCl_2$ decreases as the temperature decreases. This indicates that, as the temperature is decreased, there is an increase in the number of atomic groups whose energy is unaffected by the application of a magnetic field. Since a decrease of temperature increases the population of the lowest energy levels, the assumption (2), that the atomic groups with zero resultant moment have the minimum energy, is substantiated. $CrCl_3$ does not behave the same as $FeCl_2$, but an explanation of this effect, not in contradiction with the above, will be presented later.

TABLE II. *Layer lattice dimensions of the iron group anhydrous chlorides*

Compound	Metal Atom Distances (Angstroms) Between Layers	Between Nearest Neighbors	Metal Ion Radius	Ratio of Nearest Neighbor Distance to Ion Radius
$CrCl_3$	5.76	3.46	0.70	4.95
$FeCl_3$	5.75	3.42	0.67	5.10
$MnCl_2$	5.86	3.682	0.83	4.43
$FeCl_2$	5.84	3.580	0.80	4.48
$CoCl_2$	5.79	3.546	0.78	4.55
$NiCl_2$	5.78	3.544	0.74	4.79

The theoretical development will be based upon the simple model suggested by the above analysis of the general character of the experimental results. Below the Curie point the atoms are assumed to behave as groups. Within each group the atomic magnetic moments may be parallel or antiparallel. The antiparallel configuration produces a zero resultant moment for the group and has the minimum energy. The resultant moment produced by the parallel configuration is assumed to be in the same or opposite direction as an applied magnetic field. Thus, in the presence of an applied field there are three group energy levels, the lowest one of zero resultant moment, a higher one with the effective resultant moment parallel to the field direction, and the highest one with the effective resultant moment antiparallel to the field direction. Above the Curie point the spontaneously formed groups no longer exist, although the interaction between near neighbors is such that the antiparallel and parallel energy levels are applicable to the atoms individually. The further assumption is made that the average field acting on any one group due to the neighboring groups is proportional to the average magnetization of the crystal. Finally, only one zero moment configuration is assumed to exist. This model is obviously oversimplified by the restrictions upon the direction of the resultant moments and upon the number of zero moment configurations. However, from the point of view of the analysis and general consideration of the experimental

[14] L. Landau, Phys. Zeits. Sowjetunion **4**, 675 (1933).
[15] L. Néel, Ann. de physique **18**, 5 (1932).
[16] F. Bitter, Phys. Rev. **54**, 79 (1938).
[17] After this paper was written, Professor Van Vleck brought to the author's attention an unpublished paper by J. Becquerel, presented in May, 1939, at the Strasbourg conference on magnetism of the Institut International de Cooperation Intellectuelle, in which similar considerations are applied to the problem of paramagnetic rotatory power.

results, such an idealized model has many advantages as compared with a more rigorous and elegant theoretical treatment.

Consider the above model at a temperature below that of the Curie point. Designate N the number of atoms per group, μ the atomic magnetic moment, σ the average magnetization per atom (averaged over the whole crystal), ϵ the energy difference between groups with a resultant moment (parallel atomic moments) and groups with zero resultant moment (antiparallel atomic moments), and H the magnetic field applied to the groups. The average magnetization per group,

$$N\sigma = kT\partial(\log Z)/\partial H,$$

where the partition function

$$Z = 1 + e^{-(\epsilon - N\mu H)/kT} + e^{-(\epsilon + N\mu H)/kT}.$$

Let $\alpha = \epsilon/kT$ and $\beta = N\mu H/kT$. Then

$$\frac{\sigma}{\mu} = \frac{2\sinh\beta}{e^{\alpha} + 2\cosh\beta}. \tag{1}$$

This is plotted in Fig. 1 for various values of α. When $\alpha = -\infty$ this equation reduces to the usual hyperbolic tangent relationship. The magnetic field acting on each group is assumed to be $H = H_a + D\sigma$ where H_a is the applied field and D is the internal field coefficient. The differential atomic susceptibility is

$$\chi = \frac{d\sigma}{dH_a} = \frac{N\mu\sigma(\mathrm{ctnh}\,\beta - \sigma/u)}{kT - DN\mu\sigma(\mathrm{ctnh}\,\beta - \sigma/u)}. \tag{2}$$

At a temperature above that of the Curie point Eq. (1) is still valid, but the atoms now act individually, $N = 1$, and ϵ is the difference in energy between the parallel and antiparallel alignment of an atom with its near neighbor.

When β is large (>2), Eq. (1) reduces to

$$\sigma/\mu = 1/(e^{\alpha-\beta} + 1). \tag{3}$$

This equation is plotted in Fig. 2, and represents the general S type form of the magnetization curve at low temperatures. Since $\alpha - \beta = (\epsilon - N\mu H)/kT$, the effect of decreasing temperature is to increase the step-like character of the curve of σ *vs.* H, so that at absolute zero the magnetization changes abruptly from zero to saturation when $N\mu H = \epsilon$. For this value of the field the magnetization is independent of temperature, and the curves of σ *vs.* H for different temperatures should all cross at the point where σ is one-half saturation. This is approximately what was found for $FeCl_2$ (Fig. 2, Part I).

When the applied field approaches zero, $\beta \to 0$, and the initial susceptibility is

$$\chi_i = \Theta/[D(T - \Theta)], \tag{4}$$

where $\Theta = 2N\mu^2 D/k(2 + e^{\alpha})$. The usual form of expressing the atomic susceptibility is $\chi(T - \Theta) = (p\mu_B)^2/3k$ where p is the effective number of Bohr magnetons and μ_B is the magnetic moment of the Bohr magneton. In comparison with the usual form, Θ is as given and

$$p\mu_B = \mu[6N/(2 + e^{\alpha})]^{\frac{1}{2}}.$$

Because of the presence of e^{α}, Θ and p are functions of temperature, decreasing as the temperature decreases. Eq. (4) may also be put into the form

$$\frac{1}{\chi_i}\frac{N\mu^2}{\epsilon} = \frac{2 + e^{\alpha}}{2\alpha} - \frac{N\mu^2 D}{\epsilon}. \tag{4a}$$

Equation (4a), without the constant term $N\mu^2 D/\epsilon$, is plotted in Fig. 3 where $kT/\epsilon = 1/\alpha$.

For high temperatures or small α, Eq. (4) reduces to

$$\chi_i(T + \epsilon/3k - 2N\mu^2 D/3k) = 2N\mu^2/3k. \tag{5}$$

If $N\mu^2 D/\epsilon$ is greater than $\frac{1}{2}$, then the Θ as measured at high temperatures will be positive, as is found in the metamagnetic chlorides. The dotted line of Fig. 3 illustrates Eq. (5) when $D = 0$.

If the difference in energy per atom between a parallel and an antiparallel arrangement is δ, then $\epsilon = N\delta$. Figure 3 is then the plot of $\mu^2/\chi\delta$ *vs.* $kT/N\delta$. Assume that δ is independent of the size of the group. Above the Curie point the atoms act individually, $N = 1$, and kT/δ is large. The applicable part of the reciprocal susceptibility curve has a positive slope (right-hand part of Fig. 3). At the Curie point, group formation spontaneously occurs, N is large, and kT/ϵ is now a fraction of its former value. This places the reciprocal susceptibility in the region of

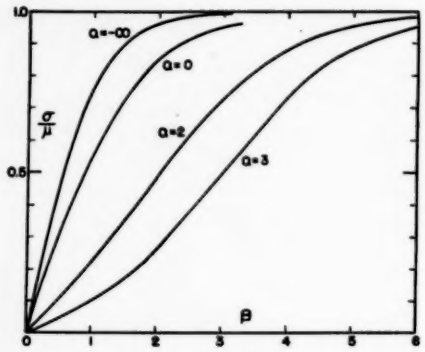

FIG. 1. The relative magnetization as a function of β, for various values of α.

negative slope (left-hand part of Fig. 3). Such a process would explain the reciprocal susceptibility characteristic of a metamagnetic chloride such as $FeCl_2$ (Fig. 1, Part I). The whole of Fig. 3 may be applicable to those anhydrous chlorides whose experimental characteristics are similar to those of chromium, nickel, copper and vanadium chlorides shown in Part I, Fig. 1. These will be discussed later.

Comparison with Experiment

The constants used in the theoretical development may be approximately determined from the experimental results by means of the appropriate theoretical equations. Below the Curie point μ, N, and ϵ are assumed independent of temperature and field strength. The experimental values for $FeCl_2$ (Table II, Part I) result in $\epsilon/k=59°$. With this value of ϵ/k the magnetization curves determined from Eq. (1) are plotted in Fig. 4 for the two temperatures, 20.4° and 13.9°. As was noted above, the two curves cross for

$$N\mu H=\epsilon=59k \quad \text{and} \quad \sigma/\mu=\tfrac{1}{2}.$$

Figure 4 should be compared with the experimental curves for $FeCl_2$ of Fig. 2, Part I.

The outstanding differences between the theoretical and experimental curves are the accentuated step-like character of the 13.9° experimental magnetization curve, as compared with the theoretical, and the fact that the 20.4° experimental curve has an apparent saturation value appreciably less than that of the 13.9° curve.

If only the spin magnetic moment is effective in these compounds $\mu=4\mu_B$ for the Fe^2 ion. The saturation moment per gram mole is then 22,200 and the theoretical intersection point of the two curves is 11,100. The experimental intersection point is 11,700, in good agreement with the theory. The experimental initial susceptibilities give $N=9$ atoms per group, approximately. The value of H at the intersection point is then 24,500 gauss. The applied field at the intersection point $H_a=13{,}500$ gauss. The difference may be due to the internal field or to the fact that N and ϵ are not independent of temperature and field strength as has been assumed. It is also possible that the magnetization of the groups with an effective resultant moment increases with decreasing temperature, as in the theory of ferromagnetism. The possible ferromagnetic behavior of the small groups postulated above is not known. It may be of interest in this connection that Peierls[18] has shown that in the Ising model, which is similar to the above, all lattices except the linear chain may be ferromagnetic.

Information as to the nature of the interaction effects which give rise to the internal field coefficient D above the Curie point may be found from its value. The high temperature $\Theta=2\mu^2D/3k$ approximately, as can be seen from Eq. (5). For $FeCl_2$, $\Theta=48°$ at room temperature (Part I, Table I). The experimental result is $D=7\times10^{24}$. Actual calculation of D assuming magnetic dipole-dipole interaction in a two-dimensional hexagonal network gives a value of 10^{23} approximately. The Lorentz field (spherical cavity) value is even less. It is apparent, therefore, that the actual interaction is more than 10 times as strong as magnetic dipole-dipole interaction. In view of the small distances between near neigh-

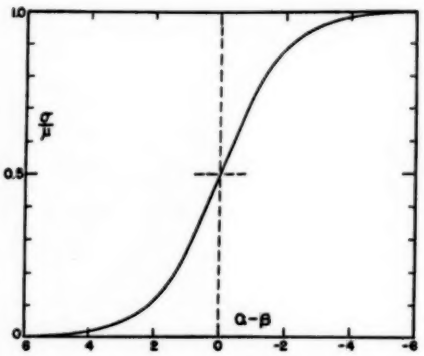

FIG. 2. The relative magnetization as a function of $\alpha-\beta$ when $\beta>2$.

[18] R. Peierls, Proc. Camb. Phil. Soc. 32, 477 (1936).

bors in these lattices (Table II), it is probable that the exchange interaction is the principal cause of these effects, as in ferromagnetics. Since the ratio of nearest neighbor distance to the ion radius in these compounds is only slightly greater than in the ferromagnetic metals (ratio is about four in Ni), it appears reasonable that the exchange interaction should be appreciable.

The magnitude of the specific heat jump at the Curie point (Part I, reference 7) is of interest. The experimental values in cal./mole were 4.54 for $FeCl_2$, 1.50 for $CoCl_2$, 0.66 for $CrCl_3$, and 0.13 and 0.18 for $NiCl_2$. If only the spin moments are effective, the theoretically predicted values for a simple ferromagnetic model[3] are 4.57 for $FeCl_2$, 4.38 for $CoCl_2$, and $CrCl_3$, and 3.97 for $NiCl_2$. The agreement in the case of $FeCl_2$ is very good but for the others the experimental value is too low. This latter discrepancy may be due to the incipient formation of groups above the Curie point, so that the total change is spread out. The specific heat anomaly is approximately the same for an antiparallel group formation as it is for a parallel group, since the entropy change is of the same magnitude.

The behavior of $CoCl_2$ and $NiCl_2$ is similar to that of $FeCl_2$, although the effects are appreciably smaller. Calculations, as above, for $CoCl_2$ result in an ϵ/k of 28°. The predicted intersection point magnetization per mole is 8300 and the experimental is 5900. The initial susceptibilities give $N=5$. The resulting intersection value of $H=28{,}000$ gauss, while the applied field at this point is $H_a=14{,}800$ gauss. Similar calculations for $NiCl_2$ result in an ϵ/k equal to 24°. No intersection point can be chosen from the results. The initial susceptibility gives $N=3$.

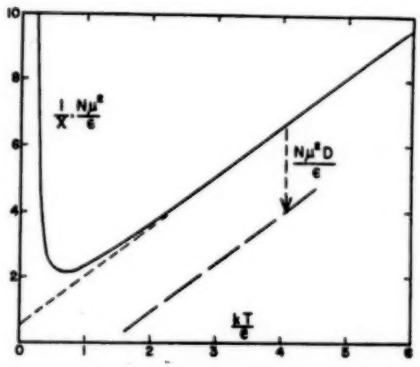

FIG. 3. The reciprocal initial susceptibility per atom, multiplied by $N\mu^2/\epsilon$, as a function of kT/ϵ.

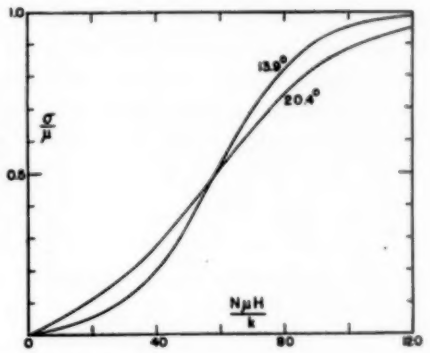

FIG. 4. The relative magnetization as a function of $N\mu H/k$ at 13.9° and 20.4° when $\epsilon/k=59°$.

The behavior of $CrCl_3$ (Figs. 1 and 2, Part I) differs from that of the other metamagnetic chlorides. The magnetization characteristics of $CrCl_3$ require that α be either very small or negative, as can be seen from Fig. 1. The fact that the slope of the experimental reciprocal susceptibility *vs.* temperature curve is constant down to low temperatures indicates that Θ is independent of temperature above the low temperature region. This requires that e^{α} be constant or negligible if Eq. (4) is to be applicable. The behavior of $CrCl_3$ may, therefore, be made consistent with the theory by assuming that $\epsilon/k=0$ or $-\infty$. Experimentally a field of 30,000 gauss at 13.9° results in a magnetization approximately 0.8 of saturation. This gives $N=4$ for $\epsilon/k=0$, and $N=2$ for $\epsilon/k=-\infty$. Since the Curie point from the specific heat anomaly is 16.8° and a field dependence occurs at 20.4°, it is probable that incipient group formation occurs above the actual Curie point temperature.

The anhydrous chlorides $CrCl_2$, $CuCl_2$, VCl_2 and VCl_3 (Fig. 1, Part I) are apparently not metamagnetic. However, they all do exhibit the behavior indicated by Fig. 3. Group formation apparently does not occur in these compounds and, therefore, they have no Curie points. The applied magnetic fields are only sufficiently large to indicate the beginning of paramagnetic saturation. These compounds all show the negative Θ predicted by Eq. (5). The theory and experiment do not agree quantitatively, but that may be due to the simplicity of the theory and the fact that other effects, such as the crystalline field, while comparatively negligible in the metamagnetic chlorides, are not negligible in these compounds.

The theory does not explain the absence of

large interaction effects in $MnCl_2$ and $FeCl_3$. The crystal structures of these compounds are the same as that of the corresponding metamagnetic chlorides. The only apparent point of difference is that the ground state of these ions is a ^6S state. This would indicate that the exchange interaction is negligible for a ^6S state, even though the electron shell is incomplete.

The author thanks Professor F. Bitter and Professor J. H. Van Vleck for their suggestions.

DECEMBER 1, 1940 PHYSICAL REVIEW VOLUME 58

Mobilities in Hydrogen at High Current Densities

WILLARD H. BENNETT
Electronic Research Corporation, Newark, Ohio
(Received August 12, 1940)

The conditions in an investigation of the silent electric discharge from sharp points and fine wires in hydrogen at atmospheric pressure are such that the discharge itself purifies the gas from electron-attaching impurities, so that the conditions of the discharge are productive of free electron conduction. Measurements are made of the generalized coefficient of mobility for the drift of free electrons in hydrogen, and of the mobility of hydrogen positive ions in hydrogen. Past observers have usually had doubts concerning the purity of the gas prepared by chemical means, but the results here reported involve a demonstrably sustained purification during the measurement itself.

WHEN the point is negative in a point-to-plane arrangement of electrodes, it is supposed that the silent discharge is caused by electrons arising at the tip of the point and producing ionizations by collision in avalanches, until the avalanche fronts have moved away from the tip of the point to a place where the electric field is no longer sufficient to support ionizations by collisions. The number of electrons freed by ionizations in an avalanche may be considered to be equal to 2^N where N is the number of ionizations an original electron makes. By considering directions of propagation of an avalanche increasingly removed from the axis of symmetry such as, for example, along the direction of the line, B, in Fig. 1, the electric field is less intense at any given distance from the metal than along a direction such as A, and so the number of ionizations that the original electron can produce is less. For example, if the number of ionizations along a direction A, is 30, while the number along a direction like B, is 20, an avalanche along the direction B will produce less than 1/1000 as much charge as an avalanche along the direction A (i.e., in the ratio 2^{10}). Thus, ionizations which are responsible for most of the current occur within a region approximating a hemispherical shell, such as CC. The region between the point and the shell and including the shell may be called the "ionizing sheath." In hydrogen, this sheath appears to be about 0.2 cm thick. Such a hemispherical cap is generally observed in this form of discharge.

Stability of Sheath

A rather detailed discussion of the negative point-to-plane discharge in air has been published by Trichel, and by Loeb and Kip.[1]

These observers report on a pulsating character of the negative corona discharge, which they attribute to the attachment of electrons to oxygen molecules to form negative molecular ions, and, due to the much smaller mobility of ions than electrons, the suppression of further ionizations in the sheath until ions have had time to move away. Their supposition is that each step in the sequence: avalanching, electron attaching, movement away of ions, *et seq.* must advance well toward completion before the next step in the sequence can begin.

[1] G. W. Trichel, Phys. Rev. **54**, 1078 (1938); L. B. Loeb and A. F. Kip, J. App. Phys. **10**, 142 (1939).

The writer also made a study of the corona discharges in air several years ago, and had observed a pulsating character of the discharge both on the negative and also on the positive polarities.

In our measurements of the negative discharge in hydrogen, observations were made to detect any pulsations which might occur. A circuit similar to Trichel's was used, except that in most of our work both on hydrogen and air, as well as other gases, a higher amplification was available and the signal was taken from a high frequency inductance in series with the discharge circuit. In this way, the bias of the first grid of the amplifier circuit was not thrown off by fluctuations of current during unsteady parts of a characteristic. It was found that a hydrogen discharge initially has more rapid and smaller pulsations than the pulsations in an air discharge, and occasionally these come in regular sequences of pulses. These pulsations gradually disappear with operation, and by the time they have disappeared, the current for any given voltage has risen to much higher values. The steady pulsation-free discharge current in purified hydrogen must be a space charge limited current with the greater density of charge near the ionization sheath at its outer boundary.

If the tube was allowed to stand idle for a few hours, the reapplication of potential showed that the tube had become partially deconditioned. It was necessary to pass current for a short time before the tube returned to the high current condition which had been attained by sustained operation previously. This reconditioning, however, did not require nearly so long as it did initially. Allowing the tube to stand idle again, the tube again might become deconditioned and if so, it could be reconditioned by operation for a still shorter time. The tube eventually reached a condition such that it remained in the high current condition even when allowed to stand idle. This showed that the deconditioning of the tube was not due to any leak. It was discovered that the initial conditioning of the tube was involved in some way with a sharpening of the tungsten wire ends. Examination with a microscope showed that the end of the tungsten wire was etched into a regular conical shape, and if, for example, a wire 0.0075 cm diameter was being used, the tip of the conical point had a radius of curvature which was less than 0.0010 cm and was usually of the order 0.0005 cm.

It had been observed in our earlier work on the corona discharges in air, that for points having a radius of curvature of 0.0010 cm or less, and of suitable metal to remain with that small a diameter, the pulsating character of the discharge reported by Trichel, Loeb, and Kip[1] did not occur. There were in air, however, some much smaller pulsations of an irregular character which did occur with these extremely sharp points. The fact that the discharge in hydrogen loses its pulsating character with the production of the extremely sharp conical tip, is probably due to the same thing, namely, the very sharp tip of the point. However, this sharpening of the tip of the point does not completely explain the deconditioning with standing, because the tip of the point did not change its shape any simply by turning off the current. It has been well established in high vacuum thermionic investigations[2] that tungsten in the presence of both oxygen and hydrogen acquires a mono-molecular layer of oxygen over which there is a mobile partial second layer of oxygen. The continued operation of the tungsten at an elevated temperature does not remove this oxygen except by the slow formation of tungsten trioxide and all of the oxygen is eliminated from the gas phase by this kind of reaction before the oxygen mono-molecular layer begins to disappear. In other words, this is an extremely quantitative means for eliminating oxygen from the gas phase.

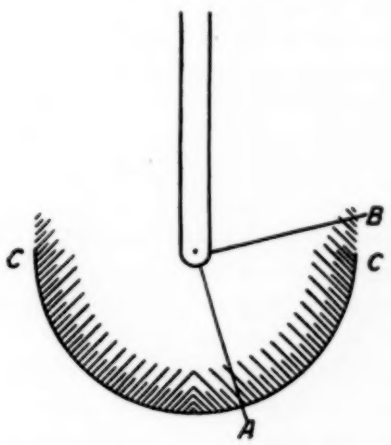

FIG. 1.

[2] Langmuir, J. Chem. Soc., 511–543 (1940).

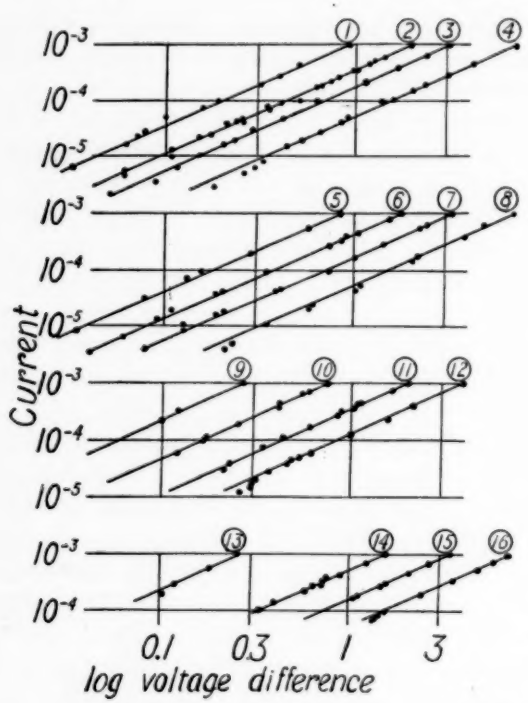

Curve	Wire diameter	Distance points to plane	Voltage subtracted
1	0.0010 cm	0.27 cm	520 volts
2		1.18	590
3		3.10	660
4		10.0	810
5	0.0025	0.29	570
6		0.98	645
7		3.00	720
8		10.0	880
9	0.0075	0.38	790
10		1.04	880
11		3.06	970
12		10.0	1170
13	0.020	0.32	1080
14		1.67	1200
15		3.24	1320
16		10.0	1620

Fig. 2. Log-log plots for point negative.

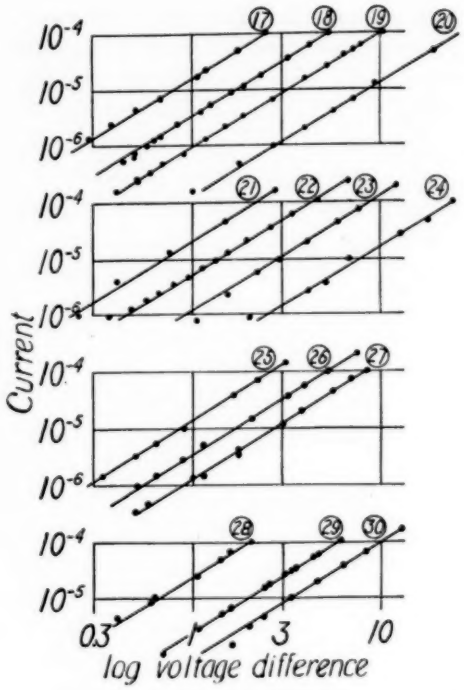

Curve	Wire diameter	Distance points to plane	Voltage subtracted
17	0.0010 cm	0.27 cm	590 volts
18		1.18	690
19		3.10	810
20		10.0	950
21	0.0025	0.29	640
22		0.98	740
23		3.00	860
24		10.0	1100
25	0.0075	0.38	900
26		1.04	1000
27		3.06	1120
28	0.020	0.32	1350
29		1.67	1500
30		3.24	1650

Fig. 3. Log-log plots for point positive.

In the present corona investigations in hydrogen, the faintest trace of oxygen would go to the tungsten wire end, and adhere so as to change the work function of the tip of the point. This change of work function at the tip of the point where field conditions are so extremely critical for the initiation of the avalanches responsible for the conductivity is observed as the conditioning of the tube up to the high current condition (or as explained later, a decrease in potential drop in the ionizing sheath) and so, the high current operation of the tube is really a very sensitive and reliable index of whether the oxygen has been removed from the gas phase. It seems reasonable to suppose that the other electron-attaching impurities should behave more or less like oxygen with respect to adsorption on tungsten, and so the disappearance of pulsations accompanied by the rise of the current to the high current condition is a reliable index of whether the conduction is really free electron conduction. The effects of sharpening of the points by etching are being separated from the effects of work function at the tip in some investigations now being made, and it is expected that a detailed report of these two different effects can be made at a later date.

Brass targets were used in most of this as well as all of the later work with cylinders because it was found that a harder surface sometimes acquired specks of material which gave a back ionization when the wire was negative and this back ionization might produce serious errors in measurements of mobilities.

The Current Voltage Relation

Although the shape of electrodes used in the first half of the work was that of a fine wire discharging toward a plane electrode which does not permit an exact solution for the space charge limited current, a dimensional argument can be used as follows. It will be supposed that the drift velocity of electrons is proportional to the nth power of the electric field intensity.

$$u=KE^n,$$

where u is the drift velocity, E is the electrical field intensity and K is a generalized coefficient of mobility. There is supposed to be a potential drop between the wire and the hemispherical shell V_0 so that the potential difference applied between the shell and the collecting plane equals the total applied voltage V_1, minus the sheath drop V_0.

Between the shell and the plane, the charge satisfies Poisson's equation.

$$\rho=\nabla^2 V/4\pi.$$

It is supposed that for some value of current and voltage, there exists a solution, $V(x, y, z)$. Multiplying the potential at every point by a constant multiplier λ gives a function $\lambda \cdot V$ which satisfies Poisson's equation and which satisfies boundary conditions where the potential applied between the sheath and the plane is greater by the same constant multiplier, $\lambda(V_1-V_0)$. The charge density is likewise proportional to V and so is increased by the ratio λ to $\lambda\cdot\rho$.

The total current flowing can be found by integrating the current density over any equipotential surface. If j is the current density so that $j=\rho\cdot u$, the total current is:

$$I=\int\int j\cdot dS=\int\int \rho\cdot u\cdot dS=\int\int \rho\cdot K\cdot E^n dS,$$

which gives the value of the current for the conditions for which it was assumed that there exists a solution. For the circumstances resulting in the potential distribution λV the current is

$$I_\lambda=\int\int \lambda\rho K(\lambda E)^n dS=\lambda^{n+1}\int\int \rho\cdot K\cdot E^n dS.$$

The value of the current when the potential applied across the gap was increased by the factor, λ, is

$$I_\lambda=\lambda^{n+1}I$$

or

$$I=\alpha(V_1-V_0)^{n+1}$$

gives the current as a function of the applied voltage, where α is a proportionality constant.

Discharge from Sharp Points

The data plotted in Figs. 2 and 3 were taken with tungsten wire in hydrogen after continued operation at 0.1 ma rising to about 1 ma for each set-up, or until pulsations had completely disappeared and the current had reached a steady value. Wires with diameters of 0.001, 0.0025, 0.0075, and 0.02 cm were used at various distances from point to plate, 0.3, 1, 3 and 10 cm. The diameter of the plane target was 15 cm so that the deviation from a point-to-plane arrangement, as well as the erratic effect of charges on the walls, distorts somewhat the observations for the 10 cm distance. It was further observed that the sheath did not present the smooth regular appearance with the 0.02 cm wire that it did with the finer wires. There appeared to be a tendency toward channeling through the sheath at the larger current for the largest wire. The assumption of a substantially constant sheath drop is probably in error for this largest wire.

It will be seen from Fig. 2 that the data generally can be adjusted in a log-log plot to

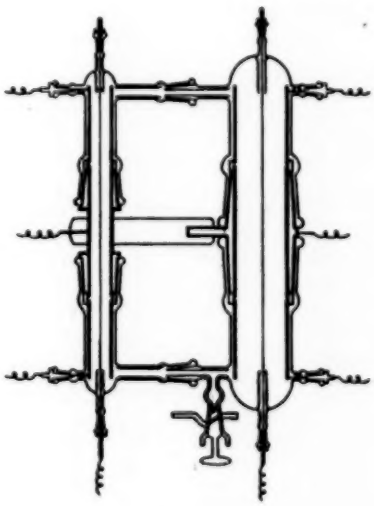

Fig. 4. Diagram of tubes.

straight line relations only by subtracting amounts assumed for the sheath drop which gives slopes of $\frac{3}{2}$. The current voltage relations have the form:

$$I_-=\alpha(V_1-V_0)^{\frac{3}{2}}.$$

Observations were also made when the point was positive with respect to the plane, and these data are plotted in Fig. 3. Here the only good fits to straight lines could be obtained by assuming sheath drops yielding slopes of 2. The current voltage relations are

$$I_+=\beta(V_1-V_0)^2.$$

These observations show that the conduction in hydrogen which is purified by sustained discharge from negative tungsten points until the pulsations have disappeared, is due to electrical charge whose drift velocity is given by an expression of the form.

$$u=KE^{\frac{1}{2}}$$

and that the discharge when the point is positive is due to charge whose drift velocity is given by an expression of the form:

$$v=CE.$$

It should be noticed that the value of sheath drop changes very little, if at all, for relatively very considerable changes in wire size, and target distance except for the largest size and largest target distance where irregularities of obvious nature can cause very considerable distortions of apparent sheath drop.

Discharge from a Straight Wire

Measurements were made of the negative and positive discharges from 0.0075 cm straight tungsten wires held axially in cylinders as shown in Fig. 4. Guard cylinders were used in order to obtain cylindrical symmetry. Cylinders with two different radii were used in order to separate out the conditions in the ionization sheath from those in the rest of the gap. The two arms of the tube were connected to insure the same composition of hydrogen in the tube for corresponding measurements.

Table I. *Values of K calculated from the data.*

I (MA)	V_2 (VOLTS)	V_1 (VOLTS)	V_2-V_1 (VOLTS)	K (E.S.U.)
10	3940	2395	1545	6.8×10^5
8	3660	2330	1330	6.8
7	3540	2290	1250	6.6
6	3360	2265	1095	6.9
5	3160	2200	960	7.0
4	2950	2160	790	7.5
3	2735	2100	635	6.7
2	2600	2010	590	5.8
1	2425	1895	530	3.4
0.6	2300	1830	470	4.1

If the ionization sheath, with wire negative, has a radius r_0 the field at the outer surface of the sheath is E_0, the potential drop through the sheath is V_0, and the electrons have a drift velocity in the rest of the gap proportional to the square root of the field:

$$u=KE^{\frac{1}{2}},$$

the current I to a guarded cylinder with radius r and length L, is related to the voltage between the wires and the cylinder by:

$$V-V_0=\left(\frac{2I}{KL}\right)^{\frac{1}{2}}(r-r_0)\left\{1+\frac{1}{3}\left(1-\frac{KLE_0^{\frac{1}{2}}}{2I}\right)\times\frac{r_0}{r+(rr_0)^{\frac{1}{2}}}-\frac{1}{18}\left(1-\frac{KLE_0^{\frac{1}{2}}}{ZI}\right)^2\frac{r_0(r_0+r)}{r^2}+\cdots\right\}.$$

For sufficiently large values of current, that is

$$I\gg KLE_0^{\frac{1}{2}},$$

the series is convergent and can be written as

$$V-V_0=(2I/KL)^{\frac{1}{2}}r\times\{1-0.722r_0/r-0.333(r_0/r)^{\frac{1}{2}}+\cdots\}.$$

The radius of the larger cylinder used was 2.70 cm, and the smaller cylinder was 1.15 cm in radius. Each guarded section was 15.15 cm long. If the voltage applied to the larger cylinder is V_2 and that to the smaller cylinder V_1, when the same current is passing to the central cylinder of each, I,

Table II. *Calculated values of C.*

I (MA)	V_2 (VOLTS)	V_1 (VOLTS)	V_2-V_1 (VOLTS)	C (E.S.U.)
0.5	7750	4115	3635	3.2×10^5
0.4	7100	3900	3200	3.0
0.3	6500	3650	2850	3.2
0.2	5600	3340	2260	3.4
0.1	4725	2990	1735	2.8
0.01	3140	2500	640	2.1

$$V_2-V_0=(2I/KL)^{\frac{1}{2}}r_2 \times\{1-0.722r_0/r_2-0.333(r_0/r_2)^{\frac{1}{2}}+\cdots\},$$

$$V_1-V_0=(2I/KL)^{\frac{1}{2}}r_1 \times\{1-0.722r_0/r_1-0.333(r_0/r_1)^{\frac{1}{2}}+\cdots\},$$

so the difference in these voltages is

$$V_2-V_1=\left(\frac{2I}{KL}\right)^{\frac{1}{2}}(r_2-r_1)\left\{1+\frac{0.333r_0^{\frac{1}{2}}}{r_2r_1^{\frac{1}{2}}-r_1r_2^{\frac{1}{2}}}+\cdots\right\}.$$

The mobility coefficient can be obtained from the data by

$$K=\frac{I}{(V_2-V_1)^{\frac{1}{2}}}\cdot\frac{2(r_2-r_1)^{\frac{1}{2}}}{L}\left\{1+\frac{0.5r^{\frac{1}{2}}}{r_2r_1^{\frac{1}{2}}+r_1r_2^{\frac{1}{2}}}+\cdots\right\},$$

which is relatively insensitive to the assumed value of r_0. Putting an outside limit on r_0 of 0.6 cm,

$$1+\frac{0.5r_0^{\frac{1}{2}}}{r_2r_1^{\frac{1}{2}}+r_1r_2^{\frac{1}{2}}}\leqslant 1.05.$$

It was observed that the discharge with the 0.0075-cm wire negative was localized in spots, and that increasing the current produced more discharging spots and crowded them more closely together.

Table I shows the data and calculated value of K.

The values for K do not show a monotonous change with decreasing current so it appears that the assumption of I large enough was justified. However, the fluctuations in values of K for the smaller currents is easily understood from the randomness of likelihood that the discharging spots should fall inside the collecting cylinders if near an end. From the data for the five largest current values,

$$K=6.8\times10^5 \text{ e.s.u.}$$

The current with wire positive, limited by space charge where drift velocity is proportional to field ($v=CE$) is related to voltage by

$$V-V_0=(2I/CL)^{\frac{1}{2}}\{r-1.542r_0 +0.500r_0(r_0/r)+0.042r_0(r_0/r)^3-\cdots\},$$

if $I\gg CLE_0^2$. Again in terms of voltages for the two cylinders for the same current as before,

$$V_2-V_1=\left(\frac{2I}{CL}\right)^{\frac{1}{2}}(r_2-r_1)\left\{1-\frac{0.5r_0^2}{r_1r_2}+\cdots\right\}.$$

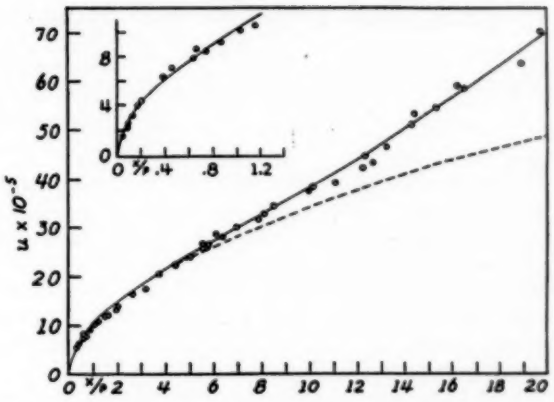

FIG. 5. Comparison of the present value of 6.8×10^5 e.s.u. for the mobility of electrons in hydrogen with the results of Bradbury and Nielsen. The experimental points are from Bradbury and Nielsen. The dotted curve is calculated from the above value of the mobility.

Table II shows the data and calculated values of C.

DISCUSSION

The results for the mobility of electrons in hydrogen may be compared with those of Bradbury and Neilsen[3] as shown in Fig. 5 where the dotted line represents the relation

$$u=6.8\times10^5E^{\frac{1}{2}} \quad (\text{for } p=760 \text{ mm}, E \text{ in e.s.u.})$$

or

$$u=10.8\times10^5(X/p)^{\frac{1}{2}} \quad (\text{in volts/cm and mm})$$

and agrees well with these data for field intensities up to $X/p=5$.

Larger field strengths than about 4000 volts per centimeter produced arc-over so that a mobility of electrons at greater than about $X/p=5$ could not be measured.

The result for the mobility of positive ions in hydrogen

$$C=3.2\times10^3 \text{ e.s.u.}$$
$$=10.7 \text{ cm/sec. per volt/cm}$$

agrees much better with Bradbury's[4] value of 8.2 rather than with those of Mitchell, which Tyndall[5] notes.

---

[3] N. E. Bradbury and R. A. Nielsen, Phys. Rev. **49**, 391 (1936).
[4] N. E. Bradbury, Phys. Rev. **40**, 519 (1932).
[5] A. M. Tyndall, *The Mobility of Positive Ions in Gases* (Cambridge University Press, 1938), p. 35.

Interpretation of Torsional Frequencies of Crystal Specimens

WILLIAM FULLER BROWN, JR.
Palmer Physical Laboratory, Princeton University, Princeton, New Jersey

(Received September 12, 1940)

A crystalline cylinder when subjected to a harmonically varying twisting moment in general not only twists but bends. A correct interpretation of the response frequencies is important in dynamical determinations of the elastic constants of crystals, and it is desirable that the measurements be made under such conditions that a simple formula, similar to that for isotropic materials, may be used without fear of serious error. In static measurements two such formulas are required, one for twist with bending prevented and the other for twist with bending unrestrained. It is shown here that each of these is a good approximation in dynamic measurements over certain ranges of frequencies and of specimen lengths, and formulas are derived by which the errors may be estimated. A simple straight-line plot based on approximate values of the elastic constants gives all the information that is needed for the selection of good working conditions in the final measurements. For the sodium and copper-gold crystals on which measurements have been reported, the pure torsion formula is a good approximation when no parasitic response frequencies are observable; but it would cease to be a good approximation for specimen lengths below about 3 cm.

IN a crystalline cylinder whose axis is oriented arbitrarily with respect to the crystal axes, application of either a bending or a twisting moment alone produces both bending and twisting. In static experiments the effective Young's modulus E' and rigidity G' measured under these conditions differ from the values E and G obtained when only pure bending or pure twist is allowed to occur.[1] If the specimen axis is Oz and if the plane of the torsion-coupled bending is taken as the zx plane, then in terms of the elastic moduli s_{ij}' referred to the xyz axes

$$E'=E(1-\epsilon)=1/s_{33}',$$
$$G'=G(1-\epsilon)=2/(s_{44}'+s_{55}'), \qquad (1)$$
$$\epsilon=s_{34}'^2/s_{33}'(s_{44}'+s_{55}').$$

In dynamic measurements of the elastic constants of crystals, it has usually been possible to choose an orientation for which $\epsilon=0$; the interpretation of the observed resonance frequencies under torsional excitation then offers no difficulty.[2] In recent measurements on metal crystals this has not been possible.[3,4] The experimental results have been consistent with the assumption that the effective rigidity was G, but a theoretical analysis of the problem seems desirable. The formulas derived by Goens[5] are unsatisfactory because in their rigorous form they are inconvenient for numerical calculation, and the first-order correction derived from them is not always reliable.

THEORY

The elastic properties of the specimen are completely described by three quantities E or E', G or G', and ϵ. Let E^* and G^* represent whichever values of Young's modulus and the rigidity are chosen for this purpose. Then the actual properties may be regarded as produced by a gradual increase of ϵ from zero to its actual value in an originally isotropic specimen with the same E^* and G^*. The actual frequencies emerge during this process from original unperturbed frequencies which may be classified unambiguously as flexural or torsional but whose values will depend on the meanings of E^* and G^*. Since the "free" frequencies ($E^*=E'$, $G^*=G'$) may be as much as 20 percent lower than the "pure" frequencies ($E^*=E$, $G^*=G$), it is clear that a first-order correction for the perturbation, if it is adequate at all, can be so only when the "unperturbed" frequencies are properly chosen.

In terms of E and G, the differential equations of motion of a cylinder of density ρ and radius a

[1] W. Voigt, *Lehrbuch der Kristallphysik* (Teubner, 1928), pp. 638, 734, 738.
[2] F. Rose, Phys. Rev. **49**, 50 (1936); M. Durand, Phys. Rev. **50**, 449 (1936).
[3] S. L. Quimby and S. Siegel, Phys. Rev. **54**, 293 (1938).
[4] S. Siegel, Phys. Rev. **57**, 537 (1940).
[5] E. Goens, Ann. d. Physik **15**, 455 and 902 (1932). See also R. Kimura, Proc. Phys.-Math. Soc. Japan **21**, 686 (1939).

may be written[6]

$$\rho\ddot{\phi}=-\tfrac{1}{4}a^2E\partial^4\phi/\partial z^4+2C\partial^2\psi/\partial z^2,$$
$$\rho\ddot{\psi}=-\tfrac{1}{4}a^2C\partial^4\phi/\partial z^4+G\partial^2\psi/\partial z^2, \quad (2)$$

where

$$C=(\epsilon EG/2)^{\frac{1}{2}}. \quad (3)$$

(Here rotatory inertia about the transverse axis Oy has been neglected.) The variables ϕ and ψ are the bending and twisting moments exerted across a cross section, divided by the moments of inertia $\frac{1}{4}\pi a^4$ and $\frac{1}{2}\pi a^4$ of the cross section about the corresponding axes. These are more convenient variables than the transverse displacement and angular twist because they make it possible to write the boundary conditions in a form not containing ϵ. For a rod with free ends at $z=\pm l/2$ the boundary conditions are

$$\phi=\psi=0, \quad \partial\phi/\partial z=0; \quad (4)$$

only this case will be considered in detail.

The differential Eqs. (2) may be written in three other forms, corresponding to other choices of E^* and G^*; these may be obtained from (2) by means of (1). If E^* and G^* are held constant but ϵ is set equal to zero, the equations reduce to the form for isotropic specimens, and for vibrations of frequency $p/2\pi$

$$\rho p^2\phi=\tfrac{1}{4}a^2E^*\partial^4\phi/\partial z^4, \quad \rho p^2\psi=-G^*\partial^2\psi/\partial z^2. \quad (5)$$

The corresponding flexural frequencies $p_i^*/2\pi$ and torsional frequencies $\omega_j^*/2\pi$ are given by[7]

$$p_i^*=n_i^2\frac{\pi^2}{l^2}\frac{a}{2}\left(\frac{E^*}{\rho}\right)^{\frac{1}{2}}, \quad \omega_j^*=j\frac{\pi}{l}\left(\frac{G^*}{\rho}\right)^{\frac{1}{2}}; \quad (6)$$

j is an integer, and n_i is the ith nonvanishing root of

$$\tanh^2(n\pi/2)=\tan^2(n\pi/2) \quad (7)$$

($n_1=1.506$, $n_i=i+\frac{1}{2}$ to four figures for $i>1$). If the frequencies are plotted logarithmically as functions of specimen length l, the torsional frequencies lie on straight lines of slope -1 and the flexural on lines of slope -2; these are the fine lines (both solid and dashed) in Fig. 1. The free frequencies ($E^*=E'$, $p_i^*=p_i'$ etc.) are lower than the pure ($E^*=E$, $p_i^*=p_i$ etc.) in the ratio $(1-\epsilon)^{\frac{1}{2}}$.

[6] Reference 1, p. 673, or reference 5.

[7] H. Lamb, *Dynamical Theory of Sound* (Arnold, 1910), p. 124.

The normalized eigenfunctions ϕ_i, ψ_j corresponding to p_i^* and ω_j^* are

$$\phi_i=l^{-\frac{1}{2}}[\cosh k_iz/\cosh(k_il/2) - \cos k_iz/\cos(k_il/2)], \quad i \text{ odd},$$
$$=l^{-\frac{1}{2}}[\sinh k_iz/\sinh(k_il/2) - \sin k_iz/\sin(k_il/2)], \quad i \text{ even}; \quad (8)$$

$$\psi_j=(2/l)^{\frac{1}{2}}\cos j\pi z/l, \quad j \text{ odd},$$
$$=(2/l)^{\frac{1}{2}}\sin j\pi z/l, \quad j \text{ even}; \quad (9)$$

$$k_i=n_i\pi/l. \quad (10)$$

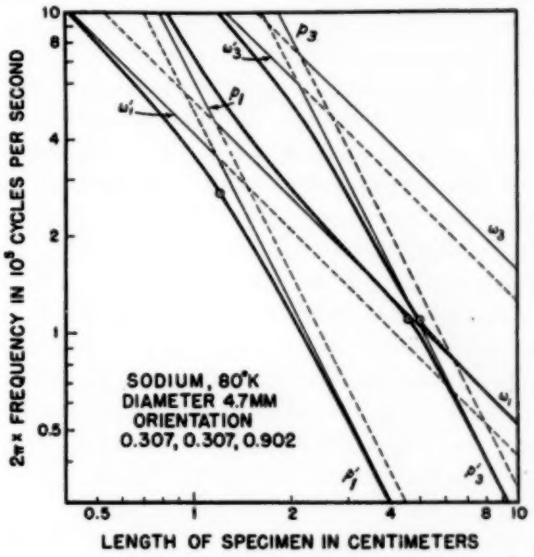

FIG. 1. Unperturbed and perturbed torsional and flexural frequencies for a hypothetical sodium crystal cylinder of the diameter used by Quimby and Siegel, with specimen axis in an orientation for which the coupling between torsion and bending is large. $E=5.47\times10^{10}$, $G=2.804\times10^{10}$ dyne/cm², $\epsilon=0.3628$. The fine solid and dashed lines represent the unperturbed frequencies as functions of specimen length: the p's are flexural, the ω's torsional; the primed are "free," the unprimed "pure." Of these, the ones represented by solid lines are a better approximation to the actual frequencies, which are given by the heavy curves and the circles. The circles have been calculated by a rigorous but laborious method, the curves by the approximate methods of this article. The subscripts are the number of moment loops in the specimen; the strongest interaction is between torsional and flexural modes of vibration for which this number is the same.

The solution for $\epsilon\neq0$ may be expressed in the form

$$\phi=\sum_i A_i\phi_i, \quad \psi=\sum_j B_j\psi_j. \quad (11)$$

Equations determining the A_i's and B_j's may be found by substituting (11) in (2) (with $\partial^2/\partial t^2=-p^2$), using the differential equations satisfied by the ϕ_i's and ψ_j's, multiplying the first of the resulting equations by ϕ_k and the second by ψ_l, and integrating over the length of the

specimen. This gives

$$(p^2-p_k^2)A_k-(2C/G)\sum_j c_{kj}\omega_j^2 B_j=0,$$
$$-(C/E)\sum_i p_i^2 c_{il}A_i+(p^2-\omega_l^2)B_l=0, \tag{12}$$

where

$$c_{ij}=\int_{-l/2}^{l/2}\phi_i\psi_j dz. \tag{13}$$

For i and j both even or both odd,

$$|c_{ij}|=(4\sqrt{2}/\pi)n_i^2 j/(n_i^4-j^4); \tag{14}$$

the other c_{ij}'s vanish. Thus Eqs. (12) break up into two sets. One set contains only odd i's and j's and refers to modes of vibration in which ϕ and ψ are symmetrical about $z=0$ (see Fig. 2); the other contains only even i's and j's and refers to antisymmetrical modes. There is no interaction between a flexural mode of one type and a torsional mode of the other type.

From (14), $c_{11}^2=0.972$, $c_{22}^2=0.952$, $c_{33}^2=0.919$, $\cdots$, $c_{jj}^2\to 0.810$ as $j\to\infty$; and since $\sum_i c_{ij}^2=\sum_j c_{ij}^2=1$, the other c_{ij}'s are small. Therefore a torsional mode interacts chiefly with the flexural mode for which the number of moment loops in the specimen is the same ($i=j$, Fig. 2), and only weakly with the others. As a first approximation, account may be taken of this strongest interaction alone by setting $|c_{ij}|=1$ for $i=j$, $=0$ otherwise. Then Eqs. (12) separate into pairs; the kth pair contains only A_k and B_k, and for non-vanishing values of these

$$(p^2-p_k^2)(p^2-\omega_k^2)-\epsilon p_k^2\omega_k^2=0, \tag{15}$$

whence $p^2=p_k^2$ or $\omega_k'^2$ for $p_k^2\gg\omega_k^2$, and $p^2=p_k'^2$ or ω_k^2 for $p_k^2\ll\omega_k^2$. Thus if the strongly interacting frequencies are not too close together, the effect of their interaction is that the lower of them is approximately free and the upper approximately pure. These frequencies correspond to the fine *solid* lines in Fig. 1.

To obtain a better approximation, the best choice of unperturbed frequencies is p_i and ω_j' for lengths below that at which the frequency under consideration and its strongest perturbing frequency become equal; p_i' and ω_j for lengths above this. The fact that the lengths actually used in the experiments lie in the latter range explains the success of the pure torsion formula. The following corrections to the unperturbed frequencies may be derived by standard methods

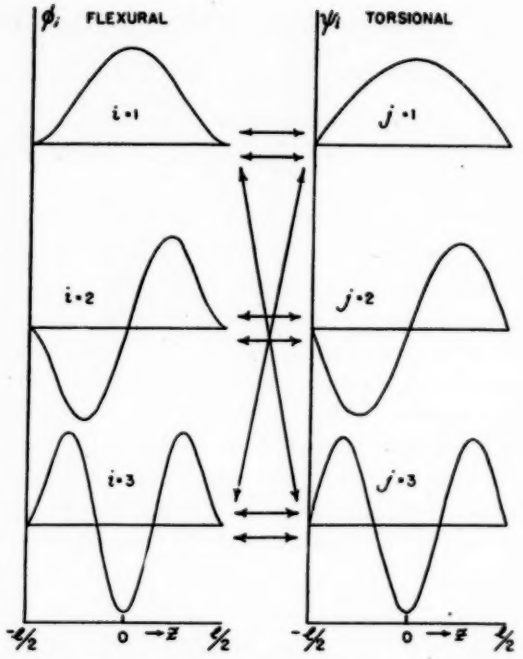

FIG. 2. Unperturbed flexural and torsional modes o vibration and relative degrees of interaction between them ϕ is proportional to the bending moment and ψ to the twisting moment. The double arrows indicate strong interaction, the single arrows weak interaction.

from the equations that now replace (12); the range in which each formula is to be used will be evident from the frequencies occurring in it.

Very near a perturbing frequency, provided the effect of other perturbing frequencies is negligible,

$$p^2=\tfrac{1}{2}[b\pm(b^2-4c)^{\frac{1}{2}}],$$

where

$$b=p_i'^2+\omega_j^2+\eta c_{ij}^2 p_i'^2$$

or

$$b=p_i^2+\omega_j'^2+\eta c_{ij}^2\omega_j'^2, \tag{16}$$

and

$$c=p_i'^2\omega_j^2=p_i^2\omega_j'^2,$$
$$\eta=\epsilon/(1-\epsilon).$$

Far from all perturbing frequencies,

$$(p^2-\omega_j^2)/\omega_j^2=\eta\sum_i c_{ij}^2 p_i'^2/(\omega_j^2-p_i'^2),$$
$$(p^2-p_i'^2)/p_i'^2=\eta\sum_j c_{ij}^2 p_i'^2/(p_i'^2-\omega_j^2),$$
$$(p^2-\omega_j'^2)/\omega_j'^2=\eta\sum_i c_{ij}^2\omega_j'^2/(\omega_j'^2-p_i^2), \tag{17}$$
$$(p^2-p_i^2)/p_i^2=\eta\sum_j c_{ij}^2\omega_j'^2/(p_i^2-\omega_j'^2).$$

Occasionally it is necessary to take account simultaneously of two perturbations, one due to a weakly interacting frequency too close for use of

(17), the other to a strongly interacting frequency still not distant enough to neglect. This is true for instance in Fig. 1 of frequencies produced by interaction of ω_1 and p_3' near their crossing point, where p_1' and ω_3 still produce a considerable effect. Formulas for such cases need not be given here; in the application to experiments the unfavorableness of such a situation is evident without detailed calculation.

Application

In the experiments mentioned, the specimen is joined end-to-end to a quartz crystal equipped with electrodes, and torsional vibrations are excited piezoelectrically. The frequencies observed are the resonance frequencies of this composite system, but the lengths are so chosen that the junction of the two cylinders is approximately a moment node for torsion. The frequencies are therefore almost the same as the natural frequencies of vibration of the specimen, as long as there is no torsion-flexion coupling. The effect of such coupling on the observed frequencies cannot be computed accurately by using the formulas derived above for the effect on the natural frequencies of the specimen by itself. If, however, that calculation shows that the natural frequency of the specimen alone differs negligibly from the "pure" frequency, it is safe to assume that the observed frequency also differs negligibly from the one that would be observed if bending could be prevented.

The simplest procedure is therefore the following. From the observed frequencies, the elastic constants may be computed by means of the pure torsion formula; the values obtained will be at least approximately correct. From the elastic constants, the unperturbed frequencies may be calculated and plotted as in Fig. 1, for each specimen used. An inspection of the plot will reveal whether any of the experimental points fall in a range where the error is likely to be excessive, and in such ranges the error for a single free rod can be calculated by the formulas given above. Points for which the error is objectionably large may be rejected and the elastic constants recomputed without them; or the whole preliminary measurement and calculation may be used merely as a means of selecting specimen lengths for the final set of measurements.

Figure 1 has been calculated for a hypothetical sodium specimen in a particularly unfavorable orientation, from the values of the elastic constants given by Quimby and Siegel.[3,8] The heavy curves are corrected frequencies of free vibration. These have been calculated by the method of this article. The circles are check points computed by means of a rigorous formula similar to that of Goens; this calculation consists in solving a cubic equation for some value of p, calculating and plotting a function f of the three roots and of p and l for a number of values of l, and thus finding a combination of l and p for which $f=0$. The calculation for given l would be still more laborious.

It can be seen that the fundamental torsional frequency is practically identical with the unperturbed "pure" frequency for lengths greater than 3 cm, except when the perturbing frequency is very close; in this case two response frequencies would probably be observed and the data would automatically be rejected.[9] The only possibility of serious error, therefore, lies in the use of too short a length. For the lengths used by Quimby and Siegel one would expect the pure torsion formula to hold quite well, as they found it did. The length range for which the *free* torsion formula would be valid is of no interest, at least for specimens of this diameter, for at such short lengths the specimen can no longer be regarded as thin ($a^2 \ll l^2$).

Siegel in his torsional measurements on copper-gold crystals used two specimens.[4,10] One had an orientation so close to [100] that the frequency correction at room temperature is only 0.004 percent. In the other ω_2, which was measured, was rather close to p_4' and was still appreciably perturbed by p_2'; the effects are 0.7 percent and 0.3 percent, respectively, and additive. The analogous situation in Fig. 1 is a measurement of ω_1 at about $l=6$. Here a correct choice of E^* and G^* is essential; for if p_3 instead of p_3' is chosen as unperturbed frequency, the perturbation is shifted to the right and the whole calculation is erroneous.

[8] For cubic crystals, in the notation of reference 3, $1/E'=s_{11}-2s\Gamma$, $1/G'=s_{44}+4s\Gamma$, $\epsilon=2s^2E'G'(\Gamma-4\Gamma^2+3\chi)$.
[9] Reference 3, footnote 12.
[10] The data required for this calculation were kindly provided by Dr. Siegel.

LETTERS TO THE EDITOR

Prompt publication of brief reports of important discoveries in physics may be secured by addressing them to this department. Closing dates for this department are, for the first issue of the month, the eighteenth of the preceding month, for the second issue, the third of the month. Because of the late closing dates for the section no proof can be shown to authors. The Board of Editors does not hold itself responsible for the opinions expressed by the correspondents.

Communications should not in general exceed 600 words in length.

A Study of the Frequencies ν_2 and ν_4 in the Infra-Red Spectra of SiH_4 and GeH_4

The infra-red spectra of the molecules SiH_4 and GeH_4 have been investigated by Steward and Nielsen[1] who report intense regions of absorption near 4.5μ and 11.0μ in both cases. These bands were found, under higher dispersion, to resemble those occurring in the spectrum of methane in a general way and were accordingly identified as the optically active frequencies ν_3 and ν_4, respectively, in each case. These measurements revealed, moreover, that the rotational absorption pattern was much more complex than could be accounted for on the basis of the prevalent theory for such molecules. In the case of SiH_4 a secondary peak was found in the spectrum near 10.3μ to which no real interpretation was given.

In a series of papers by Childs and Jahn[2] and by Jahn[3] this complex structure of ν_4 was accounted for on the basis that there exists a resonance Coriolis interaction between the frequency ν_4 and the optically inactive frequency ν_2 both of which have nearly the same values here. These results have been verified more recently by Shaffer, Nielsen and Thomas[4] who have presented a theory of the rotation-vibration problem of the tetrahedrally symmetric xy_4 type molecule accurate and complete to second order of approximation. The Coriolis interaction manifests itself in somewhat the following manner. If ν_4 is larger than ν_2 the effective moments of inertia in these states will be, respectively, larger and smaller than the moments of inertia in the normal vibration state. This should give rise to convergence of the rotation lines in ν_4 toward higher frequencies and in the frequency ν_2, if it were active, toward lesser frequencies. If, on the other hand, ν_4 is smaller than ν_2 a situation just the reverse of the above should prevail.

It was even suggested by Childs and Jahn with regard to the SiH_4 molecule where ν_4 and ν_2 are separated only by some 60 cm^{-1} that a mixing of the wave functions of the two states might occur because of this Coriolis perturbation, sufficient to induce an optical activity into the otherwise inactive frequency ν_2. In this manner, they suggest an explanation of the weaker maximum found by Steward and Nielsen near 10.3μ.

In the light of what has gone before it has been considered important to re-examine the spectra of the above molecules under the higher resolving power which is now practicable.

In the case of the silane spectrum the absorption pattern verifies in a general way the pattern reported by S. and N. except that here almost complete resolution has been accomplished, separations of the order of 0.25 cm^{-1} being frequently observed. In the present data the secondary peak near 10.3μ is clearly discernible as a Q branch of a much weaker band extending to 9.0μ. It is apparent that although the Q branch near 11.0μ is unsymmetrically broadened toward smaller frequencies this Q branch is broadened unsymmetrically toward higher frequencies. This makes it possible with certainty to identify the bands at 11.0μ and 10.3μ with the frequencies ν_4 and ν_2, respectively.

With regard to the spectrum of GeH_4, the present measurements again verify those reported by S. and N. near 10μ. They show, however, that there exists immediately beyond the region studied by S. and N. at longer wavelengths a region of far more intense absorption. The conclusion drawn is evidently that the region originally studied was not ν_4, but in reality ν_2. The complete region from 9μ to 13μ has been measured and as in the case of SiH_4 the bands are almost completely resolved. They reveal, as before, a convergence toward higher frequencies in the band ν_4 and toward smaller frequencies in the band ν_2.

The results of this preliminary investigation are summarized in Table I.

Complete details of these measurements with wavelengths will be published in a later communication.

J. W. STRALEY
C. H. TINDAL
H. H. NIELSEN

Mendenhall Laboratory of Physics,
Ohio State University,
Columbus, Ohio,
November 7, 1940.

TABLE I. *Values of the frequencies ν_2 and ν_4 in the spectra of SiH_4 and GeH_4.*

	SiH_4	GeH_4
ν_2	975 cm^{-1}	932 cm^{-1}
ν_4	910 cm^{-1}	818 cm^{-1}

[1] W. B. Steward and H. H. Nielsen, Phys. Rev. **47**, 828 (1935); **48**, 861 (1935).
[2] W. H. J. Childs and H. A. Jahn, Nature **141**, 916 (1938); Proc. Roy. Soc. **A169**, 451 (1939).
[3] H. A. Jahn, Proc. Roy. Soc. **A168**, 469 (1938); **A168**, 495 (1938).
[4] W. H. Shaffer, H. H. Nielsen and L. H. Thomas, Phys. Rev. **56**, 895 (1939); **56**, 1051 (1939).

Rotatory Power of Nickel Sulphate at Low Temperatures*

An investigation of the natural and magnetic rotatory powers of crystalline $\alpha-NiSO_4\cdot 6H_2O$ at liquid-air temperature has been undertaken in this laboratory. Preliminary results for several visible wave-lengths are reported below.

The crystals were cooled by direct immersion in liquid "air" which was assumed to be largely oxygen. Observations were made through the double cylindrical Pyrex glass walls of the container (outside diameter 1.3 cm). The rotations actually measured ranged from 1° to 7° and satisfactory agreement was obtained between visual observations with a Lippich half-shade polarimeter, and photographic measurements by a method previously described.[1] Control measurements indicated that no serious errors arose from double refraction in the glass walls, or from lack of parallelism of the light rays in the crystal.

The results so far obtained, with corresponding room-temperature data for comparison, are given in Table I.

TABLE I. *Rotatory power of nickel sulphate.*

WAVE-LENGTH IN ANGSTROMS	4358	5461	5780
Natural rotatory power, in degrees/mm:			
At 90°K	+1.2	−2.0	−2.3
At room temperature[1]	+1.7	−0.75	−1.25
Difference	−0.5	−1.25	−1.05
Magnetic rotatory power, in min./cm-oerst.:			
At 90°K	+0.072	+0.044	+0.034
At room temperature[2]	+0.044	+0.026	+0.022
Ratio	1.64	1.69	1.54

[1] F. G. Slack and P. Rudnick, Phil. Mag. (7) **28**, 241 (1939); N. Underwood, F. G. Slack, and E. B. Nelson, Phys. Rev. **54**, 355 (1938).
[2] F. G. Slack, R. T. Lageman, and N. Underwood, Phys. Rev. **54**, 358 (1938).

The natural rotations are thus seen to be displaced in the negative (i.e. "abnormal") direction at the low temperature. The magnetic rotations, although in the positive (diamagnetic) direction, are increased at the low temperature, as in the presumably parallel case of $NiSiF_6\cdot 6H_2O$ which has recently been observed and discussed by Becquerel and collaborators.[2] The two values just given for the Verdet constant at 5461A can be represented by the relation:

$$V=0.018+2.3/T,$$

which agrees qualitatively with the earlier observations (see footnote 2 to Table I) made over a much more restricted temperature range.

We acknowledge gratefully the assistance of the American Philosophical Society in support of this investigation.

PHILIP RUDNICK
F. G. SLACK
JOHN O'CONNOR

Vanderbilt University,
Nashville, Tennessee,
November 7, 1940.

* Work conducted with the aid of a grant from the Penrose Fund of the American Philosophical Society.
[1] L. R. Ingersoll, P. Rudnick, F. G. Slack, and N. Underwood, Phys. Rev. **57**, 1145 (1940).
[2] J. Becquerel and J. Van Den Handel, Physica **6**, 1034 (1939); J. Becquerel and W. Opechowski, Physica **6**, 1039 (1939).

Scattering of 20° Neutrons in Ortho- and Parahydrogen

Since our last report on this subject,[1] we have completely rebuilt our scattering chamber and have incorporated several new features in the neutron monochromator.[2] A rotating cadmium shutter was placed immediately in front of the BF_3 chamber to keep neutrons with energies above 50°K from entering the detector. The scattering hydrogen was in the gas phase to eliminate the complicating effects of liquid forces. A jacket of liquid hydrogen boiling at atmospheric pressure maintained the gas at 20.4°K. The scattering chamber was 10 cm in diameter and 46 cm long; it was placed midway between source and detector, which were seven meters apart. The intensity of the beam was monitored by passing it alternately through the scattering chamber and through a dummy chamber. The ratio of neutron transmission through these two chambers was measured for 20°K neutrons to be 1.00 ± 0.01.

Fifty thousand counts were recorded during the experiment and the probable errors computed from the fluctuations agreed well with those expected from the total number of counts. The linearity of counting rate with cyclotron beam intensity was checked before and after each run, and all parts of the experimental set-up worked exceedingly well throughout the course of the experiment. This fact is worth noting in view of the complex nature of the apparatus. The neutron temperature calculated from boron absorption measurements, assuming a $1/v$ dependence, agreed exactly with that obtained from the velocity measurements, i.e., 20.2°K. (This is in sharp disagreement with the work of Fertel, Gibbs, Moon, Thomson and Wynn-Williams,[3] who were unable to observe a change in the boron absorption cross section with neutron velocity.)

The parahydrogen was prepared by allowing liquid hydrogen to remain in contact with active charcoal for 36 hours. The pressure difference between the charcoal chamber and a surrounding liquid hydrogen bath was observed at frequent intervals. This indicated that the equilibrium state was approached very closely. The parahydrogen was then vaporized and the gas passed immediately into the scattering chamber where it was maintained at 20.4°K for the duration of the experiment. We believe that the composition of this sample was certainly within 0.2 percent of the equilibrium value, 99.8 percent parahydrogen.

With one atmosphere of *n*-hydrogen in the scattering chamber $I/I_0=0.238\pm0.005$. With an equal pressure of parahydrogen, $I/I_0=0.868\pm0.01$. The corresponding molecular cross sections are $\sigma_0=103\times10^{-24}$ cm² and $\sigma_p=7.40\times10^{-24}$ cm². To obtain the true scattering cross sections, the capture cross section of two protons per molecule must be subtracted. If one assumes a $1/v$ law, this is 2.24×10^{-24} cm² at 20°K. The scattering cross sections for 20°K neutrons in ortho- and parahydrogen are then

$$\sigma_0=(100\pm3)\times10^{-24}\text{ cm}^2$$
$$\sigma_p=(5.2\pm0.6)\times10^{-24}\text{ cm}^2$$
$$\sigma_0/\sigma_p=19.$$

The earlier work in this field[4-6] gave values of σ_0/σ_p from two to five. It may be concluded, as was suggested by those who performed these experiments that their ratios

were reduced by excess scattering of faster neutrons in parahydrogen. The theoretical implications of these data will be discussed in a companion note by Dr. Schwinger. We had planned to repeat the work, to improve the statistical accuracy and to search for possible systematic errors, but pressure of other work now makes that impossible for some time.

Our thanks are due the Research Corporation for financial assistance in this work.

LUIS W. ALVAREZ
KENNETH S. PITZER

Radiation Laboratory,
Departments of Physics and Chemistry,
University of California,
Berkeley, California,
November 8, 1940.

[1] L. W. Alvarez and K. S. Pitzer, Phys. Rev. **55**, 596 (1939).
[2] L. V. Alvarez, Phys. Rev. **54**, 609 (1938).
[3] G. E. F. Fertel, D. F. Gibbs, P. B. Moon, G. P. Thomson, and C. E. Wynn-Williams, Proc. Roy. Soc. **175**, 316 (1940).
[4] J. Halpern, I. Estermann, O. C. Simpson and O. Stern, Phys. Rev. **52**, 142 (1937).
[5] F. G. Brickwedde, J. R. Dunning, H. J. Hoge, and J. H. Manley, Phys. Rev. **54**, 266 (1938).
[6] W. F. Libby and E. A. Long, Phys. Rev. **55**, 339 (1939).

Neutron Scattering in Ortho- and Parahydrogen and the Range of Nuclear Forces

Experiments on slow neutron scattering in ortho- and parahydrogen[1] have proved useful in distinguishing between the alternative possibilities of a real or a "virtual" singlet state of the deuteron. It is the purpose of this note to stress that experiments of the nature described by Alvarez and Pitzer[2] provide invaluable information concerning the neutron-proton interaction in the triplet state, in particular the effective range of the forces. The information ultimately available from such investigations is embodied in values for the singlet and triplet scattering amplitudes a_0 and a_1, which are related to the corresponding cross section, σ_0 and σ_1, by $\sigma_{0,1}=4\pi a_{0,1}^2$. The sign of a_0 relative to that of a_1 is the experimental criterion for the nature of the singlet state. That the relative sign is negative is the essential result of previous investigation. The magnitude of a_0 coupled with a detailed assumption concerning the range and shape of the singlet interaction potential serves to determine the magnitude of the interaction energy. The magnitude of a_1 and the triplet binding energy will determine both magnitude and range of the triplet interaction energy with a definite assumption concerning the shape of the interaction potential. Thus the essence of the investigation is an accurate determination of the triplet scattering amplitude.

The transition cross sections among the various levels of the hydrogen molecule involve different combinations of a_1 and a_0. The cross sections for transitions among the para-levels are proportional to $(3a_1+a_0)^2$, transitions among the ortho-levels are proportional to the combination $(3a_1+a_0)^2+2(a_1-a_0)^2$, while transitions between the ortho- and para-level systems involve $(a_1-a_0)^2$. Only the quantity $(3a_1+a_0)^2$ is sensitive to the precise numerical value of a_1, for a_0 is large and of opposite sign compared to $a_1(a_0/a_1\sim-4)$. Parahydrogen at the low temperatures required for the nonexcitation of rotational levels, irradiated by neutrons of energy insufficient for excitation is therefore the experimental medium appropriate to the determination of this quantity; for this enables one to measure the elastic scattering cross section of parahydrogen in its ground rotational level, free from contamination by other, large, cross sections, save for the small capture cross section. To avoid the disturbing influence of molecular binding forces, it is necessary to use molecular hydrogen in the gaseous phase. This, however, introduces a complication occasioned by the large thermal motion of the molecules. If the target molecules are not stationary, but possess a distribution in the molecular velocity $\mathbf{u}$, the effective cross section for a neutron of velocity $\mathbf{v}$, $\sigma_{eff}(\mathbf{v})$, is not the usual cross section $\sigma(\mathbf{v})$, but rather

$$\sigma_{eff}(\mathbf{v})=\frac{1}{v}\int|\mathbf{v}-\mathbf{u}|\sigma(\mathbf{v}-\mathbf{u})N(\mathbf{u})(d\mathbf{u}).$$

Here $N(\mathbf{u})$, the molecular velocity distribution function, represents the Maxwellian distribution appropriate to the temperature of the gas, T. Thus, were the actual cross section independent of velocity,[3] the effective cross section would exhibit a velocity dependence represented by[4]

$$\sigma_{eff}(E)=\sigma\left\{\left(1+\frac{1}{2\xi^2}\right)\Phi(\xi)+\pi^{-\frac{1}{2}}\frac{1}{\xi}e^{-\xi^2}\right\},\quad \xi=(2E/kT)^{\frac{1}{2}}$$

considered as a function of the neutron energy E. Under the conditions employed by Alvarez and Pitzer ($E/k=T=20°\text{K}$), this yields $\sigma_{eff}=1.247\sigma$. The actual correction factor for parahydrogen will be only somewhat smaller, since the cross section decreases but slightly in the small energy range under consideration ($E=0.00173$ ev).

The cross section curves necessary for the evaluation of σ_{eff} have been computed by Schwinger and Teller,[5] with extensions and improvements by Hamermesh.[6] The effective cross section for the $0\to0$ rotational transition, the elastic scattering of para H_2, is simply

$$\sigma_{\text{para}}=\sigma_{0\to0}=6.473(3a_1+a_0)^2.$$

The cross section for scattering by orthohydrogen will consist additively of the elastic scattering cross section ($1\to1$) and the cross section for the inelastic process in which the molecule is converted to parahydrogen in its ground state ($1\to0$). For these, one obtains

$$\sigma_{1\to1}=6.291[(3a_1+a_0)^2+2(a_1-a_0)^2]$$
$$\sigma_{1\to0}=1.447(a_1-a_0)^2.$$

Combined with the experimental results of Alvarez and Pitzer,

$$\sigma_{\text{para}}=(5.2\pm0.6)\times10^{-24}\ \text{cm}^2,$$
$$\sigma_{\text{ortho}}=(100\pm3)\times10^{-24}\ \text{cm}^2,$$

these formulae imply that

$$(3a_1+a_0)^2=0.803\times10^{-24}\ \text{cm}^2,\quad (a_1-a_0)^2=6.77\times10^{-24}\ \text{cm}^2.$$

These equations have four sets of solutions but may, by the theoretical prediction that a_1 be of negative sign, be restricted to the two sets:

(I) $\quad a_1=-4.26\times10^{-13}\ \text{cm},\quad a_0=21.8\times10^{-13}\ \text{cm},$
(II) $\quad a_1=-8.74\times10^{-13}\ \text{cm},\quad a_0=17.3\times10^{-13}\ \text{cm}.$

Had we used the lower limit of the experimental para cross

section (4.6×10^{-24} cm^2), the triplet amplitude of the first set would have been -4.49×10^{-13} cm. The theoretical triplet amplitude increases in magnitude with increasing range and has the value

$$-1/\alpha(=(\hbar^2/M|E_0|)^{\frac{1}{2}})=-4.37\times10^{-13}\text{ cm}$$

for zero range. Thus to within the statistical uncertainty of the observations the two admissible values of a_1 are (I) $a_1=-1/\alpha$, (II) $a_1=-2/\alpha$. These correspond, respectively, to (I): zero range, (II): a rectangular-well range $\sim8\times10^{-13}$ cm. Both values are theoretically untenable, the expected range being $\sim2.8\times10^{-13}$ cm. A further difficulty is revealed by computing the cross section for slow neutron scattering by free protons, *viz.*:

$$\tfrac{3}{4}\sigma_1+\tfrac{1}{4}\sigma_0,$$

which may be written

$$\tfrac{1}{4}\pi[(3a_1+a_0)^2+3(a_1-a_0)^2]=16.6\times10^{-24}\text{ cm}^2.$$

This result is considerably less than the directly measured value[7] of $(20\pm1)\times10^{-24}$ cm^2.

The consequences of these ortho-para measurements are at such complete variance with present theoretical concepts that it would be highly desirable to repeat these measurements and search for possible systematic errors.

JULIAN SCHWINGER*

Department of Physics,
University of California,
Berkeley, California,
November 14, 1940.

[1] F. G. Brickwedde, J. R. Dunning, H. J. Hoge, and J. H. Manley, Phys. Rev. **54**, 266 (1938).
[2] L. W. Alvarez and K. S. Pitzer, Cf. accompanying note.
[3] This situation is realized in the scattering of slow neutrons by helium. The cross section (1.5×10^{-24} cm^2) obtained by H. Carroll and J. R. Dunning, Phys. Rev. **54**, 541 (1938), is not the true cross section σ but σ_{eff} averaged with respect to the thermal energy distribution of the neutrons. The corrected value is $\sigma=1.25\times10^{-24}$ cm^2.
[4] $\Phi(\xi)=2\pi^{-\frac{1}{2}}\int_0^\xi\epsilon^{-x^2}dx$.
[5] J. Schwinger and E. Teller, Phys. Rev. **52**, 286 (1937).
[6] M. Hamermesh and J. Schwinger, Phys. Rev. **55**, 679 (1939).
[7] V. W. Cohen, H. H. Goldsmith and J. Schwinger, Phys. Rev. **55**, 106 (1939); H. B. Hanstein, Phys. Rev. **57**, 1045 (1940).
* This work was done while the author held a National Research Fellowship, 1939–1940.

Spectroscopically Pure Mercury (198)

For some time, spectroscopists in the national laboratories have been searching without much success for a line more nearly monochromatic than the red line of cadmium, to use as a standard of length. Professor W. E. Williams pointed out to us that if it were ever possible by some means to separate the isotopes of mercury, the green line λ5461 produced by one of the even isotopes would be admirably suited for the purpose. There would be no hyperfine structure, no isotope shift, and little Doppler broadening because of the high mass.

We have bombarded gold with slow neutrons from the 60″ cyclotron, and have collected enough of the transmutation product, mercury, to observe its spectrum. Since gold has only one isotope, 197, slow neutron capture gives rise to a single radioactive isotope, Au^{198}. This artificially radioactive product emits negative beta-rays with a half-life of 2.7 days and therefore turns into Hg^{198}, one of the stable isotopes of Hg. The experimental procedure is as follows:

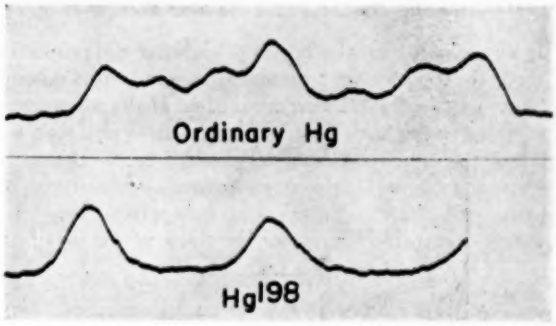

FIG. 1. Microphotometer traces for λ4047 from ordinary Hg and from Hg^{198}.

A cylinder of gold 15 cm long, 2.5 cm in diameter, and with a wall thickness of 0.2 mm is placed in a quartz tube of slightly larger diameter. To one end of this tube is fused a quartz capillary with an inside diameter of 2 mm. The whole system is evacuated and heated for 36 hours in a furnace almost to the melting point of gold. The gold is thus freed of any ordinary mercury contamination. Spectroscopically pure argon is then admitted to a pressure of 6 mm of Hg, and the quartz system is sealed off from the pumps. The gold cylinder in its quartz container is now placed in a paraffin-lined box near the target of the cyclotron, where it is bombarded with "stray" neutrons for about a month. At the end of this time the gold is again heated, while the end of the capillary tube is cooled in liquid air. After an hour of this treatment, a 3-cm length of the cooled capillary is sealed off. When the spectrum of the gas in this tube is excited by a 3-meter oscillator, the mercury lines are quite brilliant, but the argon spectrum is quenched. The mercury lines are visible after a neutron bombardment of a few hours, but they last for only a few seconds; under these conditions the Hg vapor is driven into the walls by the discharge. With a bombardment of a month, however, equilibrium between gas space and walls is apparently attained, so the spectrum is visible for some time. A microphotometer trace of a Fabry-Perot etalon spectrogram of the line λ4047 is shown in Fig. 1. The absence of the hyperfine components shows that the mercury is actually a transmutation product.

Since the Hg^{198} is a by-product of bombardments for biological purposes, no expenditure of "cyclotron time" is involved in its preparation. We will therefore be able to satisfy a reasonable demand for tubes filled with pure Hg^{198}, and we invite requests for such tubes. We gratefully acknowledge the support given to this work by the Research Corporation.

JACOB WIENS
LUIS W. ALVAREZ

Radiation Laboratory,
Department of Physics,
University of California,
Berkeley, California,
November 9, 1940.

On the Nature of the Nuclear Forces

It was shown recently by one of us,[1] that the properties of the wave equation for a particle with spin 1 in a Coulomb field are essentially different from those of the wave equation for particles with spin 0 or $\frac{1}{2}$. It turns out that the solutions of this equation corresponding to the total momenta $j \geqslant 1$ and orbital momenta $l=j+1$ have an essential singularity in the coordinate origin. The wave equations are in the vicinity of the origin of the form

$$\psi''+f(r)\psi=0 \qquad (1)$$

with $f\sim(e^2/\mu c^2)(1/r^3)$ (μ is the mass of the particle).

However, it is necessary to hold in mind that the applicability of the Proca equations is limited by distances of the order $r_0=e^2/\mu c^2$, as was shown by one of us.[2] If we note that (1) is of the form analogous to that of the Schrödinger equation the qualitative picture of the motion can be formally described as the motion of a fictitious nonrelativistic particle with mass 1 in a potential hole with the radius r_0 and of the depth $U\sim\hbar^2/r_0^2$. It is known that the levels corresponding to the motion of the particle inside the hole exist if $U>\pi^2\hbar^2/8r_0^2$. As in the present case U is itself of the order $\hbar^2/r_0^2$, it is *a priori* impossible to decide if there are states which correspond to the motion limited by the distances of the order r_0. In particular such states can prove to be possible only for certain values of the momentum j.

If we identify, as is commonly done, mesotrons with particles with spin 1, and assume that the neutron consists of a proton and a negative mesotron, then we can conclude from the foregoing considerations that there is no specific interaction between the proton and the mesotron and the formation of the neutron is the result of the ordinary electrical interaction. If such a point of view is adopted we must assume that the system proton + negative mesotron possesses for the total momentum of the system equal to $\frac{1}{2}$ and the total momentum of the mesotron $j=1$ a level which corresponds to the relative motion of both particles at the distances of the order r_0.

So we are led to the view that the nuclear forces are to be regarded as originating from the electrical interaction of the nuclear particles by means of the mesotrons, and are connected with the peculiar properties of the equations of motion of the mesotrons.

It could appear that such a point of view is inconsistent with the symmetry in the properties of the neutrons and the protons, which is substantially supported by experiment. However, it follows from the mere fact that the system proton + negative mesotron possesses a level with the binding energy *ca.* μc^2, that the system neutron + positive electron forms a proton with the liberation of nearly the same energy μc^2 (the possibility of the mesotron pair creation must be held in mind).

As the radius $e^2/\mu c^2$ of the proton and of the neutron is, in this theory, small as compared with that of the nucleus, the possibility arises of calculating various effects (the scattering of the mesotrons on the nuclei, the mesotron photo-effect, etc.) without going into the detailed consideration of the unknown interaction inside the protons and the neutrons themselves (as is done in the theory of the deuteron).[3]

A detailed discussion of these problems will be published in the *Journal of Physics* (edited by the Academy of Sciences of the U. S. S. R.).

L. Landau

The Institute for Physical Problems
of the Academy of Sciences of the U. S. S. R.,

I. Tamm

The Physical Institute of the
Academy of Sciences of the U. S. S. R.,
Moscow, U. S. S. R.,
September 25, 1940.

[1] I. Tamm, Phys. Rev. **58**, 952 (1940).
[2] L. Landau, Phys. Rev. **58**, 1006 (1940).
[3] H. Bethe and R. Peierls, Proc. Roy. Soc. **A148**, 146 (1935).

On the "Radius" of the Elementary Particles

The limit e^2/mc^2 of the applicability of classical electrodynamics can be deduced most convincingly from the condition that the reaction of the field of the electron must be small.[1] But the real limit of the classical electrodynamics is, as is well known, $\lambda\gg h/mc$ which lies much higher than $\lambda\sim e^2/mc^2$. As for the limits of applicability of the electrodynamical conceptions in quantum mechanics there are no reasons to assume that they are given by e^2/mc^2, and some other way must be found to determine the real "radius" of elementary particles.

The previous discussions of this problem have always included some additional physical assumptions,[2,3] which makes the results quite unconvincing. It is our purpose here to show that in the quantum theory a simple method can be developed to find the limit beyond which the theory comes into contradiction with itself because of the neglect of the reaction of the field.

The neglect of the reaction of the field means that we assume the particle to move under the influence of the external field without taking into account the variation of this field by the electron itself. In the mathematical treatment this is expressed by calculating the matrix elements of the interaction of the charged particle and a photon with the help of free particle wave functions. Hence the smallness of the reaction force corresponds in the quantum theory to the applicability of the perturbation theory to the collision of a charged particle and a photon.

The effective cross section for the scattering of particles with an angular momentum l in the frame of reference moving with the center of inertia is $\sigma_l=4(2l+1)\pi\lambda\!\!\!^{-2}\sin^2\delta_l$, $\lambda\!\!\!^{-}$ being the wave-length (divided by 2π), δ_l– the phase of the wave function at infinity. The applicability of the perturbation theory requires $\delta_l\ll 1$. As the scattering decreases with increasing l, it suffices to require this condition to be fulfilled for $l\sim 1$; the corresponding σ_l we denote as σ_0. Thus we come finally to the condition

$$\sigma_0\ll\lambda\!\!\!^{-2} \qquad (1)$$

(it is to be noted that the condition $\sigma_l<4(2l+1)\pi\lambda\!\!\!^{-2}$ must be fulfilled quite independently of the applicability of the perturbation theory; the opposite would mean that the number of scattered particles exceeds the number of corresponding incident particles, which is impossible).

It is easy to see that in the classical theory (1) leads to the correct results. As in the classical theory all the scattering is dipole scattering, we must simply insert for σ_0 the full Thomson's scattering cross section, this leading to $e^2/mc^2 \ll \lambda$.

We now apply (1) to the quantum theory of the electron. We must first of all transform the Klein-Nishina formula to the proper frame of reference and then take part of the scattering corresponding to the angular momentum of the order 1. This gives $\sigma_0 \sim (e^2/mc^2)^2 mc^2/E$ (E being the energy of the photon in the frame of reference where the electron is at rest). σ_0 differs from the total cross section by the absence of the factor $\log E/mc^2$ which arises from the scattering with large angular momenta. The energy ϵ of the photon in the frame of reference moving with the center of inertia is given by $2\epsilon^2 = mc^2 E$ (when $E \gg mc^2$) so that $\lambda \sim \hbar c/\epsilon \sim \hbar c/(mc^2 E)^{\frac{1}{2}}$. The energy E disappears now from (1) and we get $e^2 \ll \hbar c$ which is always fulfilled. This means that in the quantum theory of the electron there are no limits of its applicability, arising from itself. The "radius" of the electron in quantum electrodynamics is in some sense equal to zero.

One gets the same result for particles with zero spin, if the corresponding expression for Compton effect[4] is used.

The Compton effect for particles with spin 1 (mass μ) was recently calculated by F. Booth and A. H. Wilson[5] and by J. Smorodinski.[6] The result is $\sigma_0 \sim (e^2/\mu c^2)^2 E/\mu c^2$. Hence the condition (1) gives $E \ll \mu c^2 \hbar c/e^2$. The "radius" of the particle is equal to the corresponding wave-length in the frame of reference in which the particle is at rest, i.e.

$$r \sim \hbar c/E \sim e^2/\mu c^2. \tag{2}$$

Hence the "radius" of the particle with spin 1 is equal to its classical value.

A more detailed discussion of the problem with the application to the scattering of particles with spin 1 by a charged particle, is to be published in *Journal of Physics*, volume 3, 1940.

L. LANDAU

The Institute for Physical Problems
of the Academy of Sciences of U. S. S. R.,
Moscow, U. S. S. R.,
September 19, 1940.

[1] Cf. W. Heitler, *The Quantum Theory of Radiation* (Oxford, 1936), pp. 33, 232.
[2] W. Heisenberg, Zeits. f. Physik **110**, 251 (1938).
[3] V. Weisskopf, Phys. Rev. **56**, 73 (1939).
[4] W. Gordon, Zeits. f. Physik **40**, 117 (1927).
[5] F. Booth, and A. H. Wilson, Proc. Roy. Soc. **A175**, 483 (1940).
[6] J. Smorodinski, J. Phys. **3** (1940).

Relative Intensities of $^1S-{}^3P$ and $^1S-{}^1P$ Transitions in Mg

The relative intensity of singlet-triplet and singlet-singlet transitions in cases where the spin-orbit interaction is weak is given by

$$f_3 = |S_3|^2 (\nu_3/\nu_1) f_1, \tag{1}$$

where the subscripts 3 and 1 denote singlet-triplet and singlet-singlet values, respectively. The factor S_3 is the coefficient which represents the contamination of the singlet state by the triplet state; that is, approximately

$$\psi(^1P) = \psi_0(^1P) + S_3 \psi_0(^3P), \tag{2}$$

where the ψ_0's are Russell-Saunders wave functions. One has from perturbation theory

$$|S_3| = H(ij)/h\nu_{ij}, \tag{3}$$

where $H(ij)$ is the matrix element of the Hamiltonian. Furthermore, the deviation of the central component of the triplet from the interval rule is

$$\Delta W = [H(ij)]^2/h\nu_{ij}. \tag{4}$$

According to Houston,[1] we may take for P states

$$H(ij) = [l(l+1)]^{\frac{1}{2}} A = \sqrt{2}A, \tag{5}$$

if A is the constant of the spin-orbit interaction $AL \cdot S$. In practice A is determined from the over-all width of the triplet, $3A$. The theoretical expression for A is

$$A = \frac{\hbar^2}{16\pi^2 m^2 c^2} \int R_{3P}^2 \left(\frac{1}{r}\frac{\partial V}{\partial r}\right) r^2 dr. \tag{6}$$

The radial wave function, R_{3P}, of the triplet state is here assumed to be identical with that of the singlet state.

Since the relative intensities found from (1), (3), and (5) are in only fair agreement with observation, King and Van Vleck[2] have suggested that an undetermined parameter λ be inserted in (5) and (6) to account for the difference between R_{3P} and R_{1P} which was previously neglected. Then A refers to the integral (6) with R_{3P}^2 in the integrand while λA denotes the integral with $R_{3P}R_{1P}$. The value of λ is determined so as to make the deviation (4) from the interval rule correct. In this way King and Van Vleck[2] find for the atoms Hg, Cd, Zn, Ba, Sr, and Ca that $\lambda \sim 0.8$. If, however, we try to apply their procedure to the transition $3s^2\,{}^1S - 3s3p\,{}^3P$ of Mg, we find $\lambda = 2.4$, a value out of line with those previously found. It seems, then, that in this case the deviations from the interval rule are not due simply to perturbations by ^1P but that other effects enter. Mg is so light that spin-spin interaction may contribute appreciably to the observed deviation, 0.3 cm^{-1}, from the interval rule. One should therefore not place much trust in the value of λ for Mg derived above.

It is thus uncertain whether to use the value $\lambda = 0.8$ by analogy with previous calculations, or merely to use the Houston formula, where $\lambda = 1$. The relative intensities found in the two cases are

$$\begin{aligned} f_1/f_3 &= 340{,}000 \quad \text{for} \quad \lambda = 1, \\ f_1/f_3 &= 530{,}000 \quad \text{for} \quad \lambda = 0.8. \end{aligned} \tag{7}$$

We may consider these values as correct within a factor 2 or 3.

I am indebted to Professor D. H. Menzel for suggesting this problem and Professor J. H. Van Vleck for his guidance and advice.

PEARL J. RUBENSTEIN

Harvard College Observatory,
Cambridge, Massachusetts,
November 8, 1940.

[1] W. V. Houston, Phys. Rev. **33**, 297 (1929).
[2] G. W. King and J. H. Van Vleck, Phys. Rev. **56**, 464 (1939).

Gamma-Radiation from Rhenium

We have produced by proton bombardment of tungsten (purity 99.95 percent) the long period rhenium isotope which Fajans and Sullivan[1] obtained by $W(D,n)$ and $Re(n,2n)$ and assigned to Re^{184}. We have also produced the 90-hour and 30-minute periods by proton bombardment and checked the fact that they follow rhenium chemistry.

After removal from the cyclotron, the tungsten strip which had been bombarded intermittently for four months with currents of the order of 20 microamperes, was allowed to age for two months before observations began, so that the shorter periods might die out, after which the activity was followed for four months. The original intensity of the long period was about 100 divisions per minute on the Lauritsen electroscope. Our value of the half-life is 54 ± 2 days. See Fig. 1.

Absorption measurements of the radiation showed negative electrons of three kinds, of ranges 12, 50, and 350 mg/cm² of aluminum, corresponding to energies of roughly 0.1, 0.22, and 0.86 Mev, respectively, and gamma-radiation of about 1 Mev, as seen from Fig. 2. The highest energy group may be conversion electrons from this gamma-ray, which was also reported by the above authors.[1] The intermediate energy electrons were too few for careful study, and indeed may be from a tungsten isotope produced from the neutrons around the cyclotron.

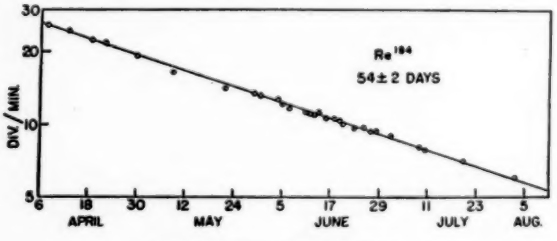

FIG. 1. Decay curve of Re^{184}.

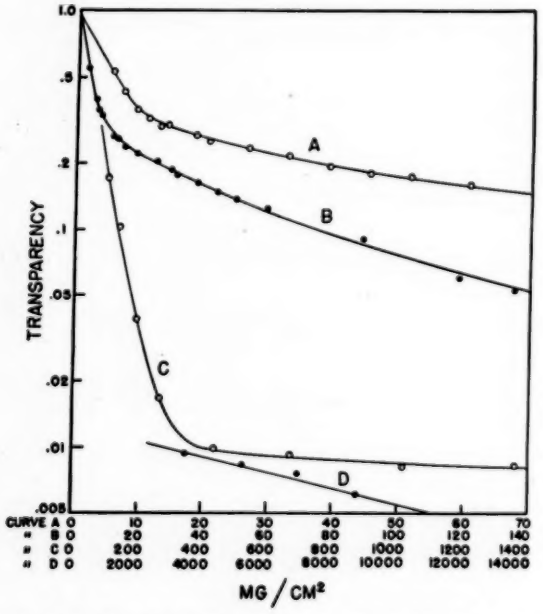

FIG. 2. Absorption of radiation from 54-day Re. Curves *A*, *B*, and *C*; absorption in Al. Curve *D*; absorption in Pb.

FIG. 3. Conversion electrons from tungsten bombarded with protons.

Previous experience had shown that a beta-ray spectrograph could be used to photograph a line of electrons of around 100 kev energy if the intensity was such that the equivalent of about 10^5 divisions of the electroscope were available. This corresponds roughly to 10^9 particles. Since the fraction of these striking the photographic film in our spectrograph is about 10^{-5}, as an estimate 10^6 electrons are required to produce a usable image. Because various workers[2] have shown the reciprocity law to be valid for electrons, it seemed worth while to attempt a long exposure to measure the low energy group from our target. A twenty-one-day exposure showed a line at 0.096 Mev, reproduced in Fig. 3. If these are *K*-conversion electrons, there must be a gamma-ray from the 54-day rhenium isotope of 0.096 ± 0.071 (Re *K* edge) $=0.17$ Mev.

E. CREUTZ
W. H. BARKAS*
N. H. FURMAN†

Palmer Physical Laboratory,
Princeton University,
Princeton, New Jersey,
November 13, 1940.

* Now with Bureau of Ordnance, U. S. Navy, Thirteenth Naval District, Seattle, Washington.
† Department of Chemistry, Princeton University.

[1] K. Fajans and W. H. Sullivan, Phys. Rev. **58**, 276 (1940).
[2] A. Becker and E. Kipphan, Ann. d. Physik **10**, 15 (1931); also M. J. Nacken, Physik. Zeits. **31**, 296 (1930).

The Electric Fields in Vibrating Polar Crystals

Within a vibrating polar crystal there are electric forces caused by the polarization, **P**, associated with the displacements of the ions of the crystal during the vibration. These forces give rise to an electric field, **E**, and an electric displacement, **D**, which, according to Lyddane and Herzfeld,[1] are connected with the polarization by

$$\mathbf{E}=-4\pi\mathbf{P}, \quad \mathbf{D}=0, \tag{1}$$

if the wave-length of the vibration is short compared to the size of the crystal but long compared to the lattice distance. This result is stated to be independent of whether the waves in the crystal are longitudinal or transverse. On the other hand, Fröhlich and Mott[2] have given formulae that agree with (1) for the longitudinal displacement but become

$$\mathbf{E}=0, \quad \mathbf{D}=4\pi\mathbf{P} \tag{2}$$

for the transverse case.

That the latter result is the correct one becomes apparent from the following direct calculation based on formulae given by Lyddane and Herzfeld[1] for the electric force, **F**, within a crystal. When the wave-length is long compared to the dimension of a crystal slab, these formulae are:

(1a) $\mathbf{F}=-(8\pi/3)\mathbf{P}$ if P is perpendicular to the face of the slab,

(1b) $\mathbf{F}=(4\pi/3)\mathbf{P}$ if P is parallel to the face of the slab.

Should the wave-length be short compared to the dimensions of the slab but long compared to the lattice distance:

(2a) $\mathbf{F}=-(8\pi/3)\mathbf{P}$ for the longitudinal vibration

(2b) $\mathbf{F}=(4\pi/3)\mathbf{P}$ for the transverse vibration.

According to the conventional definition, the electric field is the electric force in a slot in the crystal with its short dimension perpendicular to the direction of the electric force. We consider a slot of dimensions short compared to the wave-length. Then $\mathbf{E}$ is obtained by subtracting from (2a) or (2b) the effect of the material that has been removed to form the slot. Since the electric force is always parallel to $\mathbf{P}$, the effect of this material is just the force (1b). Therefore

$$\mathbf{E}=-4\pi\mathbf{P} \text{ for the longitudinal vibration,}$$
$$\mathbf{E}=0 \text{ for the transverse.}$$

The displacement, $\mathbf{D}$, is given by the electric force in the slot when its short dimension is parallel to the polarization. Therefore, subtracting (1a) as the effect of the material in the slot from (2a) and (2b)

$$\mathbf{D}=0, \quad \mathbf{D}=4\pi\mathbf{P}$$

for the longitudinal and transverse vibrations, respectively.

These formulae are consistent with $\mathbf{D}=\mathbf{E}+4\pi\mathbf{P}$, and they also lead, according to (2a) and (2b), to the Lorentz-Lorenz force for both types of vibration; that is:

$$\mathbf{F}=\mathbf{E}+(4\pi/3)\mathbf{P}.$$

At first sight, the fact that the electric displacement does not vanish for the transverse vibration may appear to be inconsistent with the absence of an impressed external field. However, the polarized crystal itself gives rise to an external field which is just $4\pi\mathbf{P}$ at the surface and vanishes exponentially with distance from the surface. This may be seen by considering a charge distribution on a plane surface that is periodic in one direction with wave-length λ and constant in the perpendicular direction. Such a charge distribution gives rise to a field proportional to $\exp(-2\pi x/\lambda)$, if x is perpendicular to the surface. A transversely displaced crystal with the polarization perpendicular to the face of the slab may be considered as made up of a series of such planes, and it is apparent that there will be an exponentially decreasing external field over a distance approximately given by the wave-length of the vibration under consideration. The result obtained directly from the lattice sums by Kellerman[3] is in agreement with this qualitative argument.

R. H. LYDDANE

University of North Carolina,
Chapel Hill, North Carolina.

K. F. HERZFELD

Catholic University,
Washington, D. C.

R. G. SACHS

George Washington University,
Washington, D. C.,

November 1, 1940.

[1] R. H. Lyddane and K. F. Herzfeld, Phys. Rev. **54**, 846 (1938).
[2] H. Fröhlich and N. F. Mott, Proc. Roy. Soc. **A171**, 496 (1939).
[3] E. W. Kellerman, Phil. Trans. Roy. Soc. **A238**, 513 (1940).

The $C^{12}H_2-N^{14}$ Mass Difference

Three years ago the author, in an attempt to obtain more accurate mass values, undertook to construct a new type of mass spectrograph having a very high resolving power and dispersion. This instrument was completed last spring and reported[1] at the Washington meeting of the American Physical Society.

Its constants are given in Table I together with those of other instruments being used at the present time to study the light element doublets.

The mass scale is correction free, mass differences being obtained directly by taking the mean of the ratios of the doublet separation to the forward and backward dispersion line separations. In the case of the $C^{12}H_2-N^{14}$ doublet, this method of calculation gives the mass difference directly to 0.000015 mass unit, a figure which is several times smaller than the error introduced in making a single doublet distance measurement. In addition, exact methods have been worked out for correcting this small deviation and it is estimated that the resulting error due to the method of computation alone is approximately three to four units in the sixth decimal place. The above relation holds true regardless of the plate position within rather wide limits.

Recently a considerable number of matched as well as unmatched $C^{12}H_2-N^{14}$ doublets were obtained in a series of spectra which were photographed under different conditions and used to verify the theoretically expected relations. The values of the mass differences corresponding to these doublets are listed in Table II in order that a birds-eye view of the variations may be obtained. These data result from measurements taken on three different plates, three to five measurements of the doublet distance being made in each instance. Although the difference in density between the doublet lines is not large in any case, only about half the doublets corresponding to the values listed are matched. It so happens that if the matched doublets alone are considered, the same average value is obtained, the probable error also being approximately the same.

For comparison purposes, this mass difference, together with other published values for the light element doublets is listed in Table III. Although no cross check doublets

TABLE I. *Mass-spectrograph constants.*

Mass Spectrograph	Resolving Power $M/\Delta M$	Dispersion (mm for 1% mass diff.)
Aston	2,000	4.5
Mattauch	6,500	1.4
Asada and others	17,000	4.65
Jordan	30,000	14.6

TABLE II. *The $C^{12}H_2-N^{14}$ doublet mass differences.*

0.01255	0.01255	0.01257	0.01258	0.01254
0.01258	0.01254	0.01263	0.01254	0.01255
0.01256	0.01252	0.01258	0.01257	0.01251
0.01253	0.01260	0.01256	0.01265	0.01252
			0.01254	0.01256

Average 0.01256 ± 0.000015*

* This error is three times the probable error computed from the internal consistency of the data.

TABLE III. *Mass differences in terms of 10^{-4} mass unit.*

DOUBLET	$H_2'-D^2$	$D_2^2-C^{12++}$	$C^{12}H_4'-O^{16}$	$C^{12}H_2'-N^{14}$
Aston	15.2 ±0.4	423.6 ±1.8	360.1 ±1.6	124.5 ±0.7
Bainbridge and Jordan	15.3 ±0.4	421.9 ±0.5	364.9 ±0.8	127.4 ±1.1
Mattauch	15.39 ±0.021	422.39 ±0.21	364.06 ±0.40	125.81 ±0.23
Asada and Others			364.2 ±0.9	125.7 ±0.6
Jordan				125.6 ±0.15

have been measured as yet, it seemed worth while to publish this value in view of the fact that it was obtained on an instrument which not only has extremely high constants but also differs radically from any of the others in use at the present time. Other measurements on the light element doublets are in progress.

E. B. JORDAN

Physics Department,
University of Illinois,
Urbana, Illinois,
October 28, 1940.

[1] E. B. Jordan, Phys. Rev. **57**, 1072A (1940).

Cosmic Rays and Comets

The conjecture that the comets are contraterrene bodies,[1] which accounts, if only in a rough qualitative way, for some of the more conspicuous features of comets, can be properly tested as follows: (a) by investigating its usefulness in detailed quantitative interpretation of the now known properties of comets; (b) by performing experiments, involving cosmic-ray measurements, during meteor showers known to be of cometary origin; and (c) by performing appropriate cosmic-ray experiments while a sufficiently active comet is sufficiently near to the earth. Method (a) is indirect; and since it involves detailed study of the intricacies of cometary behavior, as well as a knowledge of the distribution of meteoric material within the solar system, it is difficult. Method (b) implies the acceptance of the idea that certain meteor showers are of cometary origin, but is otherwise quite direct; and the requisite experiments can be done, for example, almost every August. Method (c) is in principle the most direct; but the occasions on which it can be tried are very rare.

One purpose of this note is to call attention to the fact that if the comet recently discovered by Cunningham proves sufficiently active, it might, within the next few weeks, provide opportunities for performing the experiments involved in method (c). Lacking the appropriate data, however, the writer is at present unable to venture an estimate whether, if comets are contraterrene, the cosmic-ray effects of Cunningham's comet would be sufficiently intense for experimental purposes.

If comets are contraterrene, their activity depends not only on the solar energy that they receive, but also on the rate at which they encounter ordinary meteoric matter. In the absence of a theory of interaction of terrene and contraterrene matter, it is impossible to say with certainty what the primary products of their mutual annihilation would be. It is reasonably safe to guess, however, that among these products there should be photons having energies of about a billion electron volts. Therefore experiments designed to determine whether any high energy photons do originate in a comet should best be performed in the upper atmosphere.

The second purpose of this note is to mention that among the products of mutual annihilation of terrene and contraterrene matter there may be free mesons. This possibility is of interest not only in view of the present conjecture concerning comets, but also in connection with cosmic rays in general; for it suggests that: (1) The continual release of mesons at the top of the earth's atmosphere may be caused by contraterrene matter coming from interstellar space and impinging upon the atmosphere, and (2) the non-ionizing particles which release mesons deeper in the atmosphere may be contraterrene neutrons, which have themselves been set free in the earlier stages of the annihilation of the impinging contraterrene atomic nuclei.[2]

V. ROJANSKY

Union College,
Schenectady, New York,
November 4, 1940.

[1] V. Rojansky, Astrophys. J. **91**, 257 (1940). We call "contraterrene" a body composed of hypothetical atoms consisting of negatively charged nuclei surrounded by positrons; an ordinary body we call "terrene."

[2] The possibility of production of high energy photons in the upper atmosphere by the annihilation of negative protons arriving from interstellar space was discussed by F. Zwicky, Phys. Rev. **48**, 169 (1935). See also F. Zwicky, Proc. Nat. Acad. Sci. **22**, 266 (1936), esp. Section *F*.

Erratum: On the Angular Distribution of Fast Neutrons Scattered by Hydrogen, Deuterium and Helium

(Phys. Rev. **58**, 590 (1940))

The captions of Fig. 3 and Fig. 4 on page 592 should be interchanged.

H. H. BARSCHALL
M. H. KANNER

Palmer Physical Laboratory,
Princeton University,
Princeton, N. J.,
November 15, 1940.